Delft University of Technology

Master Thesis

Evaluation of a *smart electrosurgical knife* – assessing the feasibility of tumour detection with Diffuse Reflectance Spectroscopy in breast conserving surgery.

A thesis submitted in fulfilment of the requirements

for a degree in Master of Science

in the

Department of Biomedical Engineering

Specialization Medical Instruments and Medical Safety

Author:
M.W. Adank
MSc. Student Biomedical Engineering
4102894

Supervisors:
Prof. Dr. B. H. W. Hendriks
Prof. Dr. J. Dankelman

TU Delft Delft University of Technology

PHILIPS

Delft University of Technology

Faculty of Mechanical, Maritime and Materials Engineering (3mE)

Delft Institute of Biomedical Engineering

Evaluation of a *smart electrosurgical knife* - assessing the feasibility of tumour detection with Diffuse Reflectance Spectroscopy in breast conserving surgery.

A thesis submitted to the

Delft Institute of Biomedical Engineering

In partial fulfilment of the requirements

for the degree of

MASTER OF SCIENCE

in

BIOMEDICAL ENGINEERING

by

MAARTJE ADANK

Delft, the Netherlands,

May 2017

Preface

Before you lies the culmination of this thesis project, performed in partial fulfilment of the requirements for the degree of Master of Science in Biomedical Engineering. Eight months of reading literature, formulating research questions, designing experiments – changing the experiments if they did not worked out - and obtaining the results from these experiments led to this master thesis.

The impact this project can have – improving the margin assessment for all woman with breast cancer – kept me focused even when the project got difficult at some times. When I started this project last September 2017, my knowledge about light and how light travels was limited to the knowledge obtained in high school. It took me quite some time to get used to the terminology and understand the techniques. In addition, designing, making and using an experimental setup was new to me. I really enjoyed testing the setup designs and adjusting them to be able to answer a specific research question. It feels satisfying to end this project – of which I was a bit afraid to start with in the beginning – with results that can help this innovation further.

Besides the thesis project itself, I also learned a lot from working at Philips Research. I found it interesting to work on this project in the inspiring atmosphere with people who were always helpful to me. I enjoyed the experience of the internship at Philips Research and living in another city for half a year.

Before reading this thesis, I would like to speak out my gratitude to some people without whose support I could not have finished this master thesis. First of all, I would like to thank prof. Benno Hendriks who provided daily support. Your door was always open if I had a question about one of the many topics this thesis covers. Next, I owe my gratitude to prof. Jenny Dankelman for her support from Delft University of Technology. She kept me on track and asked questions from a more zoomed out perspective.

Akash Swamy, helped me out with practical information, the Monte Carlo simulation and always made me think of why I was taking a specific step in my process. Jarich Spliethof and Christian Reich, both from the In-Body systems department of Philips Research, provided me specific information about the use of DRS and on how to use tissue in the experiments respectively. I would also like to thank Lisanne de Boer for making it possible to attend some surgical procedures in the Netherlands Cancer Institute and providing me pictures of breast tumours obtained by the pathologist.

Finally, a brief acknowledgement to my family, boyfriend, roommates and Philips interns of the In-Body Systems department for their informal support in every way.

Abstract

Every year, 1.7 million woman are diagnosed with breast cancer worldwide. Breast Conserving Surgery (BCS) – where not the whole breast but only the tumour is dissected – is the most common and preferable treatment for these woman. However, 20 to 55% of the patients' needs a second surgery because of positive margins. A dissected tumour has a positive margin if it lacks a border of 2mm healthy tissue at any point. Currently, no instruments are available to provide intraoperative distinction between adipose and muscle tissue with real-time feedback. This thesis evaluates a 'smart' electrosurgical knife, which uses Diffuse Reflectance Spectroscopy (DRS) to discriminate between tumour and adipose tissue to assess margins intraoperative with real-time feedback.

Previous research has shown that DRS can discriminate between tumour and adipose tissue. [1] In addition, electrosurgical cutting in adipose tissue does not affect the measured DRS spectra. [2] This thesis focuses on detecting muscle tissue under a layer of adipose tissue with DRS while cutting the adipose tissue using an electrosurgical knife.

An answer to this research question is provided based on four experiments. All experiments are performed on pork muscle- and adipose tissue. DR spectra are measured with multiple probes and a 'smart' electrosurgical knife. PNSas software is used to acquire the spectra and fit the data. First, the influence of electrosurgical cutting and coagulation is described. This is accomplished by examining the shape and size of the cut and measuring DR spectra. Second, the transition from adipose to muscle tissue was identified in the resulting DR spectra. In addition, chromophore concentrations are retrieved from the fit data. The second experiment was repeated on cut muscle tissue. Moreover, the DR spectra obtained while cutting with an electrosurgical knife are presented.

It is shown that for both electrosurgical cutting and coagulation, increasing the power setting leads to an increase in deviation from the pure DRS spectra. In general, deviations are observed in cut or coagulated muscle tissue compared to adipose tissue. No trends are found for the cutting or coagulation depth and with when increasing the power setting. For muscle tissue, a coagulation zone is observed after electrosurgical coagulation. The depth of the coagulation zone increases for higher power settings.

The transition from adipose to muscle tissue is clearly visible in the DR spectra for pure tissue. A significant difference between the two tissues was found in the fat-water ratio ($p = 1.28e^{-39}$), StO_2 percentage ($p = 4.81e^{-15}$), blood percentage ($p = 9.93e^{-7}$) and b ($p = 0.014$). For cut adipose tissue, the DR spectra still provided a clear transition from adipose to muscle tissue. Again, a significant difference between muscle and adipose tissue was found for fat-water ratio ($p = 3.32e^{-39}$), StO_2 percentage ($p = 3.23e^{-27}$), blood percentage ($p = 2.36e^{-9}$) and Mie scattering ($p = 2.84e^{-8}$) in this experiment. The signal of the measurements obtained while cutting was too noisy to obtain statistically significant results.

Overall, the results of this thesis provide additional evidence in favor of the effectiveness of the 'smart' electrosurgical knife in BCS. The ability to measure DR spectra and obtain a significant difference between muscle and (cut) adipose tissue is a crucial step forward in the development of the 'smart electrosurgical knife'. The results set forth in this thesis show that no conclusion can be drawn on the possibility of detecting the tumour while cutting. If so, the 'smart' electrosurgical knife could be of great benefit for tumour margin assessment in BCS.

Contents

III Experiments

IV Validation

V Clinical setting experiments

VI Discussion, conclusion and recommendation

List of Figures

List of Tables

List of Abbreviations

Abbreviation	Meaning
CT	Computed tomography
MRI	Magnetic resonance imaging
SPECT	Single-photon emission computed tomography
PET	photon emission tomography
DRS	Diffuse Reflectance Spectroscopy
NIR	Near Infra-red wavelength region
DCIS	ductal carcinoma in situ
LCIS	lobular carcinoma in situ
BCS	Breast conserving surgery
US	Ultrasound
VIS	Visual wavelength region
PNSas	PhotonicNeedle software
ENT	Ear Nose
ES	Electrosurgical / Electro surgery
PC	Personal computer
Dt	Cutting depth
Dg	Coagulation depth
Wt	Cutting width
Wg	Coagulation width
Zg	Coagulation zone
FD	Fiber distance
MC	Monte Carlo
MCML	Monte Carlo model of steady-state light transport in Multi-Layered tissue
VAF	Variance Accounted For

List of Symbols

Symbol	Unit	Function	Description
v	$[s^{-1}]$	3.1	Frequency
c	$[m/s]$	3.1	Speed of light
λ	$[nm]$	3.1	Wavelength
μ_a	$[m^{-1}]$	3.2	Absorption coefficient
μ_s	$[m^{-1}]$	Appendix A	Scattering coefficient
$p(\theta, \psi)$	$[sr^{-1}]$	Appendix A	Scattering function
g	$[-]$	Appendix A	Anisotropy
n'	$[-]$	Appendix A	Real refractive index
μ_s'	$[m^{-1}]$	Appendix A	Reduced scattering coefficient
T	$[-]$	Appendix A	Transmitted or surviving fraction of the incident light after the incremental path length ∂L [cm]
i	$[cd]$	3.6 & 3.7	Intensity of the light traveling inside the sample towards the un-illuminated surface
j	$[cd]$	3.6 & 3.7	Intensity of the light traveling inside the sample towards the illuminated surface
I	$[-]$	3.8	Measured diffuse reflectance intensity distribution
f	$[\%]$	3.9	Fat fraction
I	$[ampere]$	3.10	Electrical current
V	$[volts]$	3.10	Voltage
R	$[\Omega]$	3.10	Resistance
$p(s)$	$[-]$	3.11 & 3.12	Probability density function
R_{sp}	$[-]$	3.13	Probability of photons being specular reflected
W	$[kg]$	3.14 & 3.18	Photon weight
s	$[m]$	3.15	Step size of photon package
μ_x, μ_y, μ_z	$[-]$	3.16	Position of photon package
x, y, z	$[-]$	3.17	Updated position of photon package
θ	$[°]$	3.19 & 3.21	Deflection angle
ψ	$[°]$	3.20	Azimuthal angle
R_θ	$[°]$	3.22	Internal reflectance
VAF	$[-]$	3.24	Variance accounted for

1. Introduction

1.1. Problem statement

Cancer is a major cause of morbidity and mortality, with approximately 14 million new cases and 8 million cancer-related deaths in 2012. This disease affects people all over the world. The number of new cases is expected to increase to 24 million by 2035. [3] Surgery remains the most important, effective and widely used treatment modality by curing approximately 45% of all patients with solid tumours. [4] [5] [6] However, a major problem in surgical treatment remains the difficulty to remove the complete tumour, leaving behind tumour-positive margins (see Figure 1, right), metastatic lymph nodes, and/or satellite tumour nodules. [4]

From an oncological perspective, it is most important to remove the complete tumour tissue and some of the healthy tissue to ensure no tumour tissue is left behind. This is called 'margin with clearances' or a negative margin, where the dissected tumour is completely surrounded by a healthy tissue layer of at least 2 mm thickness, see Figure 1, left. [7] [8] On the other hand, from a functional or/and cosmetic perspective minimizing the elimination of noncancerous tissue is more crucial. [7] Statistical data indicates that complete resection is the single most important predictor of patient survival for almost all solid tumours. [4] [9] [10] After breast conserving surgery, 20% to 55% of all patients requires a second surgical procedure to clear positive margins. [11] [12]. In lung, breast, prostate, colon, and pancreatic cancers, a complete resection has a triple to fivefold improvement in survival rate compared to partial resection. [13] [14] [15] [16] Additionally, re-excision is not always possible, as for example for soft tissue tumours or colon cancer. [7]

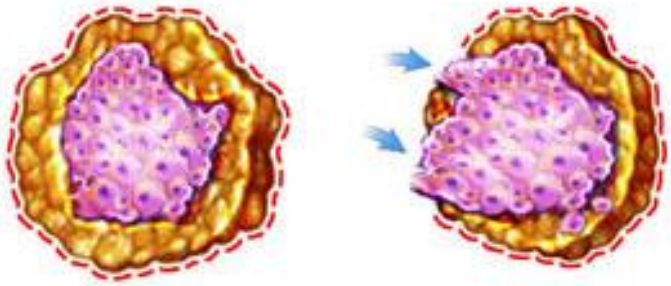

Figure 1: Left: a dissected tumour with a negative margin, surrounded by a healthy tissue layer > 2 mm thickness. Right: a dissected tumour with a positive margin, the healthy tissue layer is < 2mm thickness [1]

There are several steps to analyse tumours pre-, intra- and postoperative. Preoperative procedures include a range of non-invasive imaging modalities to detect tumours for surgical planning including CT, MRI, SPECT, PET and ultrasound. Intraoperative, the most commonly used methods to guide resection of a tumour –and its margins – are palpation and visual inspection. Both relying on the surgeon's experience and judgement. [17] The available intraoperative methods – for example ultrasound – to guide resection, often discriminate incorrectly between malignant and normal tissue, causing positive tumour margin rates up to 50% in some cancers [18] [19]. Positive tumour margins lead to a higher risk of local recurrence of the tumour. [20] [21]

A method to analyse the tissue postoperative is a histologic examination. This process is called frozen section and takes 20 to 30 minutes to complete. Hence, histologic examinations are relatively expensive. Another disadvantage of this approach is that the number of sampling points is typically small and the results are open to subjective interpretation. [7] [12] [22]

Preoperative methods to examine cancer tissue are relatively accurate but are difficult to use intraoperative due to altered body positions and tissue manipulation. The histological analysis, which can accurately locate the tumour, is time-consuming and therefore inadequate to use in situ. [7] Accordingly, the surgeon still needs to rely on gross visual- and tactile inspection during surgery. [22] [23] Currently, additional treatments for cancer such as radiotherapy, hormone therapy, chemotherapy and re-incisions are used to reduce the likelihood of local occurrence. However, these treatments have a severe impact on the quality of life of the patient by causing significant physical and emotional distress, and suboptimal cosmetic outcome. [17] [24]

There is an aim to provide a tool that correctly discriminates between healthy- and tumour tissue assisting the surgeon in improving an accurate clearance of cancer tissue. It needs to identify vital structures and discriminate healthy tissue from diseased tissue in real – or limited – time. This is particularly important for laparoscopic surgery because the surgeon lacks tactile information in this case. [22] [25]

Diffuse Reflectance Spectroscopy (DRS) is a photonic technology that has been proven to accurately distinguish tumour and healthy tissue based on surface measurements. [1] At Philips In-Body Systems, it is thought that DRS could add value to the assessment of tumour margins. Integration of this technique into the tip of an electrosurgical instrument – which is used to dissect the tumour – could give the surgeon extra information to help clearing the margins and improving patient outcome. In addition, the surgeon does not have to change between a cutting and a localization instrument any more. This thesis will be a contribution to the evaluation of DRS as a technique to assess tumour margins, in the specific case of breast tumours.

1.2. Research contribution

To evaluate the feasibility of DRS to discriminate between tissues in tumour margin assessment, already some research is performed. De Boer et al. determined the best optical parameters within the extended NIR region for discrimination between benign and malignant breast tissue. In addition, they investigated the ability of these optical parameters to detect tumour margins when there is a mixture of benign and malignant breast tissue present. [1] The relevant results of De Boer et al. for this thesis are:

- In DR spectra, the lower wavelengths are primarily influenced by their absorption in blood and higher wavelengths in fat and water. While the ultimate objective to design a tool to use intraoperatively, contamination of blood at the resected site will impair the reliability of the visual wavelengths, therefore the NIR region will be more suitable. In addition, the distinction between benign and malignant tumour tissue is clearer in the NIR region. [1]
- Besides the distinction that can be made between benign and malignant tissue by DRS on adipose/water-ratio with a specificity of 100%, a mix between benign and malignant tissue can also be detected. [1]

In addition to the research of De Boer, Fleischer also contributed to the evaluation of DRS as being an effective technique to assess tumour margins. She examined the influence of coagulation on DR spectra, a relationship that becomes relevant when using electro surgery to cut tissue. The most relevant results of Fleischer's thesis for this report are:

- Coagulation in brain, liver and chicken breast tissue increases scattering multiple times and reduces the photon penetration depth compared to non-coagulated tissue. When the DR spectra are altered, it is possible to treat the coagulated tissue as a distinct layer. [26]
- For coagulated tissue, a decrease in the large slope in the VIS region is present in the DR spectra. For heart, liver, lung and muscle tissue, increased peak values can be observed in the NIR region for normalized spectra. The fat measurements show a small rise in intensity for the 600-1100 nm plateau, but virtually no changes in the NIR region.

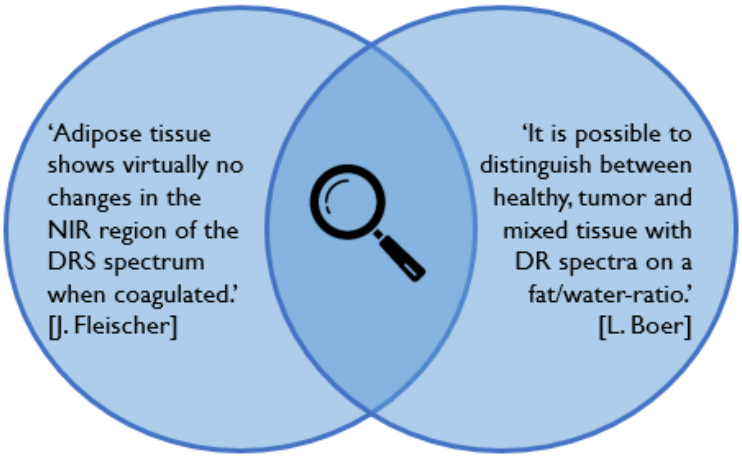

Figure 2: Indication of the knowledge gap this thesis project addresses (magnifying glass) in relationship to other research done by Philips In-Body Systems and the Dutch Cancer Institute

The results of De Boer and Fleischer are promising for DRS to be able to distinguish between healthy and tumour tissue. However, the main question that arises is whether these two results still have a positive outcome when they are combined. In other words, is it still possible to distinguish between healthy and tumour tissue through a layer of cut or coagulated tissue due to the use of an electrosurgical knife? This question will be answered in this master thesis breaking down the problem into the following sub-questions:

I. What changes in adipose and muscle tissue can be identified when cutting or coagulating with an electrosurgical knife at various settings?

a. What is the size of the cut when using an electrosurgical knife to cut and coagulate?

b. What is the size and shape of the coagulated tissue zone when using an electrosurgical knife to coagulate?

c. How does electrosurgical cutting affect DR spectra?

d. How does electrosurgical coagulation affect DR spectra?

II. Is it possible to observe the transition from healthy to tumour tissue in the DR spectrum when no electrosurgical cutting is used?

a. What are the characteristics in the DR spectra of pure adipose tissue?
b. What are the characteristics in DR spectra for pure muscle tissue?
c. It is possible to see the transition in DR spectra from adipose to muscle tissue without any electrosurgical influence?
d. How does the fiber distance of the probe influence the spectra?
e. Can chromophore concentrations provide a means to quantify the distinction between adipose and muscle tissue?

III. Is it possible to observe the transition from healthy to tumour tissue in the DR spectrum during cutting with an electrosurgical knife?

a. What are the characteristics of cut adipose tissue in the DR?
b. What are the characteristics of cut muscle tissue in DR spectra?
c. It is possible to see the transition in DR spectra from cut adipose to muscle tissue?
d. It is possible to see the transition in DR spectra from adipose to muscle while cutting?
e. Can chromophore concentrations provide a means to quantify the distinction between adipose and muscle tissue while cutting?

1.3. Thesis outline

This thesis consist of seven Sections, as can be seen in Figure 3. All Sections are visualized by a grey box and a box with a blue border refers to a Chapter. The first Section contains the theoretical part including the first three chapters about breast cancer, spectroscopy and electro surgery. The second Section describes the observations made during multiple Breast Conserving Surgeries (BCS). In addition, pictures obtained by the pathologist are discussed. Section II starts with Chapter 5, describing the steps of a BCS. Followed by Chapter 6, explaining the use of the electrosurgical knife in practice. It ends with describing the pathology of an ablated breast tumour in Chapter 7.

To answer the research question of this thesis, experiments are performed. All experiments are described in Section III. The influence of electro surgery on tissue is described in Chapter 8. In Chapter 9, experiments are performed where the transition from muscle to adipose tissue can be observed in DR spectra. In addition, the influence of a change in fiber distance is discussed. Chapter 10 and 11 will bring the experiments in a more clinical setting by measuring DR spectra on cut tissue and measuring DR spectra while cutting respectively.

Section IV, validates the performed experiments by a Monte Carlo simulation. In addition, some theoretical background is given on Monte Carlo simulations. Section V contains some small experiments on the influences of variables that will change when the experiments will be performed in clinical setting.

Finally, Section VI and VII cover the overall discussion and the conclusion and recommendation. These Sections will discuss the results of the experiments and give a conclusion on the research questions described in the introduction. An evaluation of the smart electrosurgical knife is then complete.

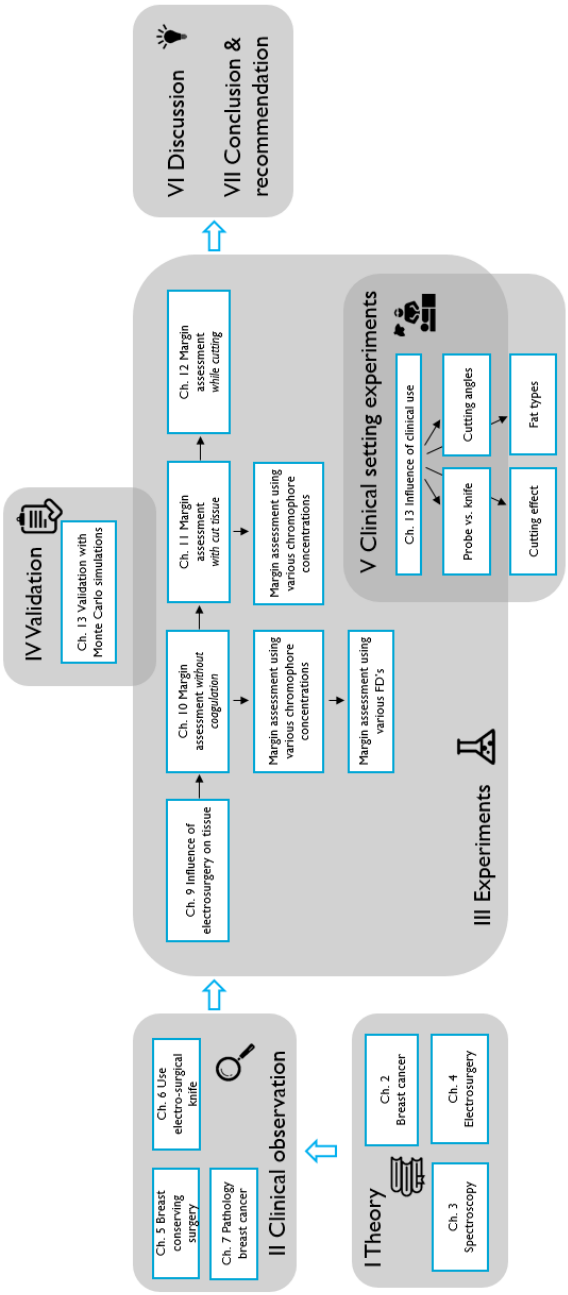

Figure 3: Visual overview of the outline of this master thesis.

I

Theory

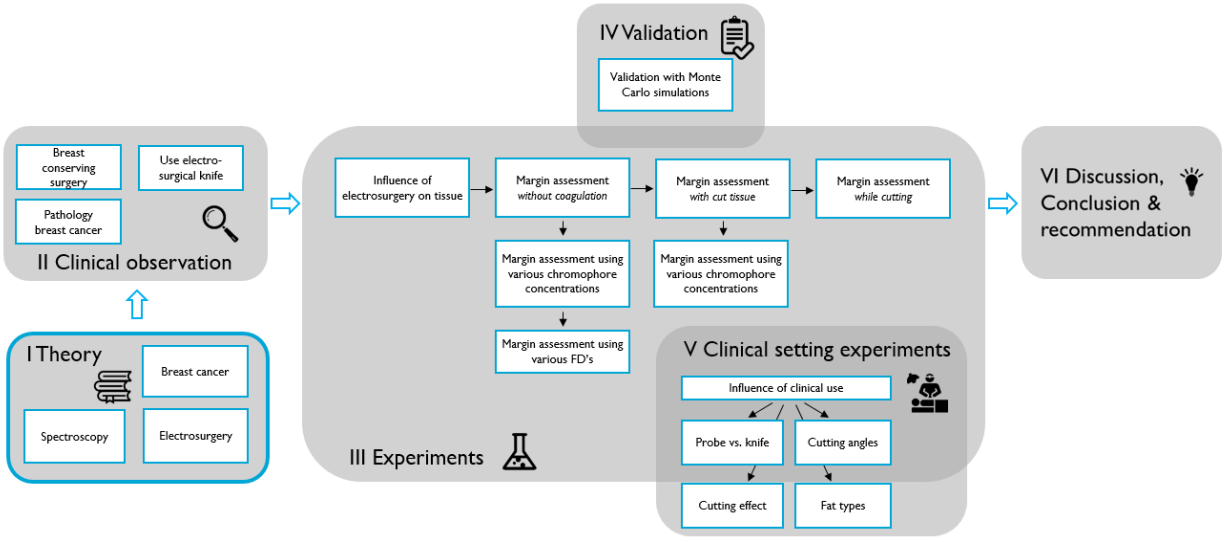
IV Validation
Validation with Monte Carlo simulations
Breast conserving surgery
Use electro-surgical knife
Pathology breast cancer
II Clinical observation
Influence of electrosurgery on tissue
Margin assessment without coagulation
Margin assessment with cut tissue
Margin assessment while cutting
Margin assessment using various chromophore concentrations
Margin assessment using various chromophore concentrations
Margin assessment using various FD's
III Experiments
V Clinical setting experiments
Influence of clinical use
Probe vs. knife
Cutting angles
Cutting effect
Fat types
VI Discussion, Conclusion & recommendation
I Theory
Breast cancer
Spectroscopy
Electrosurgery

2. Breast cancer

Breast cancer is the most common cancer for woman worldwide. [27] It affects woman of all ages and the lifetime risk of developing invasive breast cancer – where the cancer cells spread further then their origin – is 12 to13%. In the United States of America, 0.25 million woman are diagnosed with breast cancer every year. [28] The rate of survival after 5 years is high (89%) for breast cancer, compared to other cancer types. [29] In general, this cancer type is diagnosed in a relatively early stage. The most common symptom of breast cancer is a lump or mass in the breast. However, thickening, swelling, distorting, tenderness, skin irritation, redness, nipple abnormalities or spontaneous discharge can also be symptoms of breast cancer. [30] More statistical information about breast cancer – and a comparison to other types of cancer – can be found in the previously performed literature study. [29]

2.1. Pathology

Breast cancer is the collective noun of 20 subtypes of cancer in the breast. The two main overarching groups are carcinomas and sarcomas. Carcinomas arise from the structural and functional units of the breast, the lobes and ducts. These origins can be seen in Figure 4 for both normal as abnormal tumour cells. Sarcomas arise from the stromal components of the breast (i.e. the connective tissue). However, sarcomas account for less than 1% of all primary breast cancers and are therefore rare.

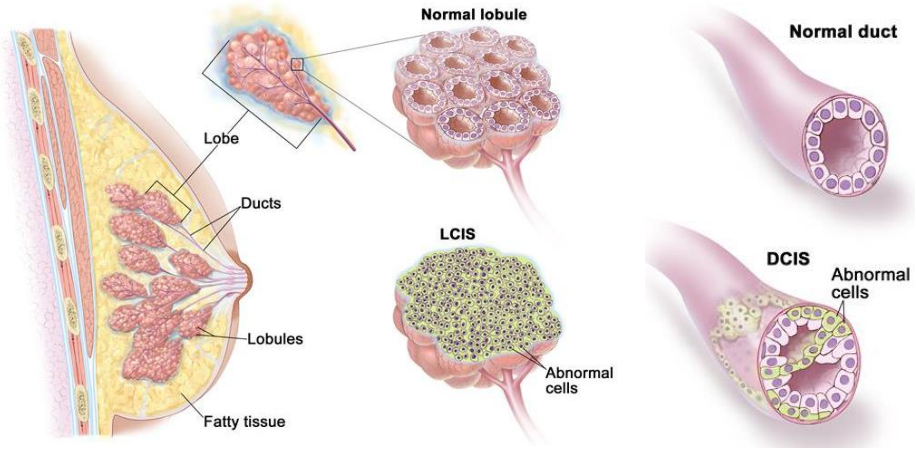

Figure 4: A breast with lobes, ducts, lobules and fatty tissue on the left. In the middle, normal and LCIS infected lobules. On the right, normal and DCIS infected ducts. [2]

Carcinomas can be divided into in situ lesions and invasive lesions. Both can be seen in a microscopic view in Figure 5. In situ carcinomas are also called pre-invasive lesions: the malignant cells are still enclosed in the ductal or lobular tree of the breast. The membrane surrounding the ducts and lobules has not (yet) been penetrated by cancer cells. This can be seen in Figure 5 (left) by the clear border that encapsulates the cancer nuclei. In situ carcinomas can become invasive carcinomas when the cancer cells infiltrate the

outside of the lobules and/or ducts and grow into the connective tissue. In Figure 5 (right), the infected connective tissue can be seen.

In situ carcinomas can be further subdivided into ductal carcinoma in situ (DCIS) and lobular carcinoma in situ (LCIS). The distinction between DCIS and LCIS is made on the architectural and cytological features of the cells. They differ in distribution and their risk at a bilateral disease. [3]

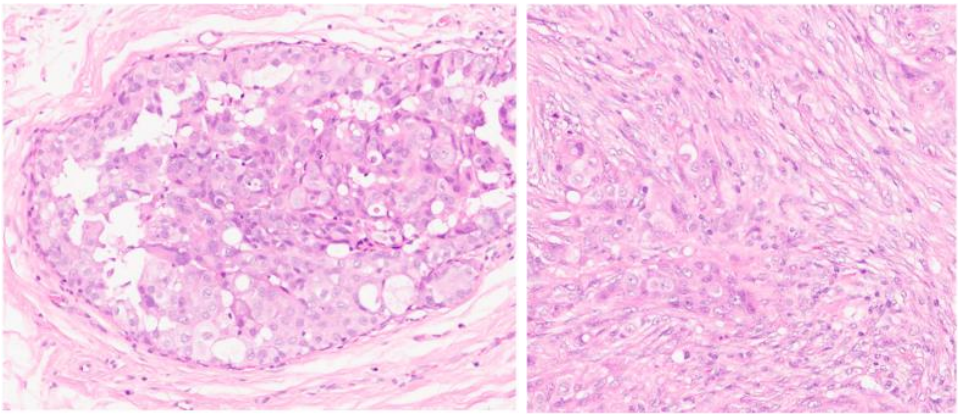

Figure 5: Ductal carcinoma in situ, DCIS (left) and invasive lobular carcinoma (right). Both are obtained by the Netherlands Cancer Institute from a dissected breast tumour by a microscopic view of 20x and later magnified 20x digitally.

2.2. Treatments

There are two types of treatment available for breast cancer namely mastectomy and breast-conserving surgery (BCS). The latter is also called partial mastectomy or lumpectomy. [31] BCS refers to the surgical removal of the breast tumour, instead of removing the whole breast. This treatment is in all cases followed by radiotherapy to eliminate the residual tumour cells. Woman diagnosed at a young age or with aggressive or multiple tumours are more likely to be treated with mastectomy. [27] The main advantage of BCS over mastectomy is preservation of the breast with improved cosmetic outcomes. [28]

The cancer stage at diagnosis is an important factor for the type of treatment a patient receives. In 2014, 61% of the woman with a breast tumour were diagnosed in stage I or II, 32% in stage III and 5% in stage IV. The remaining 2% lacks in histologic information to discriminate between stages. In Figure 6, the percentage of prescribed treatment for different breast cancer stages (I, II, III and IV) can be seen. BCS is the prescribed treatment for 61% of the patients with stage I or II, this number declines to 21% for stage III and to 7% for stage IV. [27] Mastectomy is prescribed for 19% of the patients diagnosed with stage I or II, 72% for stage III and 15% for stage IV. When BCS is combined with radiotherapy, it is found to be as effective as mastectomy. [31] [32] This master evaluates the feasibility of a 'smart' electrosurgical knife to assess tumour margins in BCS. Therefore, the focus will be on BCS instead of mastectomy.

The survival rate of breast cancer depends on the cancer stage at diagnosis, hormone receptor status, human epidermal growth factor receptor 2 (HER2) status and the tumour grade and histology. These survival rates are 89% for 5-year, 83% for 10-year and 78% for 15-year.

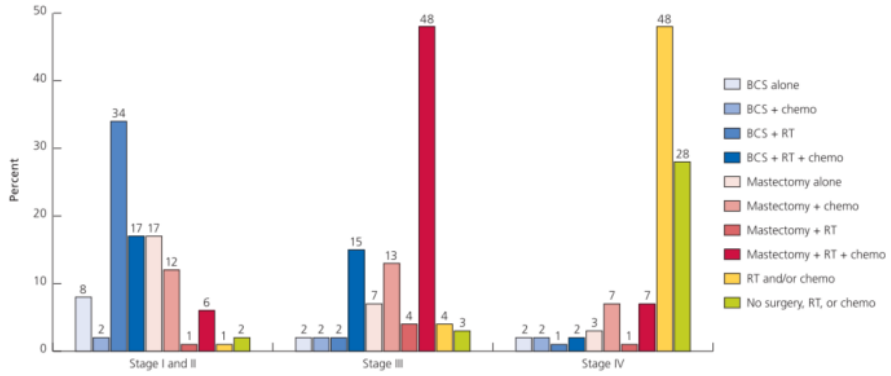

Figure 6: Female breast cancer treatment patterns (%) by cancer stage, 2013. [27]

Complications

Incorrect margin assessment is the most occurring complication in BCS. Some articles report nerve injuries after the clearance of axillary lymph nodes for breast cancer. [33] No other significant complications are mentioned in literature to the best of my knowledge. However, after breast cancer treatment 25% to 60% of the woman develop chronic pain. Other adverse side effects of BCS include numbness, tingling, or tightness in the chest wall, arms, or shoulders. In addition, psychological side effects can occur, including psychological distress (30%), fear of disease recurrence, concerns about future health and interruption of life plans often lead to anxiety and depression. [28]

2.3. Margin assessment

Surgery is the most important, effective and widely used treatment modality by curing approximately 45% of all patients with solid tumours. [4] [5] [6] However, a major problem in surgical treatment remains the difficulty to remove the complete tumour, leaving behind tumour-positive margins (see Figure 1, right), metastatic lymph nodes, and/or satellite tumour nodules. [4] The primary aim of margin assessment during a BCS is to achieve a tumour free resection and thereby prevent local reoccurrence of the tumour. This is called 'margin with clearances' or a negative margin, where the dissected tumour is completely surrounded by a healthy tissue layer of >2 mm thickness, see the left of Figure 1. [7] [8] Statistical data indicates that complete resection is the single most important predictor of patient survival for almost all solid tumours. [4] [9] [10] After a BSC, 20% to 55% of all patients requires a second surgical procedure to clear positive margins. [11] [12]. The secondary aim of BSC is a satisfactory cosmetic outcome. [7] To achieve both aims, a guideline during surgery is a resection margin of 5 to 10mm. However, a size of the tumour-free resection margin >1mm is unrelated to local recurrence. Therefore, there is no need to excise a tumour with a large volume of adjacent breast tissue. [28]

A study of Krekel et al. demonstrated an excessive volume of breast tissue is excised in the majority of patients during routine breast-conserving surgery. [28] For this study, 726 underwent a BCS of which the excised specimen was calculated using histopathological reports. For 33.6% of the patients, the excised volume was >85cm^3, which reduces the cosmetic outcome. However, 98.8% of these patients had a margin >10mm. In fact, for 54.9% an excised volume of 33.51 cm^3 would have been sufficient. In most cases, the tumour was located non-central and close to the nearest margin. The study showed a

higher rate for positive margins in palpable tumours (22.5%) compared to non-palpable tumours (17.4%). [28]

Cosmetic results after BCS are satisfactory for 60 to 80% of the patients. Besides the volume of the resected breast tissue, also the amount of radiotherapy, the site of the tumour in the breast, the type of incision and postoperative complications influence the cosmetic outcome. However, the – large – volume of the resected breast tissue is the major determinant of a poor cosmetic outcome. Volumes >85cm^3 result in a 50% rate of cosmetic failures, whereas <85cm^3 result in only a 22% rate of cosmetic failures. [28]

Instruments to assess tumour margins

In general, there are four methods available for margin assessment during a BCS: using a gamma probe, a guidewire, imaging techniques or palpation and visual information. All can be seen in Figure 7. A more comprehensive explanation about these methods can be found in the master thesis of Julie Fleischer. [2]

When using a gamma probe, small ion seeds are placed in – or as close as possible by – the tumour prior to the surgical procedure. This placement is performed using an imaging method where the tumour can be seen. The gamma probe – also known as a Geiger counter – is then used to find the ion seeds during the procedure by listening to the counting of the gamma probe. The audio signal accelerates in counts when the probe is closer to the ion seed.

A guidewire is another technique used for margin assessment. For this technique, a wire is placed inside the tumour a priori to the procedure using an imaging method to provide guidance. This wire reaches from the tumour to the outside of the patients' breast. During the procedure, the surgeon can follow this wire to the tumour and dissect the tumour at the end of the wire. Marks on the wire provide the surgeon information about the distance to the end of the wire.

In literature, some imaging techniques are mentioned to be used for assessing margins intraoperatively. The most widely used methods to improve the accuracy of tissue clearance in situ are intraoperative imaging modalities being CT, MRI, US and fluorescence-guided surgery. [7] [28] These image-guided surgeries provide the surgeon with new information such as the nature, location and dimensions of the malignant tissue. [34] The effectiveness of cancer detection depends on the minimal spatial resolution of the imaging technique. [8] A difficulty for these methods can be the lack of quantitative data available about the biomechanical properties of soft tissues. This especially accounts for the in vivo characterization of human organs due to high technical and ethical demands on these experiments. When property measurements need to be taken, direct access to the organs is needed which can disturb or prolong a usual surgical procedure. [23]

Palpation and visual information are used during every BCS to decide on the tumours location and it's margins in addition to the techniques mentioned above. However, when a tumour is palpable (i.e. large enough or deviates from the surrounding tissue) it is possible to only use palpation and visual information to assess its margins. Only pre-operative images are used to guide the surgeon to the tumours location. Furthermore, the surgeons' expertise helps him/her to distinguish between healthy and tumour tissue.

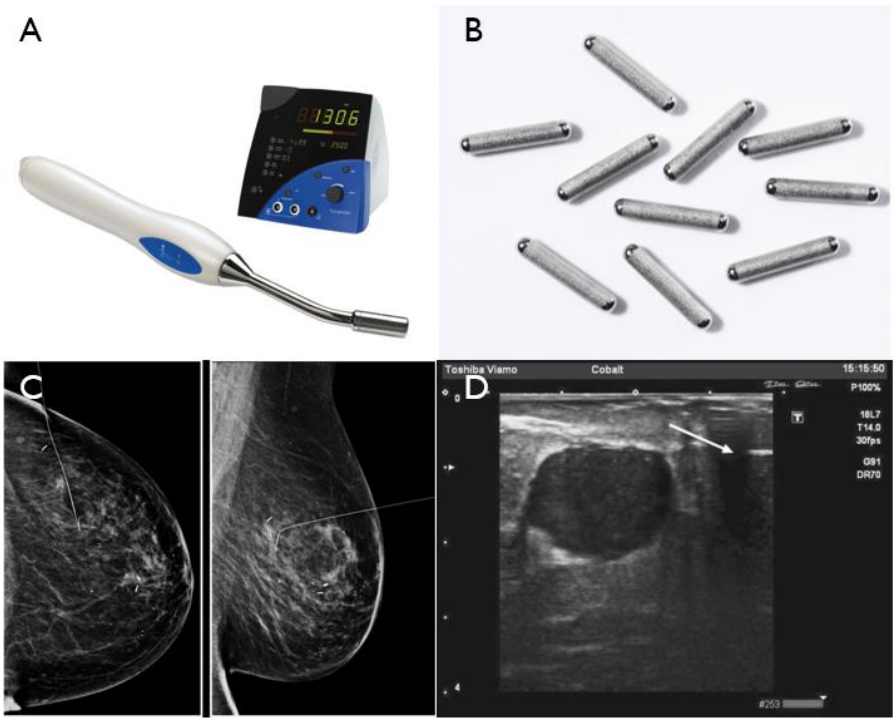

Figure 7: Methods to assess tumour margins in BCS. A: Gamma probe and interface (Medical Expo). B: Iodine seeds which are placed in the breast tumour to guide the resection. The length of one ion seed is 4.5mm. (Eckert & Ziegler) C: Guidewire, a wire is placed in the breast to assist the resection towards the end of the wire where the tumour is situated. D: Breast tumour assessment with Ultrasound. The arrow marks the incision and the dark round shape is the tumour. [28]

2.4. Discussion

The statistical numbers is this chapter indicate the importance of this research. In the United States of America, 0.25 million woman are diagnosed with breast cancer every year. Of these women, 44.2% will receive a BCS as can be seen in Table 1. After surgery, 25% will be advised to have a second surgery due to positive or close margins at the final pathology. This is – only in the United States of America – a group of 27.500 woman needs a second surgery due to positive margins.

Table 1: Percentage of women diagnosed with breast cancer at various stages. The percentage of woman receiving a BCS as treatment per stage. The percentage woman receiving BCS from all patients diagnosed with breast cancer.

Stage	Diagnosed women per stage	Prescription BCS	Percentage of total receiving BSC
I & II	61%	61%	37.2%
III	32%	21%	6.7%
IV	5%	7%	0.3%

The main problem in BSC is the margin assessment, as this fails in 25% of the surgeries. Therefore, the guideline during surgery is a resection margin of 5 to 10mm. However, the study of Krekel reports a margin >10mm for 98.8% of the patients. In addition, the tumour was located non-central and close to the nearest margin in most cases. This indicates – despite the use of localization tools as a guidewire or a

gamma probe – it is difficult to perform a margin assessment. An extra problem is the negative cosmetic outcome for at least 33.6% of the patients in the study of Krekel.

The instruments currently available for localization of the tumour in BCS are the gamma probe, guide wire and imaging techniques. Both gamma probe and guidewire are used often in clinical practice in the Netherlands, according to F.J. van Duijnhoven and A.A. Hellingman both surgeons at The Netherlands Cancer Institute. Both tools are useful for global localization, however it provides a relative distance to the probe. For example, for the gamma probe the count decreases the longer the ion seed is inside the patient. Therefore, there is no threshold on when the surgeon is – for example – 2mm from the tumour. This makes a precise margin assessment impossible. In addition, the surgeon needs to alternate between the probe – to locate the tumour – and the electrosurgical knife to dissect the tissue. Alternating costs time and will make it difficult to return at the exact same spot with the new instrument. Another disadvantage is the possibility of the incorrect placement of the ion seed(s). This will lead the surgeon to the wrong place in the breast. The guidewire, provides – as the gamma probe – a global guidance however, it does not help with assessing the margins of the tumour. In addition, the wire can be placed incorrectly or in a difficult way to follow for the surgeon.

In literature, some imaging techniques used for margin assessment can be found. However, when interviewing the surgeons in The Netherlands Cancer Institute they state these methods are not used for intraoperative margin assessment. Van der Noordaa and Snider confirm this in literature. [35] [36] A disadvantage of using imaging techniques such as ultrasound is a 2D image is provided which needs to be translated to a 3D visualization by the surgeon. The 2D image needs to be 'placed' in the patient's body with the respect to the instrument in order to be useable for the surgeon. In addition, also alternations between the imaging instrument and the electrosurgical knife are needed.

3. Spectroscopy

Spectroscopy is an analysis of the interaction between matter and any portion of the electromagnetic radiation, see Table 2. The interaction between matter and any portion of the electromagnetic radiation can give rise to electronic excitations, (e.g. ultraviolet), molecular vibrations (e.g. infrared) or nuclear spin orientations (e.g. nuclear magnetic resonance). [37] The kind of interaction, or energy transitions, depends on the wavelength and frequency of the radiation. The wavelength (λ) in meters is inversely proportional to the frequency v in Hertz (or s^{-1}) and is governed by the relationship

$$v = \frac{c}{\lambda} \tag{1}$$

where c is the speed of light in meters per second. When energy is absorbed, for example the absorption of infrared radiation, molecules are excited to a higher state. [37]

Table 2: Electromagnetic spectrum showing the wavelength, frequency and energy transitions per radiation type. [38]

Radiation	Wavelength	Frequency	Energy transitions
Gamma rays	< 10^{-3} nm	> 10^{20} Hz	Nuclear transformations in atoms
X-rays	~ 10^{-3} – 10 nm	~ 10^{16} – 10^{20} Hz	Inner electron shell transitions in atoms (bond breaking)
Ultraviolet	~ 10 – 400 nm	~ 10^{16} – 10^{20} Hz	Outer electron shell transformations in atoms
Visible light	380 – 750 nm		
Infrared	~ 750 – 106 nm	~ 10^{11} – 10^{14} Hz	Molecular vibrations
Microwaves (radar)	~ 10^{-3} – 10^{-1} m	~ 10^{9} – 10^{11} Hz	Molecular rotations and electron spin orientation transitions
Radio waves	~ 10^{-1} – 10^{3} m	~ 10^{5} – 10^{9} Hz	Nuclear spin orientation transitions

3.1. Light travel in tissue

When tissue is illuminated, three processes can occur to the outsourced photons: the light can be absorbed, scattered or reflected as can be seen in Figure 8. Light that is reflected from the surface has no effect besides decreasing the amount of light that can interact with the tissue chromophores. Scattering increases the volume of the tissue in which photons of the incident light are distributed. It increases the spot size of the light beam within the tissue and thus decreases the concentration of photons per unit volume tissue. Absorption is the transformation of light energy to another form of energy, mostly heat or vibrations, within the chromophores in the tissue. It decreases the light intensity of the light detected back at the surface of the tissue.

The components, which absorb photons, differ in composition per tissue type, organs, even within tissue types and in time. Water, oxyhemoglobin and de-oxyhemoglobin are the most relevant absorbers of photons in tissue. Blood, saturated with or without oxygen molecules respectively oxyhemoglobin and

de-oxyhemoglobin, is the main absorber in the visual region of the spectrum: 390 to 700 nm, see Figure 9. [39] [40]

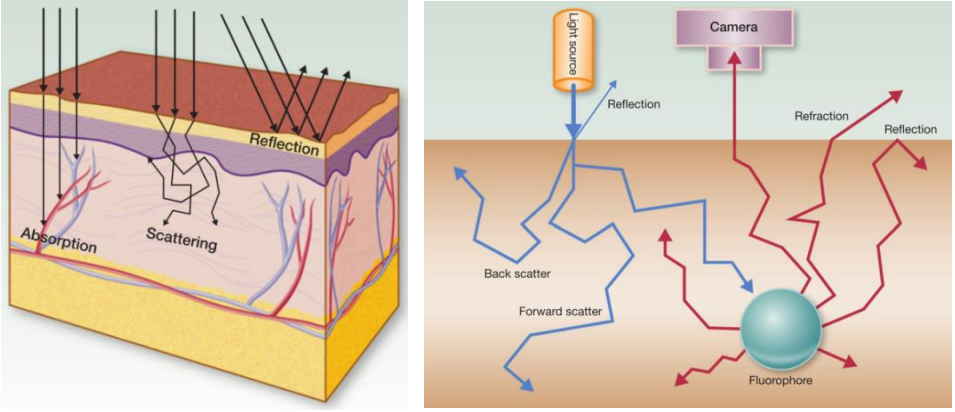

Figure 8: Light propagation through tissue: absorption, (back- and forward) scattering, reflection and refraction. [39]

The process of a photon changing direction inside the tissue is called scattering. Forward scattering is when a photon travels more or less in the same direction, while backscattering refers to a photon travelling in opposite direction of which it started. [39] In addition, reflection and/or refraction can occur in tissue. When there is a mismatch between the indices of refraction of tissue and air, the direction of the photon will change causing reflection at the surface. This same effect can occur inside the tissue where the light can be reflected or refracted in phase transitions. [39]

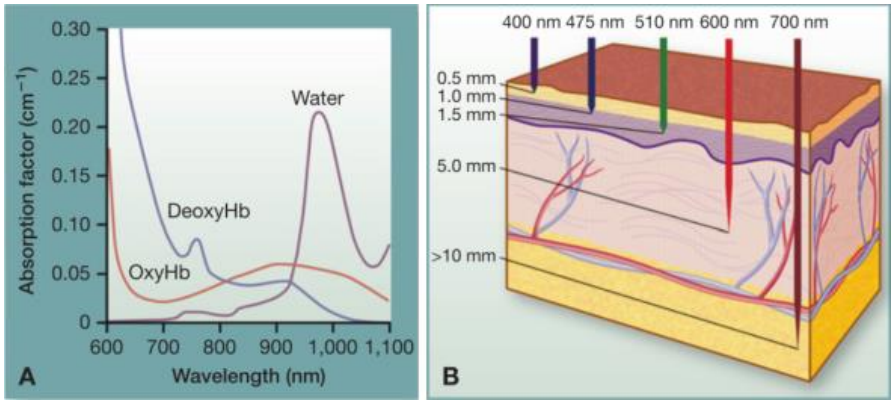

Figure 9: Light absorption. a) Absorption factor per wavelength for water, oxyHb and deoxyHb. b) Penetration depth per wavelength. [49]

3.2. Data acquisition

Spectral imaging datasets generally consist of two spatial dimensions (axial and lateral, x and y) and one wavelength dimension (λ) to make up a three-dimensional dataset shown in Figure 10. This spectral data is acquired at every pixel in the image with a minimum of three different spectral bands. In addition to regular spectral imaging, multispectral and hyperspectral analysis can be performed. The number of

collected spectral bands in hyperspectral imaging is higher than in multispectral imaging, as can be seen in Figure 11. Furthermore, the spectral bands are spaced close together, which makes it possible to construct an optical spectrum from the data. This is not possible for multispectral imaging.

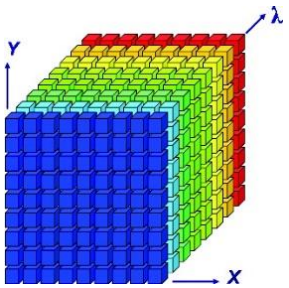

Figure 10: Diagrammatic representation of spectral image data consisting of two spatial dimensions (x, y) and one spectral dimension (λ). [41]

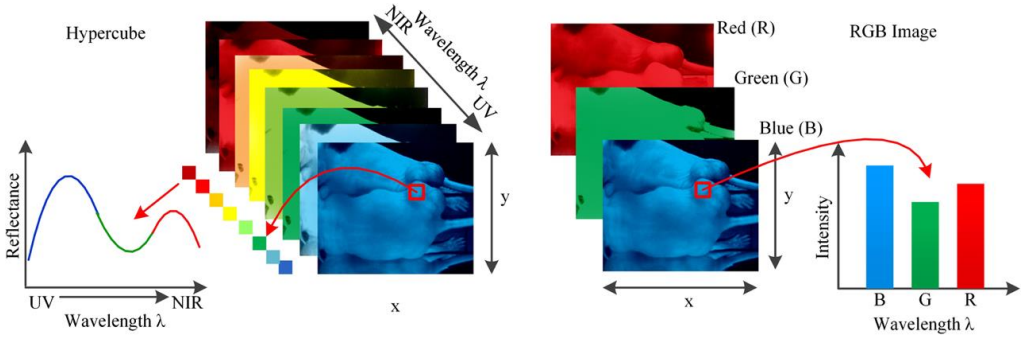

Figure 11: Left: hyperspectral imaging. Right: multispectral imaging. [42]

The most valuable strength of spectral imaging methods is the rapid delivery and collection of light via optical fibers. [25] The acquired data can present specific quantitative biochemical and morphological information of the examined tissues. [8] [12]

The main limitation of spectral imaging methods is the reduced contrast, spatial resolution and penetration depth due to strong scattering of light in biological tissues and blood. [43] However, when the device is used in situ, the light probe can be brought adjacent to the tissue, which makes it feasible to illuminate lesions and detect them. [4]

3.3. Tissue characterization

In this paragraph the notation of Stephan L. Jacques is followed. [44] Optical techniques are dependent of the spectral, angular and polarization characteristics of light scattered from the tissue. These characteristics are used as biomarkers for specific medical applications: identifying tissue types, diagnosing diseased tissues and discriminating between malignant and healthy tissues. Discrimination between cancerous and healthy tissue is possible while scattering and absorption are highly dependent on the

morphological and physiological state of the tissue. [45] The ability of light to penetrate a tissue and later escape it for detection is key to diagnostic applications. [44]

In general, tissue properties relevant for optical imaging are: the absorption coefficient, μ_a [cm^{-1}], the scattering coefficient μ_s [cm^{-1}], the scattering function $p(\theta,\psi)$ [sr^{-1}] where θ is the deflection angle of scatter and ψ is the azimuthal angle of scatter, and the real refractive index of the tissue, n'. As can be seen below, the scattering coefficient is related to the reduced scattering coefficient $\mu_s{}'$. This also holds for the anisotropy coefficient g. The scattering function is related to the anisotropy. [44]

Absorption	μ_a	[cm^{-1}]
Scattering	μ_s	[cm^{-1}]
Scattering function	$p(\theta,\psi)$	[sr^{-1}]
Anisotropy	$g =< \cos(\theta) >$	[-]
Real refractive index	n'	[-]
Reduced scattering	$\mu_s' = \mu_s(1-g)$	[cm^{-1}]

Jacques presents these formulas to be able to generate optical properties from tissues at any wavelength in the ultraviolet, VIS and NIR range, based on the amount of absorbing chromophores. [44] It is important to take into consideration that the known optical properties of tissues *in vivo* are not always accurate while variations can occur in blood content, water content, collagen content and fiber development. These variations can occur, not only between persons, but also within the same person at different sites. [44] A more elaborate description of the variables can be found in Appendix A.

Absorption coefficient

The absorption coefficient μ_a – which will be used to characterize tissues in the experiments – is described by T. T is the transmitted or surviving fraction of the incident light after the incremental path length ∂L [cm]. In addition, ∂T/T per ∂L yields an exponential decrease in the intensity of the light as a function of increasing path length L. The relation between μ_a and T is given by

$$\mu_a = -\frac{1}{T}\frac{\partial T}{\partial L} \tag{2}$$

where T can be described as

$$T = e^{-\mu_a L} = 10^{-\varepsilon C L} = e^{-4\pi n'' L/\lambda}\,. \tag{3}$$

In Equation (3), C is the concentration [mole L^{-1}] and ε is the extinction coefficient [cm^{-1} $mole^{-1}$] for the chromophore. The absorption coefficient μ_a of the tissue is the sum of all absorbing chromophores within the tissue. The individual absorption coefficient for each chromophore is proportional to the extinction coefficient multiplied by the chromophore concentration. The absorption coefficient of the tissue is described by

$$\mu_a = \ln(10) \sum_i C_i \varepsilon_i \,. \tag{4}$$

An example of this formula would be [46]

$$\mu_a = [blood]\, {\mu_a}^{blood}(\lambda) + [water]{\mu_a}^{water}(\lambda) + [fat]{\mu_a}^{fat}(\lambda) \tag{5}$$

In Figure 12, the build-up of a spectrum using Equation (5) can be seen. The absorption coefficient (μ_a) per wavelength is used to construct the spectrum obtained by DR measurements. Left, the spectra of all chromophores present in the measured tissue are combined regarding to their presence. The more chromophore of a type are present, the more this spectrum will dominate the total spectrum. Right, the chromophores present in the measured tissue can be seen separately. All chromophores have their own characteristic peaks and dips at specific wavelengths whereby they can be recognized. Fat – for example – has a characteristic peak between 1200 and 1400nm.

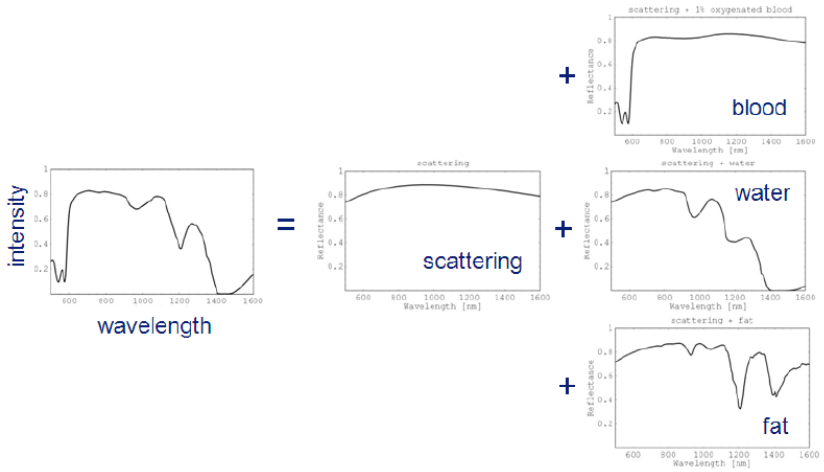

Figure 12: Composition of the measured spectrum from scattering processes and the absorption by chromophores [46]

3.4. Diffuse reflectance spectroscopy (DRS)

DRS is a spectroscopic technique to characterize tissue. Via a fiber optic probe, a broadband light source is send to the tissue where it interacts with chromophores by (single or multiple) scattering or absorption. [8] [47] [48] The scattered light that is detected at the tissue surface is gathered as a function of the wavelength. The detected light holds information on the absorption and scattering coefficients of the tissue. [48] Using mathematical models, information about the concentration and variation of chromophores, the nuclear size, morphology and structure of the scatters or components present in tissue can be extracted. Examples of these components are lipid membrane and collagen fibers. [47] [48] In addition, the absorption coefficient of each molecule can relate directly to the concentration of its absorber in the tissue. [8] This method requires two extra measurements: calibration of the wavelength scale and correction for transmission and reflection losses. [12] [49]

During the development of pre-cancers, the characteristics of the diffuse reflected light change due to biochemical and morphological changes in the tissue. There is a growth of the chromatin concentration, nuclear size and shape, nuclear to cytoplasmic ratio, and metabolic activity. [50] Due to these developments, cancerous tissue can be identified using DRS. [48]

DR spectra are described by the light travelling inside a light-scattering specimen. Kubelka and Munk [51] made a model for this description based on the equations

$$-\mathrm{d}i = -(S+K)i\mathrm{d}x + Sj\mathrm{d}x \tag{6}$$

and

$$\mathrm{d}j = -(S+K)j\mathrm{d}x + Si\mathrm{d}x \tag{7}$$

where i is the intensity of the light traveling inside the sample towards the un-illuminated surface, j towards the illuminated surface, $\mathrm{d}x$ the differential segment along the light path, S the K-M scattering coefficient and K the absorption coefficient.

These equations are applicable when the particle size is comparable to, or smaller than the wavelength of the incident light, and the diffuse reflection no longer allows to separate the contributions of the reflection, refraction, and diffraction (i.e. scattering occurs). [52]

3.4.1. Fitting the spectrum with PNSas

In this thesis, the DRS measurements are performed using a probe, which consists of optical fibers. The probe has one detecting fiber and – at least – one fiber emitting light via a console. The detecting fiber collects light for every wavelength in the VIS and NIR region and stiches it together to construct a raw spectrum from 400nm to 1600nm. This setup can be seen in Figure 13.

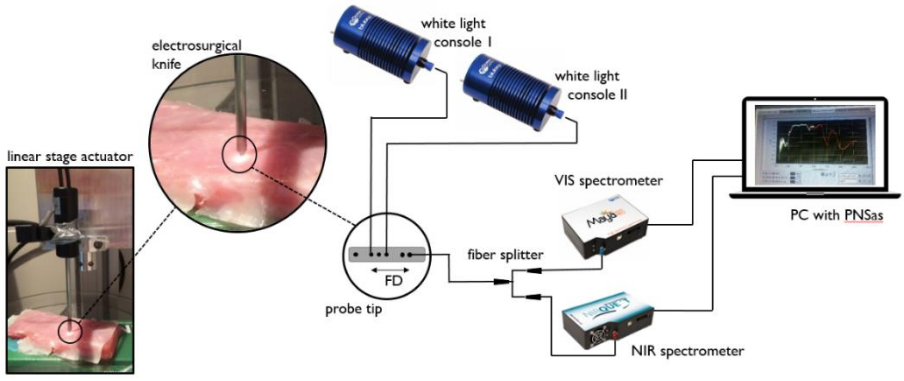

Figure 13: Experimental setup including a linear stage actuator, a probe, white light, VIS spectrometer, NIR spectrometer and a PC including PNSas software.

PhotonicNeedle software (PNSas) is a program designed by Philips Research to estimate concentrations of physiological parameters in scattering media such as biological tissue. The input of the model is a (measured) raw spectra and an excel file and the outputs are an excel document with the chromophore concentrations, a fit of the measurement and a plot of the measurement and the fit, as can be seen in Figure 14.

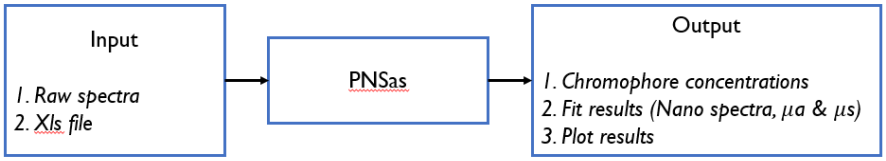

Figure 14: Visual representation of the input and output of PhotonicNeedle software, made at Philips In-Body Systems

The output of the PNSas – PhotonicNeedle software PNSas – model is constructed using a model developed by Farrell [53]. This model describes a system as in Figure 8, where two fibers are in contact with the tissue. One fiber emits light and the other detects the light. The light diffusion theory is used to translate the measured spectrum into physiological parameters and scattering properties. Light diffusion in tissue is determined by the scattering- (μ_s) and absorption coefficient (μ_a), which are described in Appendix A. The determination of the measured spectrum by the absorption of chromophores and scattering processed in tissue has a non-linear relationship. Farrell expresses the measured diffuse reflectance intensity distribution $I(r)$ like this

$$I(r) = \alpha \frac{a'}{4\pi}\left[\frac{1}{\mu_t'}\left(\mu_{eff} + \frac{1}{\tilde{r}_1}\right)\frac{e^{-\mu_{eff}\tilde{r}_1}}{\tilde{r}_1^{\,2}} + \left(\frac{1}{\mu_t'} + 2z_b\right)\left(\mu_{eff} + \frac{1}{\tilde{r}_2}\right)\frac{e^{-\mu_{eff}\tilde{r}_2}}{\tilde{r}_2^{\,2}}\right]. \quad (8)$$

The definition of all variables used in Equation (8) can be found in Appendix B. The accuracy of the fit to the measured spectrum is influenced by some assumptions made in the model. The assumptions are:

- The fluence due to highly forward directed scattering can be set equal to the fluence due to isotropic scattering, as the set of parameters are changed from (μ_s, g) to $(\mu_s(1-g), 0)$. When using the similarity principle [53] as described by Farrell, the outcome of the light scattering depends only on $\mu_s' = \mu_s(1-g)$ and μ_a.
- The diffuse approximation used is correct as long as the absorption is small compared to the scattering and as the mean free path, length is small compared to the source-detector distance.
- The details regarding emission distribution and collection distribution of the fibers is excluded in this model when the pencil beam is described as a single scatter source.

The reduced scattering coefficient is modelled as following,

$$\mu_s'(\lambda) = s_{800}\left[f_{mie}\left(\frac{\lambda}{\lambda_0}\right)^{-b} + (1-f_{mie})\left(\frac{\lambda}{\lambda_0}\right)^{-4}\right]. \quad (9)$$

The scattering coefficients – which can also be extracted from the model – are: s_{800}, the reduced scattering amplitude at λ_0, b is the Mie scattering slope and f_{mie} the Mie-to-total reduced scattering fraction assuming Mie and Rayleigh scattering as the two scattering regimes present for elastic scattering. Elastic scattering is scattering when a photon changes direction but maintains its energy as opposed to inelastic scattering when some energy is lost. λ_0 is set to 800nm and corresponds to a wavelength normalization value. In Equation (8), α describes the light intensity at the delivery fiber. This variable is also considered a scattering coefficient.

Other chromophores – used in this thesis – that can be extracted from the model are: blood, water haemoglobin saturation by oxygen (StO_2), beta-carotene (b) and fraction of lipid in water plus lipid content ($l/(w+l)$). In addition collagen, methaemoglobin, histopathological ink, R(um), bilirubin, bile, collagen, Pp9(uM), Catalase, CytoCOxi and CytoCRedu can be extracted. The characteristic DR spectrum of all scattering coefficients and chromophores can be seen in Figure 15.

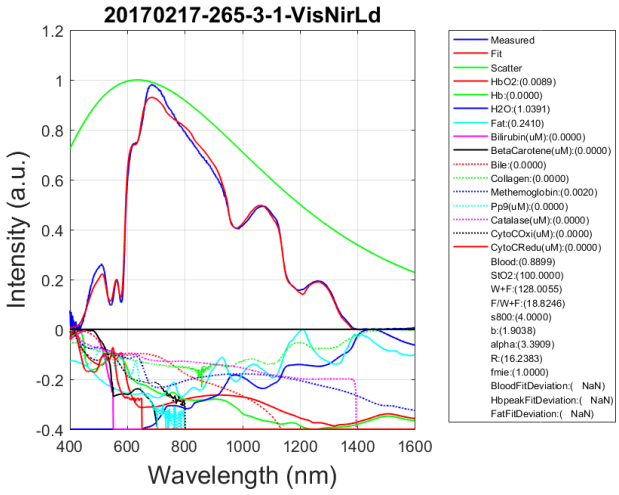

Figure 15: Measured spectra (blue) and fitted spectra (red) of DR measurement. The fitted spectra is built up of characteristic spectra for various chromophores, shown mirrored downwards.

3.4.2. Sensing depth

When measuring the DR spectra of tissue, the sensing depth is of importance while this will influence the spectrum if the tissue contains of more than one layer. A previous study at Philips Research concerning the sensing depth of a probe with two fibers in a two layer model gave this function [54]

$$f = A_2 + \frac{A_1 - A_2}{1 + \exp\frac{x - x_0}{dx}} \tag{10}$$

Where f is the fat fraction, A_1 and A_2 are the fat amounts of the top and bottom layer respectively, x is the position of the optical probe and x_0 is the interface of the two layers. dx is a parameter directly related to the fiber distance. This model was used to successfully describe the fat percentage at various distances while moving through two layers: a layer of mayonnaise (70% fat) on top of a layer of solid fat (35% fat). Figure 16 presents the measured data in blue dots – including the variance in red bars – and Equation (10) plotted in black.

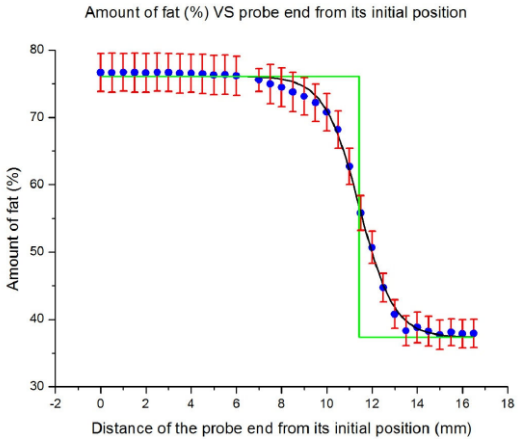

Figure 16: The amount of fat (%) as a function of the distance of the optical probe from its initial position. The estimated amount of fat (the blue dots) is forming an S-curve. The red bars represent the variance of the fitted values derived from the calculation from the calculation of the confidence interval. [54]

3.5. Discussion

In my literature study, DRS is compared to other techniques that could potentially be used for margin assessment intraoperative in real-time. Compared to fluorescence and Raman Spectroscopy, DRS will give less detailed information about the tissue. However, the data is easier and faster to obtain for DRS compared to the other two methods. [25] [52] [55] According to experiments, Haka et al. conclude the detail level of DRS is specific enough to discriminate between healthy and cancerous tissue. [12] In addition, DRS is a minimally (or non-) invasive and non-destructive to the tissue. By altering the fiber geometry, wavelength range and source-detector-separation, the technique can be fine-tuned for a particular clinical use. [47] According to a review by Budlon et al. malignant and healthy surround tissues can be distinguished based on the difference in blood oxygenation. [47]

Disadvantages of DRS are the small penetration depth of <1mm [56] and the fact that the surrounding light can affect the signal recorded from the detector.

The sensing depth – described by Philips research [54] – reports a depth of approximately half of the fiber distance (FD) of the probe. It is assumed, the sensing zone of a probe containing two fibers has a banana-like zone. In Figure 17 (left), a visualization of the sensing depth for different FD's is made. A larger FD will increase the sensing depth.

In addition, Figure 17 (right) shows the sensing zone of a probe on a two-layered tissue. When the thickness of the layer changes, the percentage of sensed tissue for that layer will change. Formula (10) describes this change in chromophore percentage. The experiments in Chapter 9, 10 and 11 will simulate a situation similar Figure 16. Therefore, it is expected the transitions in chromophore concentrations in Chapter 9, 10 and 11 will follow the same S-curve as for Equation (10). This only holds for tissue layers with a difference in the chromophore concentration which is calculated.

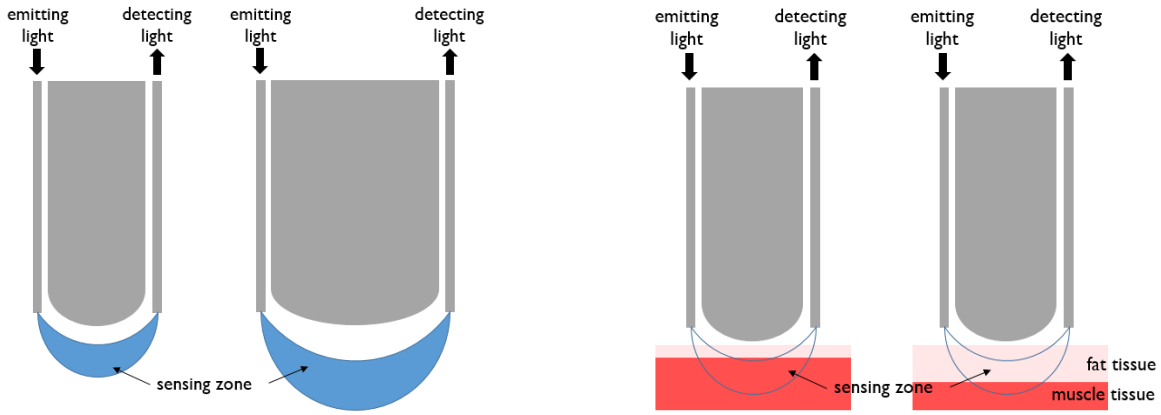

Figure 17: Sensing depth of a probe containing two fibers. Left: A larger fiber distance will increase the sensing depth. Right: the sensing zone when the sensed tissue changes.

It is important to notice, the fitted spectra – as can be seen in Figure 15 – will be used in this thesis as result of the measurements. However, all spectra need to be examined on their fit hence a wrong fit is not included into the results. In addition, all spectra are normalized by setting the maximum value at one. This is done while the intensity of the spectrum is relative.

4. Electro surgery

Electro surgery is widely used across all surgical specialties. [57] It accounts for 80% of all cutting and coagulation in surgeries performed today. [58] Weiser estimates a global volume of 234.2 million major surgical procedures using electro surgery every year worldwide. According to the World Health Organization, electro surgery is commonly used in dermatological, gynaecological, cardiac, plastic, ocular, spine, ENT, maxillofacial, orthopaedic, urological and neurological surgical procedures as well as certain dental procedures. [59] A more extensive explanation about electro surgery can be found in my literature study. [29]

4.1. Basic principles of electro surgery

To be able to understand the mechanism of electro surgery, some basic physical principles need to be introduced. These principles will be explained based on Equation 1.1. The current (I) is the flow of an electric charge. This electric charge flows through the wire in one direction: from negative to positive. Current (I) is expressed in amperes (A) expressing the electric charge in Coulomb ($6.24 \cdot 10^{18}$ charge carriers) per second. The voltage (V) is the difference in electrical potential between two points in the circuit which is measured in volts. The greater the voltage, the greater the flow of electrical current. The last component in the equation is resistance (R) which determines how much current will flow through a component. Resistance is expressed in Ohm (Ω) for a direct current, for an alternating current this concept is called impedance. [60] The relation is given by [57] :

$$I = \frac{V}{R} \tag{11}$$

Heat is produced when electrons encounter resistance when moving from one atom to a neighbouring atom. Electrical current flow can only exist when there is a continuous circuit. An electrical circuit requires a positive and a negative pole to ensure a flow of ions and/or electrons. [61] In the operating room, the circuit consists of the patient, the electrosurgical generator, the active electrode and the return electrodes, as shown in Figure 18. [60] [57] The electrical energy is converted into tissue heating when the tissue resists the flow or part of the flow of current from the electrode.

4.2. Electrosurgical modalities

Electro surgery – sometimes called electrocautery – is a technology that almost all surgical specialties have adopted. [62] [63] It achieves haemostasis – destruction and division of tissue – which limits blood loss in comparison to a 'normal' or 'cold' knife. [63] [60] The different thermal effects on tissue are shown in Table 3.

Table 3: Thermal effects of electro surgery on biological tissue at various temperatures. [64]

Applied temperature	Thermal effects of electro surgery on tissue
37 - 40	None
> 40	Hyperthermia: initial tissue damage, edema formation, depending on the duration of application, the tissue can recover or die (devitalization)
> 60	Devitalization (destruction) of the cells, shrinkage of the connective tissue through denaturation
100	Vaporization of the tissue fluid, depending on the speed of vaporization: - Tissue shrinkage through desiccation (drying out) - Cutting due to mechanical tearing of the tissue
> 150	Carbonization
> 300	Vaporization (evaporation) of the entire tissue

Monopolar and bipolar electro surgery

Electro surgery is most commonly used monopolar, which means a single electrode is used and the circuit is closed through a dispersive pad, or ground pad placed on the patient, as shown in Figure 18. The electrical current passes through the body of the patient. When electro surgery is used bipolar, the current only passes between the arms of the forceps as can be seen in Figure 18. [65] Monopolar electro surgery can be used for cutting and coagulation, while bipolar electro surgery is limited to coagulating. Cutting of tissue is also called dissection.

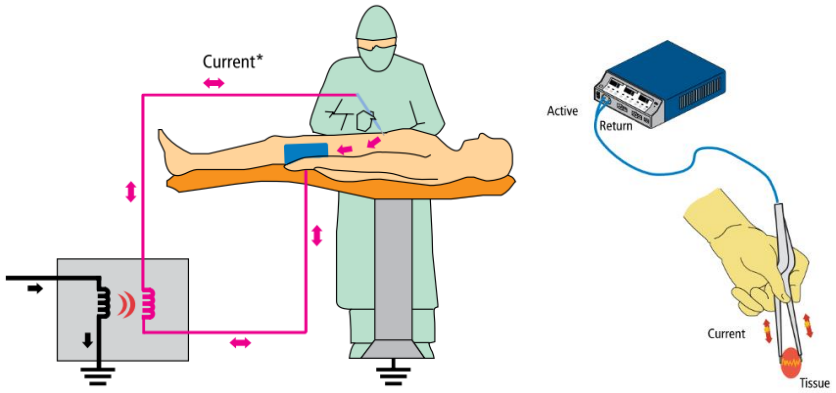

Figure 18: Visual overview of electrical circuit of monopolar (left) and bipolar (right) electro surgery. Monopolar: the current flows from the electrosurgical generator via the active electrode, which the surgeon holds, to the patient. It leaves the body at the return electrode making a continuous circuit going back to the electrosurgical generator. Bipolar: the current flows from the electrosurgical generator to one of the electrosurgical instrument forceps and flows back through the other forceps coagulating the tissue. [66]

Electrosurgical cutting and coagulation

The two types of current used in electro surgery are cutting current and coagulation current. Both use the same frequency of 300 kHz to 5 MHz [67] A frequency above 10 kHz is crucial as the susceptible tissues do not depolarize at frequencies below 10 kHz. This lower bound prevents acute pain, muscle spasms and even cardiac arrests. [61] [63] The electrical waves of coagulation and cutting current are

different, as can be seen in Figure 19. Coagulation current has a high voltage and is interrupted 30,000 times per second while cutting current has a low voltage is a continuous sinusoidal current.

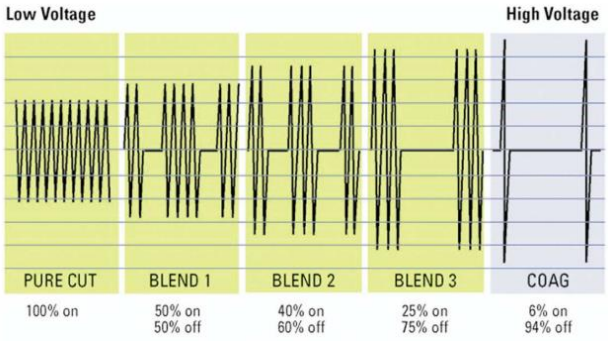

Figure 19: Wave forms of electrosurgical units with different tissue effects. [60] [68]

Different waveforms have a different impact on the tissue. The cutting current quickly heats up individual cells, which first leads to boiling and then causes cell rupture. The off time in a coagulation current allows the cells to cool down when an interruption is present. [62] Another technique is blended cutting where the number of interruptions and the voltage height differ from cutting and coagulation waveforms. This is cutting with some coagulation effect, which produces more extensive charring and neighbouring tissue damage as can be seen in Figure 20. In addition, increasing the voltage will enlarge the thermal spread and charring in the tissue.

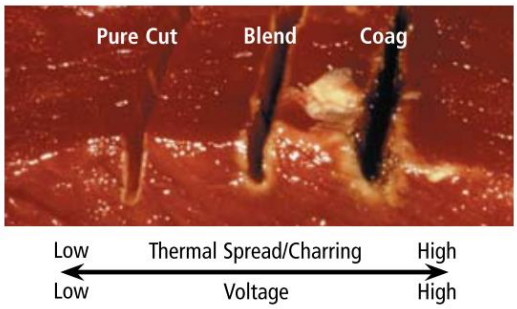

Figure 20: Tissue charring and thermal spread are inversely related to voltage setting. [60] [66]

Coagulation types: fulguration and desiccation

There are two types of electrosurgical coagulation: fulguration and desiccation. For fulguration the current travels across a gap, which is created by holding the electrode lightly above the tissue (2-5 mm), to reach the tissue, as shown in Figure 21. This gap creates an ionized current path while it travels through the air by ionizing nitrogen. The path looks like a miniature lightning strike. When the electrode is held too high (5-10 mm) above the tissue, fulguration may produce a coagulum of charred blood over the tissue which can leave bleeding tissue underneath the coagulum. In desiccation, a zone of coagulated tissue is produced by having direct contact with the tissue as shown in Figure 21. [62] Fulguration can only coagulate tissue

while desiccation can coagulate but also cut/dissect tissue. A clean incision in the tissue is made with minimal coagulation, as can be seen in Figure 20. [63]

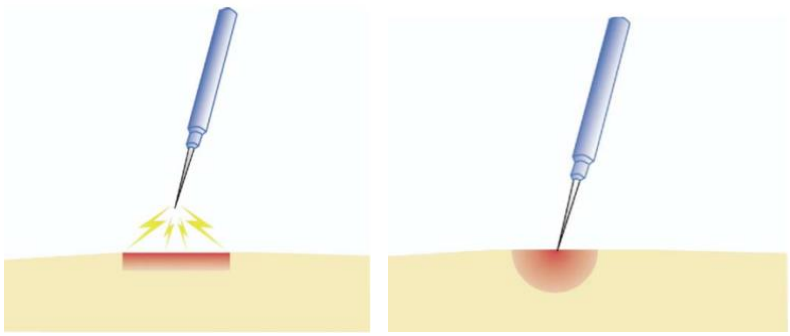

Figure 21: Left: fulguration, where the current travels across a gap to reach the tissue. Right: desiccation, direct contact between the tip of the device and the tissue.

Impedance and resistance

The tissue properties determine its impedance, and therefore how easy- or difficult it is to use electro surgery on this tissue. Tissues containing high ion concentrations, such as hydrated tissue, have a low impedance while tissues with low ion concentrations, such as scarred tissue or fat have a high impedance. A high impedance provides a high resistance to the current flow [61] In Table 4 the resistance properties of different physiological tissues are showed.

Table 4: Resistance properties of different physiological tissues. [69]

Biological tissue	Resistance in 10^3 MHz
Blood	0.16
Muscle, kidney, heart	0.2
Liver, spleen	0.3
Brain	0.7
Lungs	1.0
Fat	3.3

4.3. Electrosurgical instruments

An electrosurgical setup regardless needs an electrosurgical unit, which is connected to a power point and converts the current in the right setting to the instrument. The setting and power are set at the electrosurgical unit, which can be seen in Figure 22. In addition, the setting (monopolar or bipolar) is regulated on the instrument itself by buttons or with foot pedals. When monopolar surgery is used, a dispersive pad is used to transfer the current back to the electrosurgical unit.

Figure 22: Left: Electrosurgical unit available at Philips In-Body Systems, which was used for the experiments described in this master thesis. Right: Dispersive pad which is used to transfer the current back to the electrosurgical unit.

Electrodes

The most common electrodes – which can be seen in Figure 23 – will be discussed. For monopolar electro surgery, various cutting electrodes are available: knife electrodes, needle electrodes, (wired) loop electrodes, ball electrodes and hook electrodes. These electrodes come in different sizes and under different angles, however they are all single tipped. This is different for bipolar electrodes, where the current needs to travel from the instrument, through the tissue and coming back to the instrument. The electrodes for bipolar electro surgery available are scissors, forceps and clamps. Similarly as for monopolar electrodes, these come in various sizes and under various angles.

Figure 23: Monopolar and bipolar electrodes. Left (from the top to bottom) blade, ball, loop, needle, hook and wired loop electrodes. Right (from left to right) clamps, forceps and scissors. [70] [71]

4.4. Strengths and weaknesses

There are certain advantages of electro surgery that contribute to its widespread adoption across all surgical specialties. In comparison to the cold knife, electro surgery achieves haemostasis, which limits blood loss. [63] This is useful when operating, as blood loss can deteriorate the surgeons' sight. [57] [65] To obtain optimal clinical effects and reduce potential complications, a thorough understanding of the proper use of each energy modality is critical. [57]

Besides some advantages, electro surgery has the disadvantages of resulting in more collateral tissue damage compared to scalpel surgery. Electro surgery can create histologic changes of the tissue at the surgical margins. [65] These changes can make it more difficult to distinguish between healthy and malignant neoplasms for histopathologic analysis. The blended cutting mode causes less thermal damage than pure cutting.

4.5. Complications

Complications using electro surgery can happen in practice: 18% of the surgeons have personally experienced a complication using electro surgery. The likelihood of complications depends on its application. Of all different medical specialties, gynaecologists have reported the most personal misadventures (33.3%) compared to other subspecialists. [72] However, when used properly, unintended injuries are rare. [57]

Table 5, shows a number of complications identified during a survey conducted among 620 members of the Society of University of Otolaryngologists by Smith et al. The group of respondents performed 99.664 surgeries in a year, 324 of which resulted in an injury. The occurrence of these complications together is 0.32%. The most common complications are unanticipated direct burns (0.22%) which include applying electro surgery to the wrong structure, accidently turning the instrument on, insulation failure and direct coupling. An injury can develop when the pencil is accidently turned on when somebody steps on the pedal. Using a pencil with a button could avoid this kind of hazard. [62] [60] [59] If the generator is put on when the electrode is near to another metal instrument like a trocar, this instrument can be energized and cause an injury. This hazard is called direct coupling. [60] [66] Applying electro surgery to the wrong tissue or structure might cause collateral damage, for example when operating too close to a (major) nerve. In addition, the heat from the electrosurgical instrument that spreads through the tissue can cause injuries. [62] In addition, the electrosurgical current can diffuse through the body and concentrate in unintended ways, which can cause injuries. Currents are more likely to run through blood vessels, which have a low impedance and are less likely to travel through fat tissue, which has a high impedance, as shown in Table 4. [62]

Other complications that can occur are capacitate coupling (0.05%), electromagnetic interference (0.03%), an improperly applied return electrode (0.01%), fires (0.01%) and hair loss at the incision site (0.001%). When the current flows through a metallic retractor or instrument, it is called capacitive coupling. [73] Alternate site burns can develop due to high current density at an improperly applied ground electrode. [62] This occurs when devices attached to the patient are in direct contact with the ground surface or a metal object that is insufficiently insulated. [63] [60] [59] The latter is called electromagnetic interference. Fortunately, modern generators are better isolated hence mitigating this risk. In addition, interference with older pacemakers can lead to asystole and cardiac arrest. [63]

Besides the direct injuries that can occur, it is thought that 5% of the smoke that is produced during electro surgery is made up of potentially harmful chemicals and cellular debris. [63] [60]

Table 5: Different complications mentioned in electro surgery for 99.664 cases with 324 complications. [73] *The percentage (x/y) are x: occurrence in 99.664 cases, y: occurrence in 324 complications.*

Complications	Occurrence
Improperly applied return electrode	13 (0.01% / 4.01%)
Unanticipated direct burns: accidently turned on, applied to wrong structure, insulation failure, direct coupling	219 (0.22% / 67.6%)
Capacitive coupling	48 (0.05% / 14.8%)
Electromagnetic interference: In contact with other metal object	32 (0.03% / 9.8%)
Fires	11 (0.01% / 3.39%)
Hair loss at an incision site as a result of a cutting electrosurgical instrument	1 (0.001% / 0.31%)

4.6. Discussion

In the experiments performed for this thesis, a monopolar electrosurgical knife was used. This type of electro surgery is chosen while this was the type available at Philips Research. In addition, monopolar electro surgery is used in The Netherlands Cancer Institute where three surgical procedures were attended for this research. However, when a prototype of a 'smart' electrosurgical knife is made, both monopolar and bipolar instruments should be taken into consideration.

Electrosurgical cutting and coagulation have different waveforms and therefore a different impact on tissue. This will be confirmed in Chapter 8, where the influence of electrosurgical cutting and coagulation on tissue are tested. However, in my literature study it is concluded that there are no rules on when to use which modality. In addition surgeons use different modalities and powers for the same – parts of the – surgical procedure. Which modality is used depends on the surgeon's knowledge and expertise. In the experiments in this thesis, electrosurgical cutting and coagulation is used with a power setting of 50, 60, 70 and 80 Watt. These are the most commonly used settings for monopolar electro surgery. [60]

Complications during the use of electro surgery are rare (<0.32%). [73] However, when they occur it is most of the time due to improper use of the instrument. It is thought that electrosurgical devices are poorly understood among medical professionals. [74] This lack of electrosurgical knowledge may negatively affect the outcome of an operation and hence safety of the patient. [75] To obtain optimal clinical effects and reduce potential complications, a thorough understanding of the proper use of each energy modality is critical. [57]

To minimize the occurrence of complications during electrosurgical procedures and make surgeons aware of the differences between electrosurgical cutting and coagulation better training should be provided. More research could be performed on the influence of using different modalities in electro surgery to substantiate this new training.

II

Clinical setting

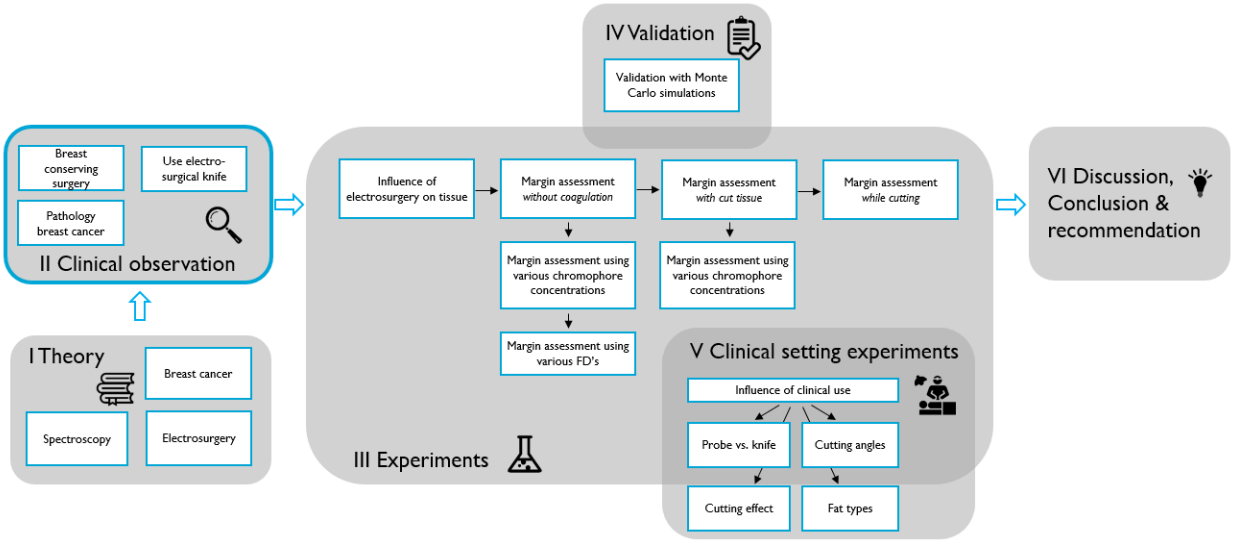

5. Breast conserving surgery

This chapter describes the workflow of a BCS to examine if the integration of a 'smart' electrosurgical knife could be beneficial for tumour margin assessment. Three surgical procedures were attended on April 12, 2017 at the Netherlands Cancer Institute to gather information about the current procedure. The procedure is described in several steps of which the duration is measured. The focus will be on the specific step of the procedure where a 'smart electrosurgical knife' could be an advantage compared to the current situation.

5.1. Workflow BCS

A BCS can be coarsely divided into four steps: the preparation of the patient, the localization of the tumour, dissecting the tumour and closing the patient. At the attended surgical procedures a gamma probe and ion seeds were used to localize the tumour. All steps of the BCS will be discussed and a timeline of the three procedures will be shown. The focus at the explanation of these steps will lay on the localization of the tumour and assessing the margins of the tumour. The preliminary steps to the surgical procedure including placing the ion seeds, the anaesthesia, and sterilization of the surface will be neglected.

1. Preparation of the patient: Before the first incision is made, the gamma probe is used to globally localize the tumour(s). With this knowledge, marks on where to make the incision are made at the breast. In addition, the surgeon can make use of the images made prior to the procedure to predict the location of the tumour. When the surgeon is confident about his/her marks, the first incision is made with a scalpel.
2. Localization of the tumour: After the first incision with the scalpel is made, the ES knife will be used for further dissection. The surgeon is guided towards the tumour by alternating the use of the gamma probe for localization of the tumour and the use of the ES knife to dissect the tissue. When the surgeon thinks he/she is close to the tumour – by taking into consideration the preliminary images made and acceleration of the audio signal of the Geiger counter – the tumour is dissected.
3. Dissecting the tumour: Estimation of the tumour margin is performed by visual inspection, palpation and using the gamma probe. However, all these methods provide a relative distance to the tumour. Therefore, the decision of dissecting the tumour is made based on the expertise of the surgeon. After dissecting the tumour, the tissue is examined *ex vivo* to visually inspect the margins. Then two markers are placed on the dissected tissue to provide information to the pathologist on the orientation of the dissected tissue in the body.
4. Closing the patient: After the dissection of the tumour, some small staples are placed on the location of the dissected tissue. These staples are used to guide the radiation posterior to the surgical procedure. After placing the staples, the patient is closed.

All steps described above were timed during the visit at The Netherlands Cancer Institute. Three procedures were attended, which included five breast tumour dissections. In Figure 24, all steps are showed in minutes. In addition, the number of alternations between the gamma probe and the electrosurgical knife in the 'searching tumour'-step are stated in parentheses. The time for 'preparing the patient' differs from 17 to 30 minutes, for 'searching the tumour' from 11 to 26 minutes, 'inspecting the

tumour' took 2 to 5 minutes and 'closing the patient' differed from 7 to 20 minutes in time. The alterations between the instruments variated between 3 and 17.

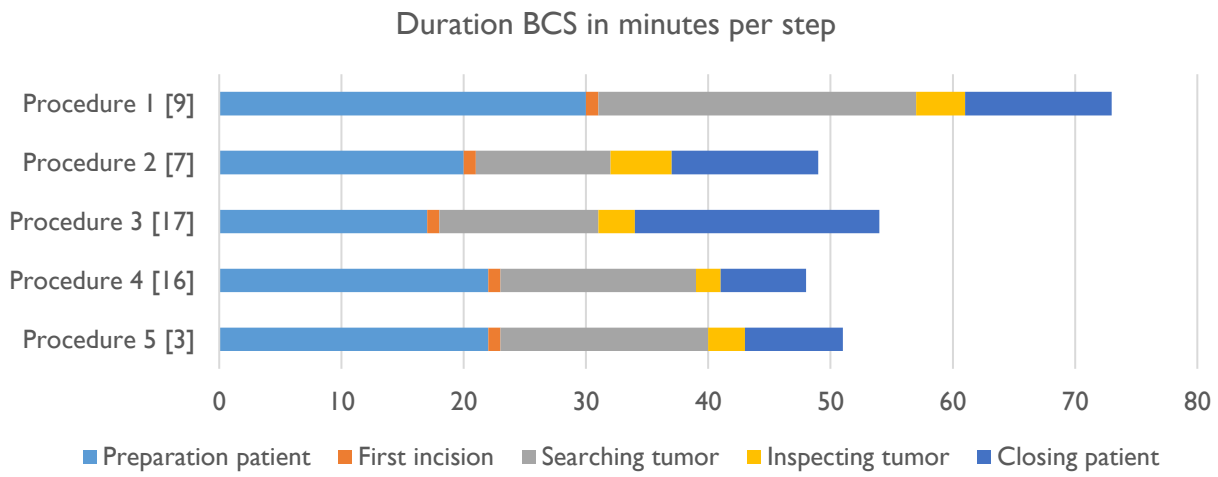

Figure 24: Bar chart of the workflow of a BCS. Five BCS's described per step in minutes. The numbers in parentheses [x] represent the number of alternations between the Gamma probe and the electrosurgical knife.

5.2. Discussion

In this chapter, the workflow for BCS is described. One must take into consideration these observations rely on three surgical procedures. Differences in workflow between surgeons, hospitals and countries can are present and therefore the description of a workflow will always be incomplete.

As described in step 2 of the BCS, the global and specific localization of the tumour is currently performed by using a gamma probe. This probe has some disadvantages: it provides a relative distance to the ion seed. Therefore, if the ion seed is placed incorrectly the probe will guide the surgeon to the wrong place. In addition, localization of the tumour can only be done by alternating between instruments (gamma probe and electrosurgical knife).

Advantages of a 'smart electrosurgical knife' (i.e. an electrosurgical knife with sensing capabilities to determine a tumours' location at – at least – 2mm in front) would be: providing the absolute distance to the tumour from 2mm, no alternation needed between instruments and focusing on the tumour itself instead of a ion seed or guidewire. Besides saving time, not having to alternate between instruments also enables the surgeon to stay focused on his/her operating site. However, for global localization another instrument than a 'smart' electrosurgical knife is needed.

The localization of the tumour takes approximately a third of the surgery time for BCS. However, making the assumption that this time will decrease – a lot – when a 'smart' electrosurgical knife is used would be incorrect. The majority of the time included in the step 'localizing tumour' is needed to reach the tumour. With the knowledge gained in this master thesis, no estimation can be made on the time a 'smart' electrosurgical knife would reduce in a BCS. However, it needs to be taken into account that an increasing amount of dissected tissue will increase the time closing the patient in a satisfying way regarding to the cosmetics.

6. Usage electrosurgical knife

The aim of this master thesis is to evaluate a 'smart' electrosurgical knife. Therefore, it is important to examine the use of the electrosurgical knife in a BCS in clinical practice. The settings and positioning of the electrosurgical knife and the cutting techniques will be discussed. These insights are helpful for the design of the experimental setups in this thesis.

6.1. Settings electrosurgical knife

The electrosurgical unit used for the surgical procedures attended at the Netherlands Cancer Institute is a Covidien ForceTriad. Monopolar electro surgery is used in both cutting (blended) and coagulation (fulguration) setting with a power of 35 Watt. Cutting was used for dissecting close to the skin and coagulation for cauterization of blood vessels. For dissecting adipose tissue – neither close to the skin nor close to a vessel – the cutting setting was used most of the time, however sometimes the coagulation setting was used. The surgeons declared there are no 'rules' for what settings to use in this case. More information about the use of electro surgery can be found in my literature study. [29]

6.2. Positioning and cutting techniques

The electrosurgical knife is held as a pencil, as can be seen in Figure 25. When needed, the knife is rotated in the hand. The tissue is held under a slight tension by pulling on the skin with surgical retractors. In general, the electrosurgical knife is used perpendicular to the tissue for dissecting in depth. However, sometimes another angle was made between the tissue and the knife to dissect a – for example – small piece of adipose tissue.

The cuts made by the surgical knife where short, compare to a scalpel. Long cuts are split in short pieces when an electrosurgical knife is used. This is mostly because of the tissue that sticks to the blade of the knife when long cuts are made. Short cuts result in a rough surface after dissection. The bottom right picture in Figure 25 shows the dissected tissue does not have a clean cut at the borders. In literature, no information is found about the velocity of cutting during electro surgery.

Before the surgery, a clean cutting blade was put on the electrosurgical knife. Figure 26 shows the cutting blade after the surgery. Especially on the tip of the blade, ablation can be seen. After using the cutting blade, it is thrown away. The electrosurgical knife is brought to the central sterile supply department to be sterilized and used again for another surgery.

6.3. Discussion

The pictures in Figure 25 show the use of the electrosurgical knife in practice. Some differences can be observed when comparing electrosurgical cutting and 'cold' cutting. First, when a scalpel is used, a straight cut is made instead of splitting the cut up in smaller pieces for electrosurgical cutting. Second, blood loss during electrosurgical cutting is limited. This is the main advantage of electrosurgical cutting. Both electrosurgical cutting and 'cold' cutting are performed on tissue under tension. In literature, it is stated spectra change when pressure is applied. This is possibly due to alteration of tissue morphology and blood

flow. [76] [77] Tension could affect DRS results as applying pressure does. However, as pressure is not the same as tension, research should be performed to examine the influence of tension on DR spectra.

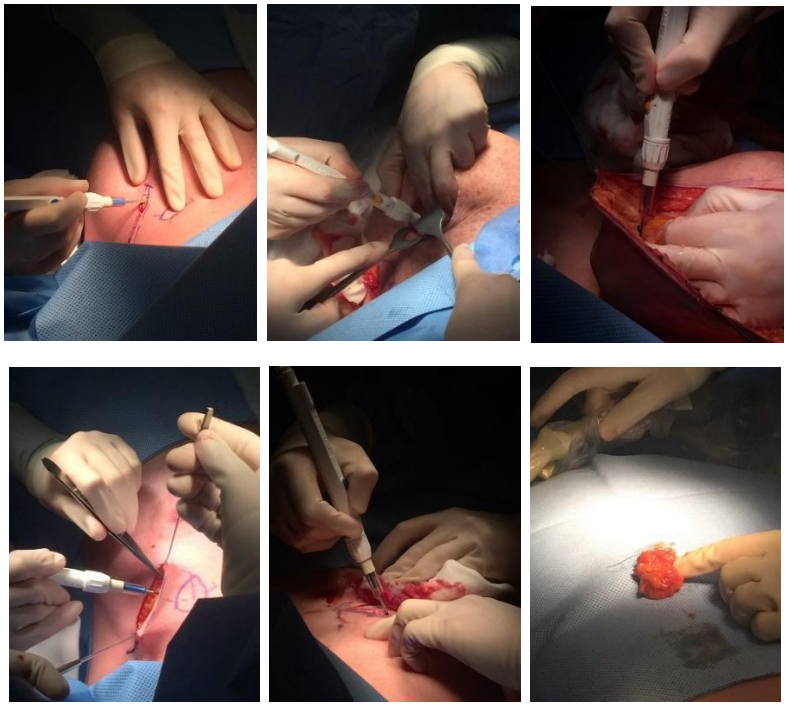

Figure 25: Five examples of the use of an electrosurgical knife while cutting. (All pictures at the top, bottom left and middle) The cuts are made when the tissue is held under a slight tension using hands or forceps. The instrument has a perpendicular orientation with respect to the tissue. All show a pen-grip with various rotations. The bottom right picture shows the dissected tumour tissue.

Figure 26: Ablation present on the electrosurgical knife after the surgery.

A difference between electrosurgical cutting and coagulation was seen when attending the surgical procedures. When cutting, the knife was held upon the tissue and the tissue split. The knife was held some mm above the tissue for coagulation. Charring developed on the tissue and more smoke was produced compared to electrosurgical cutting.

For the surgeries attended, electrosurgical cutting and coagulation was alternate and a power setting of 35 Watt was used. No explanation was given on when to use coagulation or cutting. Similar, the specific power setting was chosen while this power setting is always used for this surgery. No explanation on the used power setting was given.

7. Pathology breast cancer

Besides the visual ablation caused by electrosurgical cutting and coagulation, the effects of ablation on microscopic level are unknown. In this chapter, pathological samples of a dissected tumour with ablation is examined on the effects of ablation on microscopic level.

7.1. Pathological samples

Table 3, shows the thermal effects of electro surgery on biological tissue for various temperatures. For this research, it was wondered if these thermal effects could also be seen in microscopic view on tumours. The microscopic views used in this chapter are obtained at the pathology department of the Netherlands Cancer Institute. The pathologist rarely sees thermal ablation – which occurs for electrosurgical cutting or coagulation – on tumours. Figure 27 shows a dissected breast tumour from a microscopic view (20x). The blue marks are placed by a pathologist and refer to tissue where thermal ablation can be seen. In general, a tumour under microscopic view can be recognized by an increase in number of cells together with enlarged nuclei.

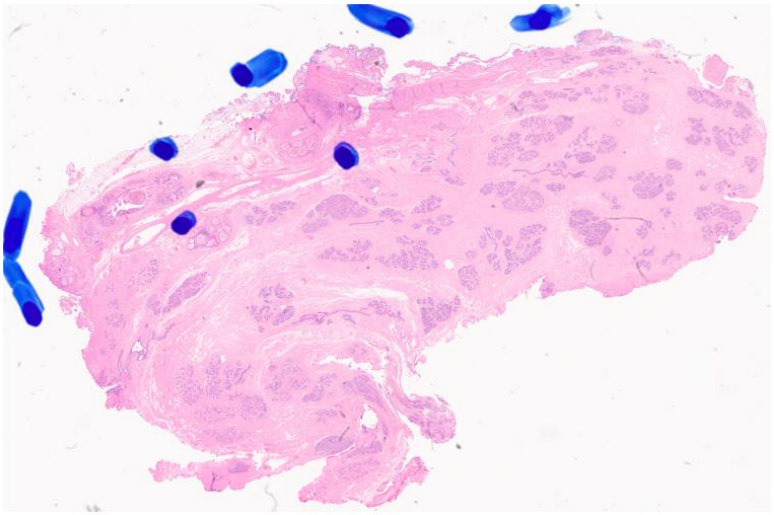

Figure 27: Microscopic view of a dissected breast tumour showing thermal ablation. This view is magnified 20x by a microscope. The blue marks are made by the pathologist to indicate thermal ablation.

Thermal ablation on the tumour makes it more difficult to distinguish between healthy and tumour tissue compared to non-ablated tumour tissue. When thermal ablation on the tumour is present, the following changes can be seen:

- The nucleus becomes blurry
- The connective tissue becomes deep red
- The endothelial becomes ropy and streaming effects occur

Figure 28 and Figure 29 are all digital magnifications of Figure 27. They show the effects described above for thermal ablation in the black boxed regions. However, it is not easy to distinguish between ablated and non-ablated tumour cells. A pathologist should examine each individual case, before a conclusion can be drawn.

Figure 28 shows DCIS and normal breast tissue. The tumour cells are not – yet – broken through the border of the ducts. A high density of dark purple dots – which represent the nuclei – is identified as the ducts. The ducts are individual units which can be recognized by the round shape and the small border of connective tissue around it. The connective tissue is pink and has a long structure. In addition, the connective tissue possesses nuclei which can – again – be identified as dark purple dots. In the corner in the bottom right of the figure, a blood vessel with red blood cells can be seen.

The ablated tissue in Figure 28 can be seen in the back boxes among others. The nuclei are blurry in some parts and a few spots of deep red connective tissue can be seen.

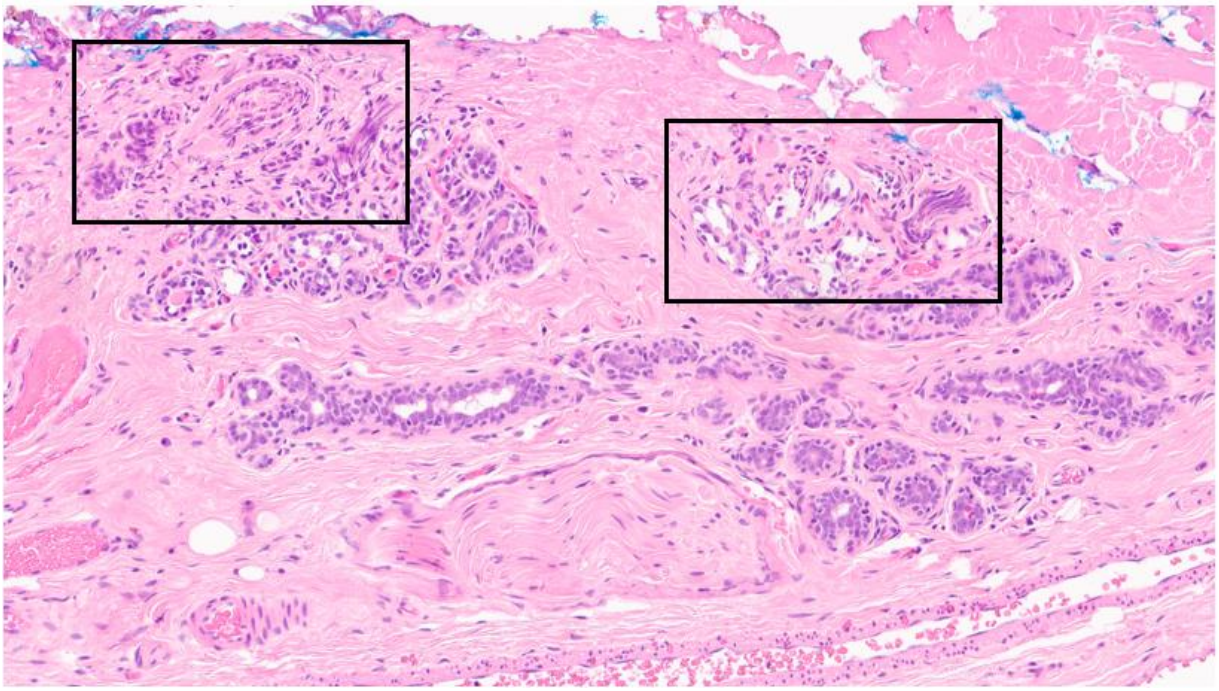

Figure 28: Magnified view of Figure 27. The black box shows the effects of thermal ablation on tumour cells. This view is magnified 20x by a microscope and 20x digitally.

Figure 29, shows a DCIS however now at the border of the dissected tissue similar to Figure 28. The ducts and the connective tissue can be identified in the same way as described for Figure 28. In the black box effects of ablation can be seen including blurry nuclei. In this figure, the dark red connective tissue is more present compared to Figure 28. In addition, some dark brown parts are visible at the border of the dissected tissue. This is charring of the tissue due to electrosurgical cutting or coagulation.

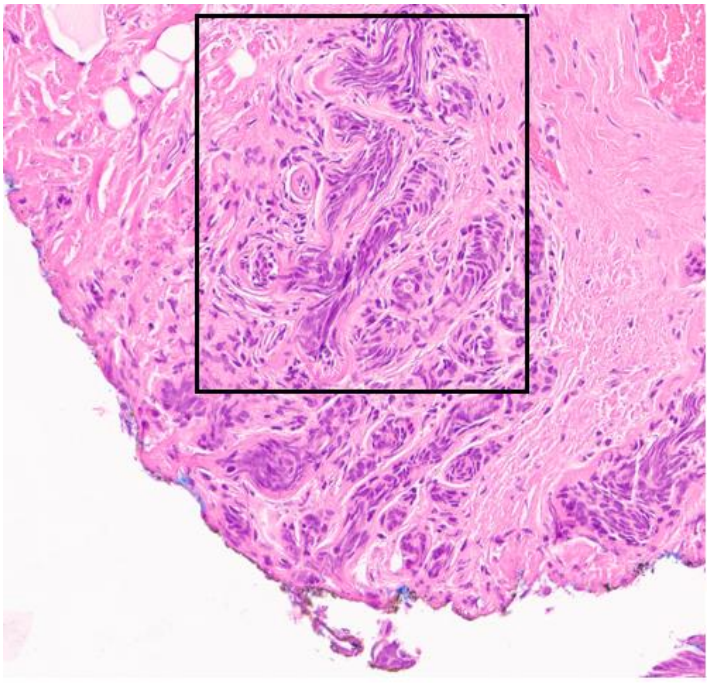

Figure 29: Magnified view of Figure 27. The black box shows the effects of thermal ablation on tumour cells. This view is magnified 20x by a microscope and 20x digitally.

7.2. Discussion

Differences are present between ablated tumours and non-ablated tumours in microscopic view. The pathologists stated that ablation on the tumour makes it more difficult to distinguish between healthy and tumour cells. This could be an additional reason to achieve negative margins at a tumour resection, next to prevent local reoccurrence of the tumour. A 'smart' electrosurgical knife could be able to detect a tumour at a certain distance and thereby preventing the tissue from being ablated. It is not known if electrosurgical cutting or coagulation causes the ablation in these samples.

It needs to be considered that the black boxes depicted in Figure 28 and Figure 29 show ablated tissue however, the surrounded tissue can also be ablated. The pathologist has verified the tissue inside the black boxes, as ablated tissue.

III

Experiments

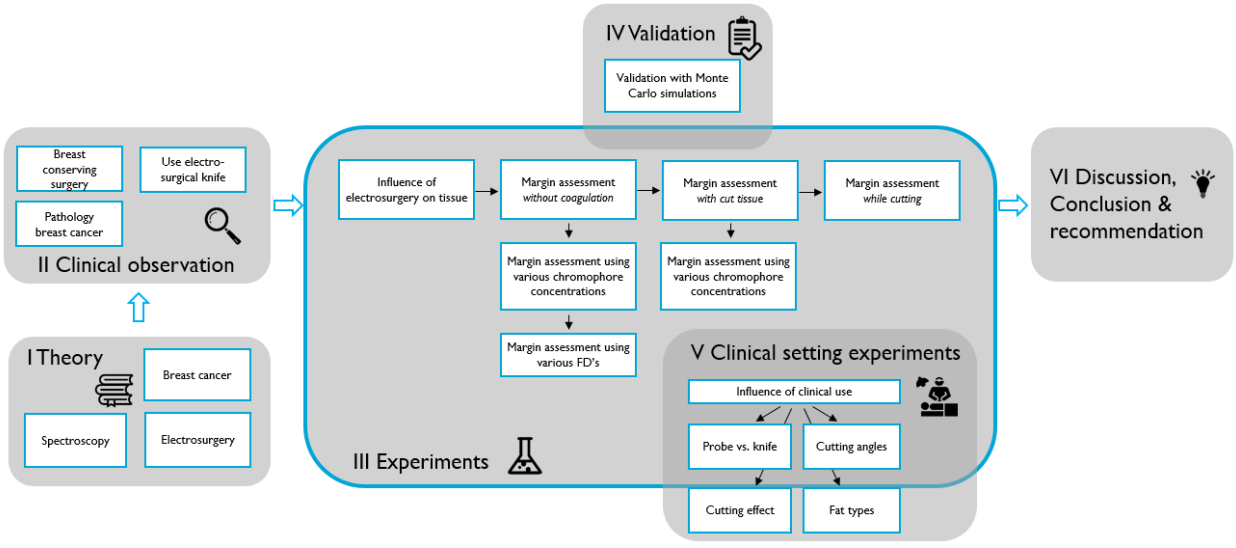

8. Influence of electro surgery on tissue

To understand the effects of electro surgery on tissue, the size and shape of tissue exposed to electro surgery is examined. The tissue concerning a BCS is tumour tissue and adipose – fat – tissue. In the experiments, porcine fat and muscle tissue will be used to simulate these tissues. Various settings as cutting and coagulating at a power of 50, 60, 70 and 80 Watt are used. Besides the visible differences due to electro surgery, also the tissue composition can change. DRS can measure the latter one.

It is known that a distinction can be made between adipose and tumour tissue by DRS. [1] In this experiment, the changes in DR spectra due to electro surgery will be examined. Based on the experiments performed in the thesis of Julie Fleischer [2] it is expected that:

- Cutting and coagulation will have different visual effect on muscle and adipose tissue
- Cutting and coagulation will have different effect on DR spectra for muscle and adipose tissue
- Higher current will result in more visual effects and a bigger difference in DR spectra

All assumption will be considered in comparison to pure tissue.

8.1. Materials

Specimens

Pork belly (Figure 30) bought at the Albert Heijn is used as specimen to cut/coagulate on. This porcine tissue exists of muscle (red) and adipose (white) tissue, both can be seen in Figure 31. Ten different pieces of tissue are used, on half of the pieces only cutting is performed, on the other half only coagulation is performed. The tissue has a thickness of approximately 10 mm.

Figure 30: Pork belly (Albert Heijn) used for the experiment

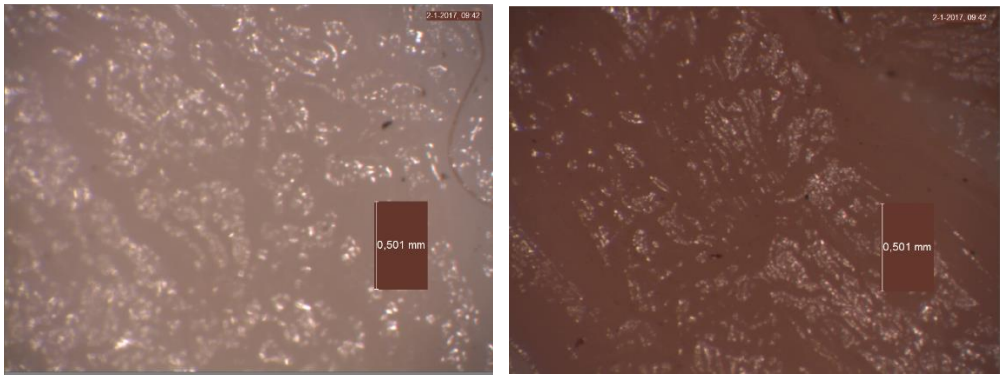

Figure 31: 40x magnification of adipose tissue (left) and muscle tissue (right) of pork belly.

Instruments

A monopolar electrosurgical knife (Reliant) is used to cut and coagulate the porcine tissue. In addition, a disposable scalpel (Swann-Morton, Sheffield, England) is used to cut the tissue for a side view examination by the microscope. Tweezers are used to pick up the tissue ones it is cut in small bars.

For measuring the DR spectra, a small probe with a maximum fiber distance of 3mm was used. The probe can be seen in Figure 33.

Figure 32: Monopolar electrosurgical knife (Reliant). Various blades can be attached to the knife, for this experiment the blade in the figure was used.

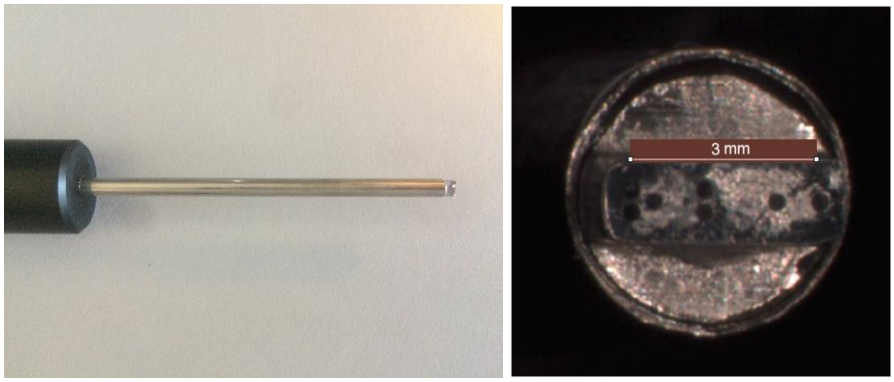

Figure 33: Small probe with a maximum fiber distance of 3mm. The fiber distances used were 2mm and 3mm.

Equipment

The setup for this experiment can be seen in Figure 34. The monopolar electrosurgical knife is connected to an electrosurgical unit Force Fx (Valleylab, Boulder, United States). The electrical current flows from this unit, through the knife to the porcine tissue. The tissue is cut or coagulated by the current from the monopolar electrosurgical knife. The current flows from the electrosurgical unit, through the body, then leaves the tissue at the dispersive pad and returns to the electrosurgical unit. The cutting and coagulated power settings used are 50, 60, 70 and 80 Watt. These are the most commonly used settings for monopolar electro surgery. [60]

To be able to cut and coagulate in a controlled setting, a linear stage actuator controlled by an ESP300 Universal motion controller (Newport, Irvine, United States) is used. This stage makes cuts of 2 mm deep and is situated 1 mm above the tissue while coagulating. The time of cutting and coagulation was timed at 1 second. After 1 second, the linear stage actuator was moved upwards again.

After cutting or coagulation, DR measurements are made. A probe is held on the cut or coagulated tissue. The probe emits white light and detects light via a VIS and NIR spectrometer. Both transfer the detected light per wavelength to the PC with PNSas software. The PC stiches the spectra together to make it a continuous spectrum from 400 to 1600nm. Following, the tissue was cut in thin slices with an scalpel. This made it possible to examine the tissue under a microscope (Leica, Wetzlar, Germany). The maximum and minimum cutting width and depth and the maximum and minimum coagulation width and depth were measured.

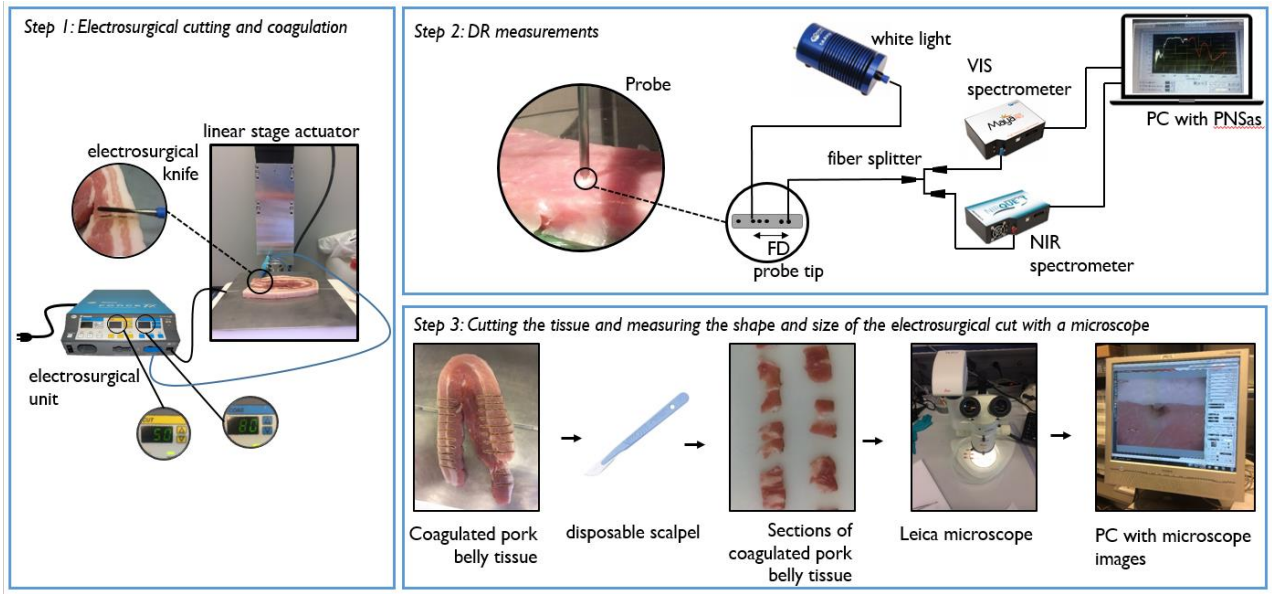

Figure 34: Setup experiment. Step 1: Cutting the tissue using an electrosurgical unit - connected to the electrical outlet - linked to the electrosurgical knife and to the dispersive pad. Step 2: Measuring the DR spectra with a probe which has a white light source and a VIS and NIR spectrometer to detect the light. A PC with PNSas software transforms the detected light into a spectrum. Step 3: Cutting the pork belly tissue in thin slices to examine its shape and size under a microscope (Leica, Wetzlar, Germany).

8.2. Method

The dependent variables for the first experiment are: the cutting depth (Dt) in mm, coagulation depth (Dg) in mm, cutting width (Wt) in mm, coagulation (Wg) width in mm and the coagulation zone (Zg). All dependent variables can be seen in Figure 35. These variables are used to examine the visual effects of electro surgery. It is important to consider that the electrosurgical knife was held 0.2mm within the tissue when cutting or coagulating. This 0.2mm is included in the Dt and Dg measurements.

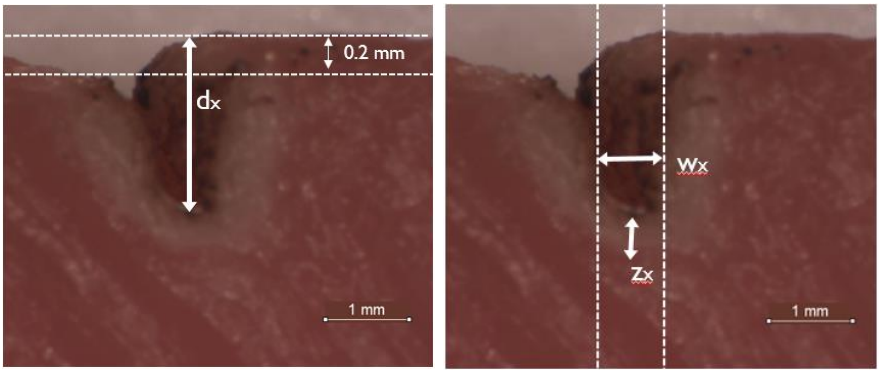

Figure 35: Dependent variables depth (Dx), width (Wx) and coagulation zone (Zx), the x can be replaced by a 't' for cutting or a 'g' for coagulation. The depth of the incision with the knife was 0.2mm for all incisions. Dx includes this 0.2 mm incision length. Wx is measured in the middle of the incision.

The independent variables were the tissue type and the power of the electrosurgical unit. Four different power amounts are used: 50, 60, 70 and 80 Watt. The tissue types used are muscle tissue and adipose tissue. Each different experimental condition is performed 30 times, which ended up in a total of 240 experiments as can be seen in the condition matrix. As approximately 25 cuts can be made on 1 piece of porcine tissue, therefore 10 pieces of porcine tissue are needed. The cut is made with a constant velocity, duration and depth with the linear stage actuator and is performed through adipose and muscle tissue in the same cut. The experiment was performed twice, first for electrosurgical cutting and then for coagulation of the tissue.

Both trials – cutting and coagulation – were randomized by the command randperm in MATLAB. First all cutting trials were performed, then all coagulation trials. By randomizing the trials, variables which could influence the results, like difference in specimen and heating of the knife after multiple cuts are cancelled out.

Table 6: Condition matrix with two different tissues (muscle and adipose tissue) and four different powers (50, 60, 70 and 80 Watt). A total of 8 conditions and 30 experiments adds up to 240 trials.

		Power			
	t = 30	**50W**	**60W**	**70W**	**80W**
Tissue	**Muscle tissue**	EC11	EC12	EC13	EC14
	Adipose tissue	EC21	EC22	EC23	EC24

After electrosurgical cutting and coagulation of the tissue, the DRS spectrum was measured. This is the dependent variable of the experiment. This spectrum is obtained using PNSas. To start the measurements, a probe with known fiber distance(s) is used. The signal is calibrated by performing a measurement on a reflectance standard (Spectralon Diffuse Reflectance Standard, Labsphere, North Sutton USA). The white reflectance standard reflects the light uniformly over the probe surface, and this spectrum was used as the system response to compensate for the spectral shape of the light emitted by the lamp and the wavelength dependent sensitivity of the detector as well as any wavelength-dependent sensitivity in the optics and gratings of the system. This calibration step was followed by a background measurement in order to minimize the impact of the ambient light, dark current, and electric offsets of the detector. The integration times – with a minimum of 0.1 second and a maximum of 1 second – were set on 0.5 second for VIS and 1 second for NIR. A larger integration time increases the accuracy of the measurement. After this steps, the measurements can be made.

The spectra are saved in a .mat file and can be used to plot spectra in MATLAB from this file. When plotted, the maximum of the spectra is set at one to normalize the spectra. This is done as the intensity of the spectrum is relative. Interesting regions in the spectrum can be pointed out, from which a specified chromophore percentage can be extracted. The chromophore percentages provide information about the changes in composition of the tissue.

After measuring the DR spectra, the tissue was examined under a microscope (Leica, Wetzlar, Germany) on a scale of 2.5x. First all cutting/coagulation lines were examined from a top view. Later, after making incisions in the tissue with a scalpel, the side views were examined. A top view can be seen in Figure 35 on the right, and a side view can be seen in on the left.

8.3. Results

8.3.1. Size and shape of cut tissue

In Figure 36, cuts made in pork belly tissue can be seen in a section and a top view. The cut is normally V-shaped with a large opening at the surface of the tissue ending in a sharp tip within the tissue. It can be seen that less charring is present in the adipose tissue versus the muscle tissue. In addition, there exists no coagulation zone in both muscle and adipose tissue. In Figure 36 – left and middle – there are no big differences in the cutting depth. However, the cutting seems a bit larger for the muscle tissue. The right picture in Figure 36 contradicts the observation of the cutting width made for the left and middle picture, while here the cutting width for adipose tissue seems to be larger than for muscle tissue. To examine these assumptions, 120 measurements are performed on cut muscle tissue and 120 measurements on cut adipose tissue.

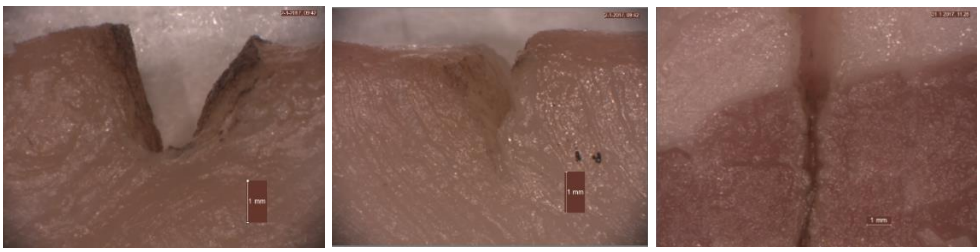

Figure 36: Section of muscle pork belly tissue (left) and adipose pork belly tissue (middle) and a top view (right). All include a cut with an electrosurgical knife.

The cutting depth (Dt) for muscle and adipose tissue can be seen in the left plot in Figure 37. The cuts are made using various powers from 50 Watt to 80 Watt. The mean of Dt is 0.72mm for muscle tissue and 0.65mm for adipose tissue. The average Dt increases for increasing powers for muscle tissue, but for adipose tissue the average Dt stays approximately the same for increasing powers. The maximum Dt is 1.5mm for muscle tissue and 1.4mm for adipose tissue. The minimum Dt is 0.27mm for muscle tissue and 0.28mm for adipose tissue.

The cutting width (Wt) for muscle and adipose tissue can be seen in the right plot in Figure 37. As described above, the cuts are made with powers ranging from 50 to 80 Watt. The mean Wt for muscle tissue is 0.82mm and for adipose tissue is 1.16mm. Both for muscle and adipose tissue, no relation can be seen between the Wt and the power. The maximum Wt is 1.52mm for muscle tissue and 2.27mm for adipose tissue. The minimum Wt is 0.31mm for muscle tissue and 0.29mm for adipose tissue.

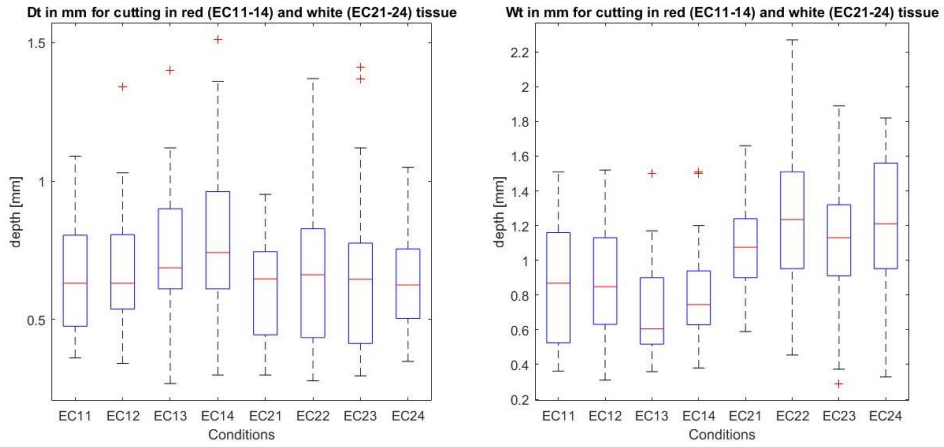

Figure 37: Dt (cutting depth) left and Wt (cutting width) for using the cutting setting on 50 Watt (EC11, 21) to 80 Watt (EC14, 24) on muscle (EC1x) and adipose tissue (EC2x)

8.3.2. Size and shape of coagulated tissue

In Figure 38, pork belly tissue is coagulated which can be seen from a section and a top view perspective. When these figures are examined in contrast with Figure 36 it can be seen that the 'incision' is less clear for coagulation than for cut tissue. More charring is present for both muscle and adipose tissue and a coagulation zone is present around the 'incision' in the muscle tissue. The incisions in Figure 38 have approximately the same size and shape. Again, 120 measurements are performed on coagulated muscle tissue and 120 measurements on coagulated adipose tissue to examine these assumptions.

Figure 38: Section of coagulated pork muscle pork belly tissue (left) and adipose pork belly tissue (middle). On the right, a top view of coagulated pork belly tissue (2x). The coagulation is present in the muscle and the adipose tissue.

The coagulation depth (Dg) for muscle and adipose tissue can be seen in the left plot in Figure 39. The coagulation is performed using various powers from 50 Watt to 80 Watt. The mean Dg for muscle tissue is 0.43mm and for adipose tissue is 0.71mm. The average Dg increases for increasing powers for muscle tissue until 70 Watt, for 80 Watt the average Dg decreased to 0.45 mm. For adipose tissue, the average Dg stays approximately the same for increasing powers. The maximum Dg is 1.16 mm for muscle tissue and 1.56 mm for adipose tissue. The minimum Dg is 0.20mm for muscle tissue and 0.23mm for adipose tissue.

The coagulation width (Wg) for muscle and adipose tissue can be found in the right plot in Figure 39. The mean Wg for muscle tissue is 0.88mm and for adipose tissue is 1.12mm. The average Wg increases for increasing powers for muscle tissue until 70 Watt, for 80 Watt the average Wg decreased to 0.91 mm. For adipose tissue, the average Wg also seems to increase. However, the average Wg value of EC22 for 60 Watt is higher than the value for EC23 for 70 Watt. The maximum Wg is 1.67mm for muscle tissue and 2.03 mm for adipose tissue. The minimum Wg is 0.40mm for muscle tissue and 0.41mm for adipose tissue.

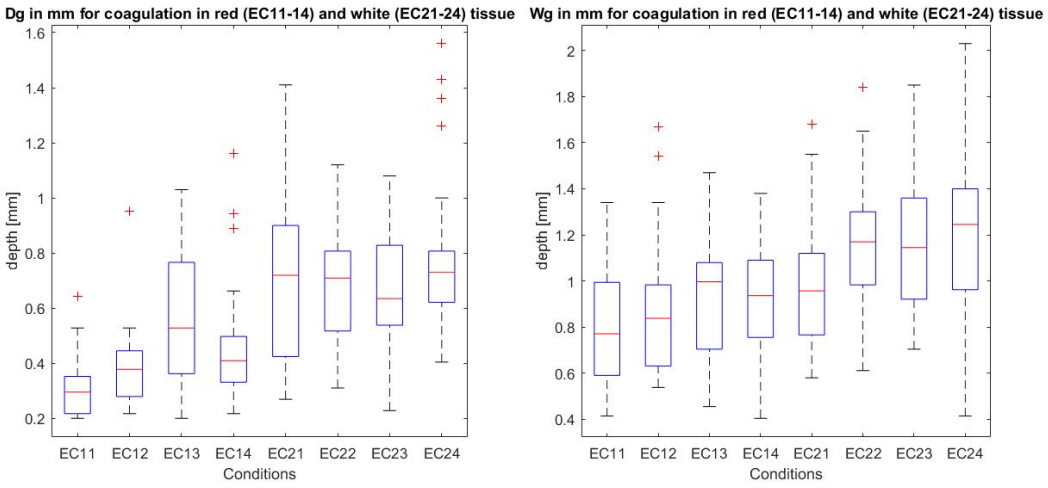

Figure 39: Dg (cutting depth) left and Wg (cutting width) for using the coagulation setting from 50 Watt (EC11, 21) to 80 Watt (EC14, 24) on muscle (EC1x) and adipose (EC2x) tissue

In Figure 40, the coagulation zone (Zg) can be seen. There is no Zg for adipose tissue, which results in a mean of 0mm. The mean Zg for muscle tissue is 0.43mm. The average Zg increases for increasing powers for muscle tissue from 0.35mm, 0.39mm, 0.46mm to 0.54mm. The maximum Zg is 1.05mm and the minimum Zg is 0.20mm, both for muscle tissue.

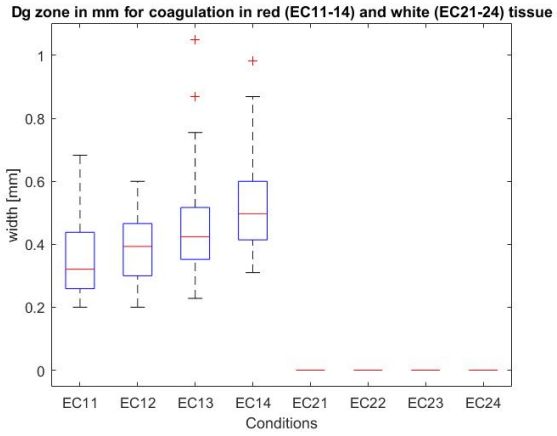

Figure 40: Zg (coagulation zone) for using coagulation setting from 50 Watt (EC11, 21) to 80 Watt (EC14, 24) on muscle (EC1x) and adipose (EC2x) tissue

8.3.3. DR spectra cut tissue

In the addition to the description of the shape and size of the cuts, the change in configuration of the tissue can be described. This has been done by the use of DR spectra. A probe with a fiber distance of 2mm and 3mm is used for these measurements. The probe can be seen in Figure 33. The influence of electrosurgical cutting at various power settings can be seen in Figure 41. This figure shows DR spectra of cut tissue with a power of 50, 60, 70 and 80Watt and the DR spectra of pure tissue. All experimental conditions, as described in Table 6 have 30 measurements which can be seen in Appendix C. In Figure 41, the means of these measurements are presented.

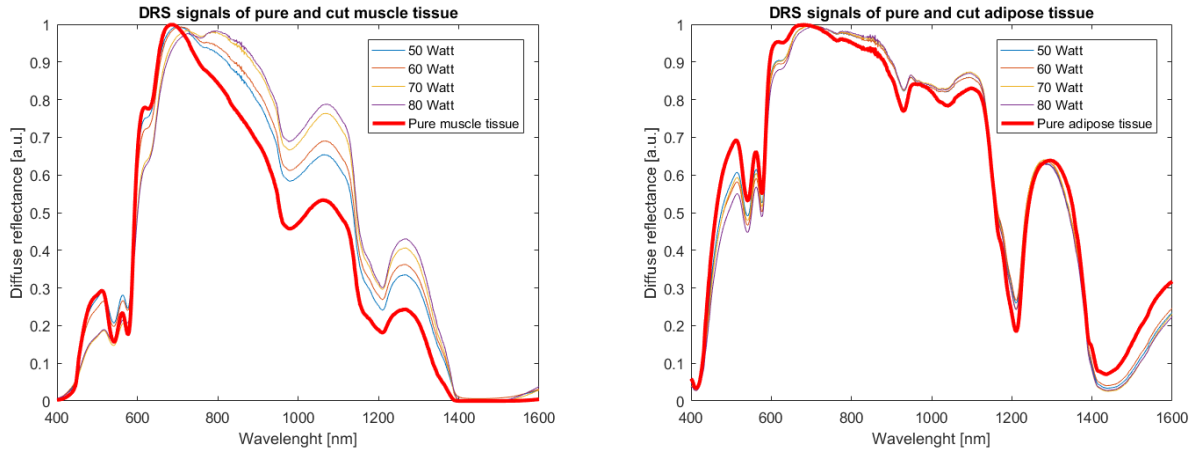

Figure 41: DR signals of pure and cut muscle tissue (left) and pure and cut adipose tissue (right). Both plot show DR spectra of all power settings used (50, 60, 70 and 80 Watt). All spectra presented are the mean spectra of multiple measurements: 30 measurements for cutting and 5 measurements for pure tissue. All obtained measurements can be found in Appendix C.

Muscle tissue

The characteristics of a spectrum of muscle tissue can be seen in Figure 41 (left). The characteristics marked by an asterisk indicate qualitative landmarks for haemoglobin tissue. [78]

- a (low) double peak between 500nm and 600nm which represents the oxygen within the muscle*
- Peak at 700 nm with a small valley just before the peak around 650nm*
- A gradually decreasing slope after 700nm
- A valley and peak at 1000nm and 1100nm
- A second valley and peak at 1200nm and 1300nm

When comparing the DRS signals of cut and pure muscle tissues along a varying power setting, it can be seen that the overall shape of the spectrum does not change. However, deviations are present, especially in the NIR region. In the VIS region, the peak at 500nm and at ±650nm has a lower intensity for cut tissue. When increasing the power of the cut, the peaks lose intensity. In the VIS region, the whole spectrum is elevated. Again, the higher the power the more deviation is present compared to the pure tissue spectrum.

Adipose tissue

The characteristics of a spectrum of adipose porcine tissue can be seen in Figure 41 (right). The characteristics marked by an asterisk indicate qualitative landmarks for adipose tissue. [78]

- A (high) double peak between 500nm and 600nm with a higher intensity than for muscle tissue
- A plateau from 600nm to 1100nm
- A double peak around 1050 nm*
- A large peak between 1200nm and 1400nm*
- An increasing slope of a peak from 1400nm*

Again, the overall spectrum of the adipose tissue without cutting in Figure 41 does not change a lot after the tissue has been cut. All characteristics are still present for cut tissue for all power settings. In addition, thee deviation after cutting is less for adipose tissue compared to muscle tissue. The double peak between 500nm and 600nm and the peak starting from 1400nm have a lower intensity in the spectra of cut tissue. The plateau between 600nm and 1100nm has a higher intensity in the NIR region – from 700nm – however, it has a lower intensity between 600nm and 700nm in the VIS region.

8.3.4. DR spectra coagulated tissue

Figure 42, shows the spectra of coagulated muscle (left) and adipose (right) tissue. Power settings of 50, 60, 70 and 80 Watt are included and plotted next to the spectrum of pure tissue.

Comparing the DR spectra of cut muscle tissue, in Figure 41 (left), to coagulated muscle tissue, in Figure 42 (left), coagulation results in more deviation in the spectrum. This deviation is present within the whole spectrum, although all characteristics are still present. In the VIS region, all peaks – the double peak between 500 and 600nm and the small peak at 650nm – are flattened. In the NIR region, all peaks are still present however; the spectra of coagulated muscle tissue are elevated compared to the spectrum of pure tissue. This is equivalent to the changes in the cut muscle tissue.

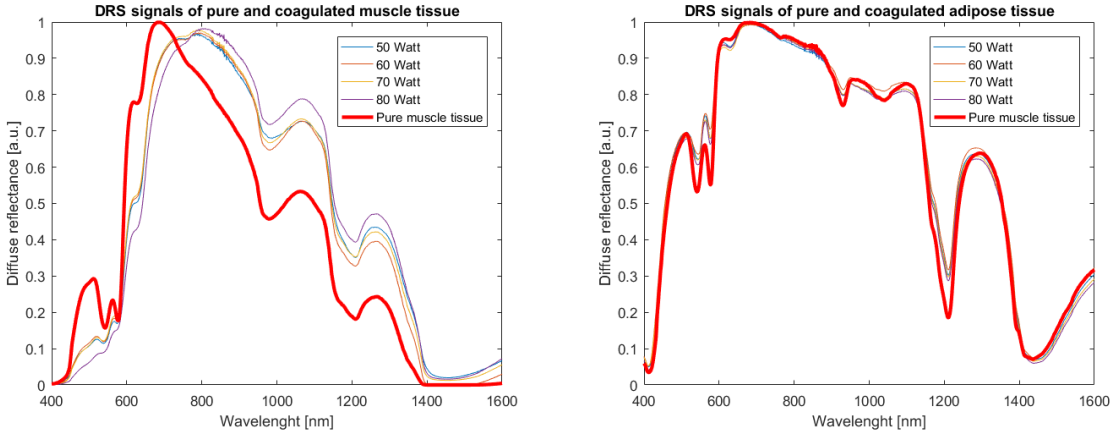

Figure 42: DR signals of pure and coagulated muscle tissue (left) and pure and coagulated adipose tissue (right). Both plot show DR spectra of all power settings used (50, 60, 70 and 80 Watt). All spectra presented are the mean spectra of multiple measurements: 30 measurements for cutting and 5 measurements for pure tissue. All obtained measurements can be found in Appendix C.

In the DR signal of coagulated adipose tissue in Figure 41 (right), all characteristics of pure adipose tissue can be found. The deviation of the coagulated adipose tissue compared to pure adipose tissue is very little. The second peak between 500 and 600nm is elevated and the double peak around 100nm is flattened.

8.4. Discussion

Measurements

Observing the Dt, Dg, Wt and Wg for various settings gave some important insights. First, for both cutting and coagulation there was no relation between the increasing power setting and an increasing depth or width of the cut. These results correspond to the findings of Julie Fleischer. [2] There was a relation observed between the increasing power setting and the Zg in muscle tissue. This results complies with the findings by Taheri et al. [67] For adipose tissue, no coagulation zone was observed. In general, the Wt and Wg was higher for adipose tissue compared to muscle tissue. The same holds for Dg.

The average Dt including power of 50 to 80 Watt is 0.72mm for muscle tissue and 0.65mm for adipose tissue. However, the depths can deviate from 0.27mm to 1.5mm in muscle tissue and from 0.28mm to 1.4mm in adipose tissue. These numbers are relevant when considering the clear margin needed for a BSC. Currently, a guideline during surgery is a resection margin of 5 to 10mm. However, the size of the tumour-free resection margin (>1mm) is unrelated to local recurrence. If the threshold of detection for a 'smart' electrosurgical knife of a tumour would lay at 2mm, it would be possible to not detect the tumour at 2.1mm distance and then cut with a maximum depth of 1.5mm or 1.4mm. This would result in a margin

of 0.6mm in muscle tissue and 0.7mm for adipose tissue. More research should be performed on the cutting depth for electrosurgical cutting and coagulation at different power setting to draw a conclusion about the margin depth that should be regulated. The same holds for coagulation with a mean Dg of 0.43mm for muscle tissue and 0.71mm for adipose tissue. The depth can deviate from 0.20mm to 1.16mm in muscle tissue and from 0.23mm to 1.56mm in adipose tissue. Therefore, a using a margin of 2mm could also jeopardize the resection margin of >1mm.

Accuracy measurements

To make the cuts and coagulation of the tissue more precise, a linear actuator was used. This made it possible to make cuts and coagulate with a specific depth of 0.2mm. An additional benefit of using the linear actuator is the minimization of vibrations and barely no variation in cutting angle while cutting. However, the tissue used was not flat. For every measurement, the knife was placed on the tissue without pressing on the tissue. From there the knife was put in the right setting and pushed 0.2mm down by the linear actuator. The non-flat surface of the tissue can decrease the accuracy of the measurement. However, by using the linear stage actuator, the experiment was limited to holding the knife parallel to the tissue instead of perpendicular. This is different from the use in the clinic as described in Chapter 6.

The measurements itself where performed with a microscope (Leica, Wetzlar, Germany). The calibration was done by putting a ruler into the image and adjusting the scale. Measuring Dt and Dg was done by measuring the deepest point of the cut to the surface of the tissue. This measurement was most of the time easy to perform. However, measuring Wt and Wg can have a decreased accuracy while the measurements points where less straightforward. The width was measured by taking the average width of the cut. In addition, the cut or coagulation layer was not always that clear, which makes the measurements prone to subjectivity. The accuracy of the measurements is estimated to be ± 0.1 mm. The coagulation zone was measurable in muscle tissue due to the change in colour, which can be seen in Figure 40. However, the coagulation zone is not uniform, which makes it more difficult to measure this correctly. The coagulation zone was therefore measured at the deepest point of the cut. Although, again the transition between layers was not always clear which makes the measurements prone to subjectivity. Repeatedly, the accuracy of the measurements is estimated to be ± 0.1 mm.

It needs to be considered that the measurements in this thesis are performed on adipose and muscle tissue of a pork instead of adipose human tissue and tumour tissue. These tissue types were easy and cheap to obtain and do not have ethical restrictions for experiments as human tissue does. The measurements – both for performed on the microscope and the DR spectra – are therefore not directly related to a breast conserving surgery. DRS measurements of human tumour tissue can be found in research of Boer et al. among others. [1] Different types of adipose tissue in DR spectra are discussed in Paragraph 13.4.

DR spectra

In general, there appears more deviation in the DR spectra for coagulated muscle tissue compared to cut muscle tissue. This corresponds to the visual changes in cut and coagulated muscle tissue during the experiments. The cut muscle tissue has less charring and no coagulation zone, while coagulated muscle tissue contained charring and has a coagulation zone. When comparing cut and coagulated muscle and adipose tissue, the adipose tissue appears to be more similar to the pure adipose tissue than the muscle tissue is with pure muscle tissue. This – again – corresponds with the visual changes during the experiments

where muscle tissue showed charring and a coagulation zone and adipose tissue did not. Increasing the power of the cut in muscle tissue increases the deviation of the spectra compared to the spectra of pure tissue. For coagulated muscle tissue, this effect is less clear.

No clear trends can be discovered when comparing Dt, Dg, Wt and Wg to DR spectra of cut or/and coagulated muscle tissue and adipose tissue. However, the Dt, Dg, Wt and Wg values of adipose tissue differ less – for various power settings – compared to these values of muscle tissue. This can be connected to the DR spectra where more deviation is present in cut and coagulated muscle tissue compared to cut and coagulated adipose tissue.

Accuracy DR measurements

To create an experiment with a high accuracy, the experimental conditions where held constant. The measurements where performed including as little light as possible, the same probe with a FD of 3nm was used and the probe was held by the linear stage actuator to prevent vibrations and variations in the angle between the probe and the tissue.

Conditions that can have decreased the accuracy of the DR spectra are the following. First, the tissue was placed in the freezer for multiple days if not directly used. This was necessary to be able to perform all depth and width measurements and DRS measurements on the same tissue. Second, it was intended to place the probe – without any pressure – on the tissue. However, while measurements are performed in the dark, this cannot be confirmed with certainty. Therefore, the measurements can be performed pressing on or not touching the tissue entirely, which could affect the accuracy of the measurement. Third, before a measurement is made, the surrounding light is measured to extract this from the detected light. However, if a measurement is made too quickly, this process can be interrupted. Both the second and third condition are thought to be the reason that single DR spectra are not similar to the other spectra in the same plot.

9. Tissue interaction: no cutting

To improve margin assessment in breast conserving surgery, the electrosurgical knife should be able to differentiate between tumour tissue and adipose tissue. For this experiment, the transition between the adipose and muscle tissue will be examined regarding the DR spectra. In Chapter 8, the differences between the DR signal of adipose and muscle tissue are described.

First, the transition in raw DR spectra will be discussed. With thin layers of adipose tissue, measurements could be made upon tissue layers laying on muscle tissue. Raw spectra of muscle tissue, a layer of 0.4mm, 0.8mm, 1.2mm, 1.6mm and 2mm adipose tissue are shown. The transition of DR spectra from muscle tissue to adipose tissue will be observed. Second, the variation in this transition will be discussed regarding a change in FD of the probe. Measurements are performed with probes having FDs of 3.25mm, 3.75mm, 5mm and 6.2mm. Third, the regions in which the transition is most dominant will be described. These transitions can be linked to transitions in chromophore concentrations, as described in Paragraph 3.4.1. The change in chromophore concentrations are plotted to examine which change in concentration is most powerful. Chromophore concentrations where a significant difference between muscle and adipose tissue is found are discussed. These curves are expected to be as described in Paragraph 3.4.2.

9.1. Materials

Specimens

For this experiment porcine adipose and porcine muscle tissue was used. The porcine muscle tissue was received from LifeTech and the adipose tissue of 'Slagerij Lelieveld'. These specimens, Figure 43, will represent the clinical setting of a tumour within the breast, the porcine adipose tissue represents the human adipose tissue and the porcine muscle tissue represents the tumour tissue. The muscle tissue was cut into slices of 1.5 cm in the lab. The adipose tissue was cut in slices of 0.4mm when frozen at the butcher. Both specimen where frozen when not used. When used for measurements, the specimen was outside of the freezer for at least two hours to thaw.

Figure 43: Specimen used for the experimental setup in Chapter 9, 10 and 11. Layers of adipose tissue with a thickness of 0.4mm on top of muscle tissue with a thickness of 1.5cm.

Instruments

Three types of probes where used to achieve various fiber distances. The 'large' probe was used for the fiber distances of 3.25mm and 3.75mm. To achieve a larger fiber distance, two small probes where attached to each other, therefore fiber distances of 5mm and 6.2mm could be made. The 'large' probe can be seen in Figure 44 and the combination of the probes can be seen in Figure 45.

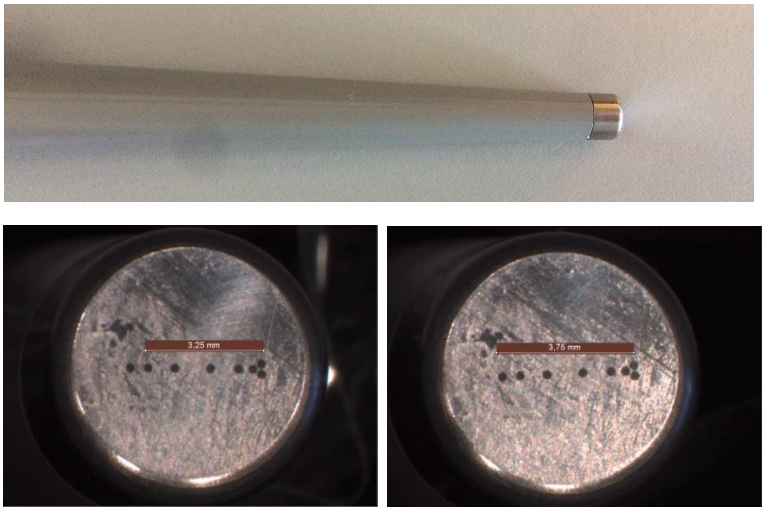

Figure 44: 'Large' probe with fiber distances of 3.25mm (bottom left) and 3.75mm (bottom right). At the top, a side view of the probe is shown. Bottom left and right are front views of the probe, made with a microscope (Leica, Wetzlar, Germany) on 2.5x.

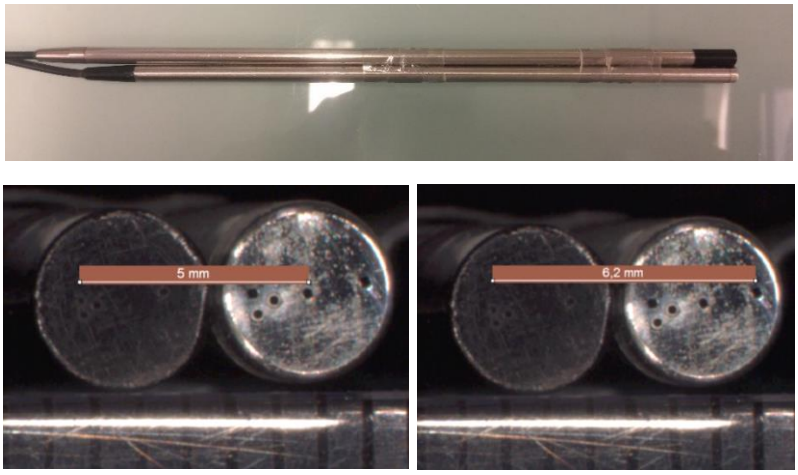

Figure 45: Two probes attached to each other in a side view (top), fiber distances of 5mm (bottom left) and 6.2mm (bottom right) can be made with this combination. Bottom left and right are front views of the probe, made with a microscope (Leica, Wetzlar, Germany) on 2.5x.

A disposable scalpel (Swann-Morton, Sheffield, England) and a stainless steel meat-knife (Albert Heijn, The Netherlands) were used to cut the tissue into slices. Tweezers are used to pick up the layers of fat tissue. The tissue was placed on petri dishes when making the measurements.

Equipment

In Figure 46 the setup of this experiment is shown. The specimen to be examined is muscle tissue with multiple fat layers of 0.4mm upon it. A probe with fiber distances 3.25mm and 3.75mm is connected to two white light consoles and a VIS and NIR spectrometer to detect the light coming from the tissue. The latter two are connected to a laptop where the PNSas software uses these inputs to create DR spectra. Before starting the measurements, the signal was calibrated on a white thing. The software uses the calibrated signal and stiches the VIS and NIR signal together. A linear stage actuator is used to place the probe precisely on the tissue and to exclude vibrations. Both would be more difficult when using a hand instead of the linear stage actuator to hold the probe.

The PNSas software requests some settings, which were an integration time of 0.5 sec for both the VIS and NIR measurement.

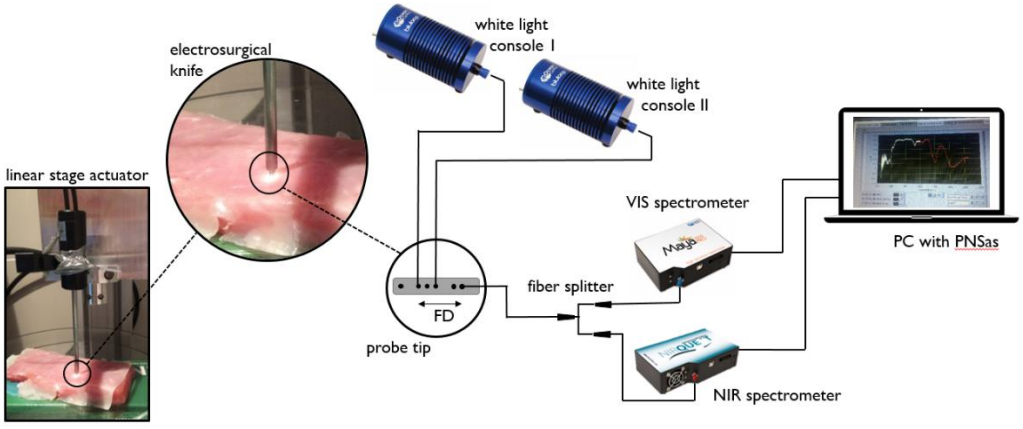

Figure 46: Experimental setup including a linear stage actuator, a probe, white light, VIS spectrometer, NIR spectrometer and a PC including PNSas software.

After obtaining the spectra, also the chromophore concentrations per measurement can be read from the XlsOut file. Calculating the significance between the measured chromophore concentrations at the muscle tissue (0mm) and adipose tissue (2.4mm) was done in excel. Both rows of chromophore concentrations are used in the command T.TEST where a two-tailed distribution and a heteroscedastic t test is performed. Heteroscedasticity is used when the two datasets have a difference in variance.

9.2. Method

The dependent variable, the one that is measured in this experiment, is the DRS signal. This signal will change due to variations in the independent variables, which can be seen in Table 7. The independent variables are the depth of the fat layer upon muscle tissue and the fiber distance of the probe. In addition,

some of the variables will be controlled to secure they will not influence the results. The controlled variables in this experiment are the angle of the probe relative to the tissue, the muscle tissue and fat layers, which stay the same for the whole experiment.

To acquire the spectra as showed in this chapter, some steps were performed. A calibration was performed – as discussed in Paragraph 8.2 – and the integration time were set on 0.5 second for VIS and 1 second for NIR. After retrieving the spectra, they were normalized by setting the maximum value at one.

Table 7: Condition matrix with 24 different experimental conditions, 30 trials per condition and the independent variables fiber distance and depth of the fat layer (upon muscle tissue). The dependent variable is the DR spectrum.

		Depth fat layer in mm (upon muscle tissue)					
Fiber distance	n = 30	**0**	**0.4**	**0.8**	**1.2**	**1.6**	**2.0**
	3.25mm	EC11	EC12	EC13	EC14	EC15	EC16
	3.75mm	EC21	EC22	EC23	EC24	EC25	EC26
	5mm	EC31	EC32	EC33	EC34	EC35	EC36
	6mm	EC41	EC42	EC43	EC44	EC45	EC46

9.3. Results

9.3.1. Raw spectra of pure tissue

In Figure 47, the DRS signals of a tissue transition from muscle tissue to adipose tissue with a FD of 6.2mm can be seen. All signals in this plot are the mean of 30 measurements for each condition. All measurements can be found in Appendix D. The red line represents the mean of the spectral measurements performed upon the muscle tissue. The blue line represents the mean of the spectral measurements performed upon 2.4mm of adipose tissue layers. The other lines represent the transition from muscle to adipose tissue. Every layer has a thickness of 0.4mm. A visualization of this setup can be seen in Figure 48.

The transition from a typical DRS signal for muscle tissue makes a transition towards a typical DRS signal for adipose tissue when increasing the depth of the adipose tissue layer. This transition starts from a layer depth of 0.8mm. The transition posterior to 0.4mm runs smoothly in the NIR region (from 700 to 1600nm). For the VIS region, the transition is less noticeable while the shape of the plots are different. However, also in the VIS region the transition from 0.8mm to 2.4mm is present.

Besides the transition of the plots, some observations can be made. Around 700nm, both 0mm and 2.4mm do not have a dip however all plots in between do have a dip here. The graph of 0.4mm has a lower intensity around 1000nm and between 1100 and 1400nm. Therefore, all other graphs – in transition between 0mm and 2.4mm – are in between these two plots and the graph of 0.4mm is not.

All characteristics for pure muscle and adipose tissue – described in Paragraph 8.3.3 – can be found in the plot for 0mm (muscle tissue) and 2.4mm (adipose tissue). However, the plateau between 600 and 1100nm is more flat in Figure 47 compared to Figure 41 (right) where the pure adipose tissue is measured.

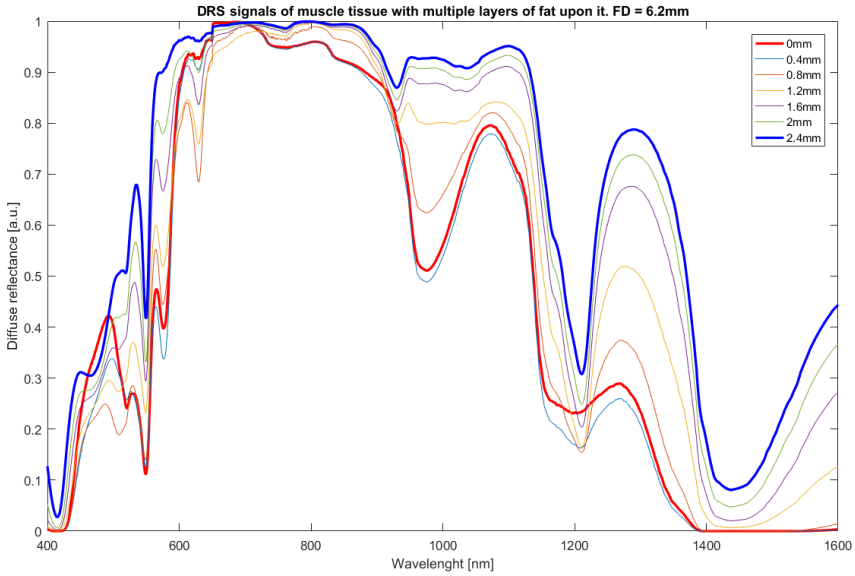

Figure 47: DR signal of the transition from muscle tissue (0mm) to adipose tissue (2.4mm) in steps of smaller layers of 0.4mm adipose tissue upon the muscle tissue. The spectra in this figure are the means of 30 measurements per condition. All measurements from which these means are constructed can be found in Appendix D. A FD of 6.2mm was use to obtain these DR spectra.

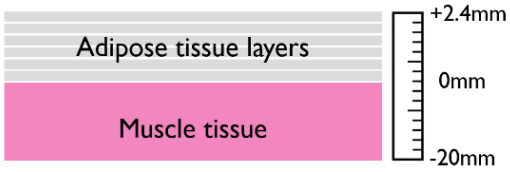

Figure 48: Visualization of the specimen used for the experiment. The 0 line is the transition from muscle tissue to adipose tissue. Every layer on top of the muscle tissue is an addition of 0.4mm of adipose tissue.

9.3.2. Raw spectra of pure tissue with various fiber distances

In Appendix D, all measurements described in Table 7 are shown. Besides the transition with a FD of 6.2mm – as described in Paragraph 9.3 – also FDs of 3.25mm, 3.75mm and 5mm are shown. For all figures, 30 measurements where performed and a mean is plotted in the same figure. Therefore, the transition from muscle tissue (0mm) to an adipose tissue layer of 2.4mm can be seen. Again, the transition is made from muscle tissue to adipose tissue within steps of 0.4mm adipose layers, as can be seen in Figure 48.

When comparing the figures, it can be seen that the plots of all fiber distances make a visible transition from muscle tissue to adipose tissue. The first change in spectra can already be seen at 0.4mm for all FDs. However, this transition is not identical for all fiber distances. For a FD 3.25mm and 3.75mm the double peak between 500 and 600nm has a higher intensity than for a FD of 5mm and 6.2mm. For all FDs, the transition from pure muscle to pure adipose tissue results in an increase in the height of the double oxygen peak between 500nm and 600nm. However, this peak has a higher starting point for the FD of 3.25mm and 3.75mm.

Another difference that can be seen in the plots is the increase in intensity of the 500nm to 700nm region for larger FDs. For muscle tissue, this region exists of a valley followed by a peak. However, this transforms into two small peaks for adipose tissue. In addition, the peak around 900nm and the peak from 1000nm to 1200nm have a higher intensity for bigger FDs.

The transition for all spectra starts at 0.4mm where a deviation in spectra can be seen compared to pure muscle tissue. However, spectra of different FDs retrieve their equilibrium at different points. A FD of 3.25mm and 3.75mm retrieves its equilibrium – the typical adipose tissue spectrum – at 1.2mm. For a FD of 5mm this happens at 2mm and for a FD of 6.2mm no major changes are observed after at 1.6mm.

9.3.3. Chromophore concentrations

As described in Paragraph 3.4.1, the DR spectra are fits composed of percentages of chromophore concentrations in the tissue. Therefore, peaks with a high intensity in the DR spectra will most likely conclude in a higher percentage of chromophore concentration for that specific condition. In the DR spectra described in Paragraph 9.3 and 9.3.2, a high peak between 1200nm and 1400nm is observed for adipose tissue. This peak is not yet present for muscle tissue. Considering this peak to be composed of adipose lipids, it can be assumed the fat/water ratio will change in the transition from muscle to adipose tissue.

In Figure 49, the chromophore concentration for the transition from muscle tissue (0mm) to adipose tissue (2.4mm) is shown. All boxplots include 30 measurements per condition. The title of the plots represents the chromophore condition described in the plot: fat-water ratio (upper left), oxygen saturation (upper right), Mie scattering (bottom left) and blood (bottom right). All measurements are performed with a FD of 6.2mm.

The fat-water ratio present an average ratio of less than 10% at 0mm while at 2.4mm the average ratio is higher than 90%. Comparing the measurements at 0mm and 2.4mm, a p-value of $1.28e^{-39}$ is found. It is common to describe a difference with a p-value <0.05 as significant. Therefore, the change in fat-water ratio is called significant. The p-values of the chromophore concentrations extracted from the PNSas model can be found in Table 8. Other chromophore concentrations with a significant difference between the muscle and adipose tissue are StO_2, blood percentage and b. All are obtained with a FD of 6.2mm. For StO_2, a difference in concentrations can be seen comparing 0mm – with an average concentration of 26% - to 2.4mm with an average concentration of less than 10%. However, the concentration StO_2 starts to increase from 0mm to 0.4mm and then declines from 0.4mm to 2.4mm. The p-value of StO_2 is $4.81e^{-15}$ and therefore the difference between muscle and adipose tissue for StO_2 is called significant. Observing the blood concentration in the transition from muscle to adipose tissue, a decline in concentration can be seen. The change in percentage is smaller than for the fat-water ratio, from a maximum of 0.5% to 0% and the dissemination of the data is high for 0mm, 0.4mm and 0.8mm. Still, the p-value of $9.93e^{-7}$ is significant. The plot describing the chromophore concentration of b for 0mm to 2.4mm shows no visible differences. However, the p-value is 0.014 and therefore the difference between the values at 0mm and 2.4mm is significant. When observing the values in the XlsOut, differences in the concentrations for b are visible at $1 \cdot e^{-10}$.

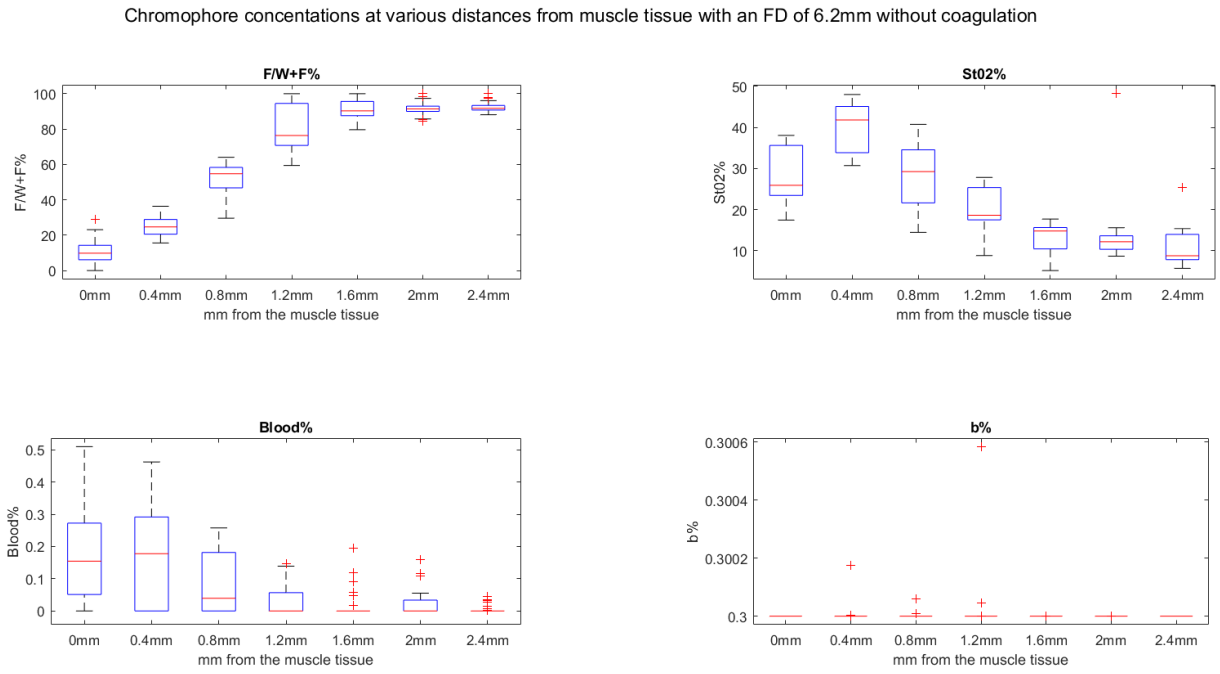

Figure 49: Chromophore concentrations for the transition from muscle tissue (0mm) to adipose tissue (2.4mm). All boxplots include 30 measurements per condition. The title of the plots represents the chromophore condition described in the plot: fat-water ratio (upper left), oxygen saturation (upper right), Mie scattering (bottom left) and blood (bottom right). All measurements are performed with a FD of 6.2mm.

Other coefficients that can be extracted from the PNSas model are α, S_{800} and F_{mie}. The concentrations of these scattering coefficients can be seen in Appendix E. S_{800} does not change for muscle and adipose tissue, they are stationary at 0.3% and 4% respectively excluding a few deviations. The concentration of α starts at 10% for muscle tissue, then the values drop for 0.4mm and 0.8mm with a minimum of 7%. From 1.2mm, the average concentration of α is at 10% again. The concentration Mie scattering starts and ends with an average of 1 at 0mm and 2.4mm respectively. However, between 0mm and 2mm values lower than 1 are measured. These values are not taken into account for calculation of the p-value as this calculation only distinguishes between the values at 0mm and 2.4mm. With p-values of 0.285, 0.05 and 0.36 for α, $s800$ and F_{mie} respectively these chromophore concentrations are not found significant.

Table 8: P-value of chromophore concentrations from the PNSas model. All p-values are obtained by comparing the 0mm values (upon muscle tissue) to the 2.4mm values (upon 6 layers of adipose tissue) from the XlsOut excel sheet. The difference in chromophore concentrations is called significant for a p-value <0.05. The p-value is calculated as 2 tailed and heteroscedastic.

Chromophore concentration	P value
Fat/water-ratio	$1.28e^{-39}$
$\boldsymbol{StO_2}$	$4.81e^{-15}$
$\boldsymbol{F_{mie}}$	0.3605
$\boldsymbol{b}$	0.014
$\boldsymbol{\alpha}$	0.285
Blood	$9.93e^{-7}$
$\boldsymbol{s800}$	0.050

9.4. Discussion

DR spectra

This chapter focused on the transition from pure muscle tissue to pure adipose tissue – in layers of 0.4mm – without cutting. The transition – showed in Figure 47 – is clearly visible. Especially when focusing on the characteristics for muscle and adipose tissue, described in Paragraph 9.3. However, minimal changes between the spectrum of pure muscle and pure adipose tissue can be seen when comparing the spectra in Chapter 8 to the spectra this chapter. A change is the intensity of the plateau between 600 and 1100nm in this chapter. This is due to the use of another type of muscle and adipose tissue. In Chapter 8, pork belly tissue was used while this is a cheap type of tissue containing both adipose and muscle tissue in one piece. This specimen is readily available at the super market. For the experiments in this chapter, larger pieces of muscle tissue were needed to provide a solid basis with a controlled height. In addition, very thin layers of adipose tissue were needed to simulate the transition from muscle to adipose tissue. These thin layers of 0.4mm could only be cut from sowbelly tissue.

Excluding the minimal changes in DR spectra between the types of muscle and types of adipose tissue, the overall transition from muscle to adipose tissue can be clearly seen. This is a satisfying starting position, which gives the confidence to proceed with the experiments including cutting. The transition can be observed for all FDs used. As described in Paragraph 3.5, it would seem logical that the transition occurs faster for small FDs compared to large FDs. This is true for the plots in Appendix E.

When a peak has a higher intensity in a plot, it can make it easier to distinguish between – in this case muscle and adipose – tissues. In clinical setting, it is important to have a high accuracy of your measurements. The regions with a high intensity and the regions where there is a considerable change in spectrum will therefore be of importance for this research. In Figure 47 the peak between 1200 and 1400nm has a high intensity. This peak refers to the fat concentration in the tissue. This clear transition can also be seen when looking at the chromophore concentrations.

Chromophore concentrations

PNSas software makes it possible to extract various chromophore concentrations from the measurements. Comparing all transitions in Figure 49 and the p-values in Table 8, the fat-water ratio is definitely the best variable to distinguish between muscle and adipose tissue. The transition for a FD of 6.2mm is smooth which could help identifying the distance to the tumour surrounded by adipose tissue in a tumour margin assessment. In addition, StO_2, b and blood percentage can also be used while a variation between muscle and adipose tissue is also present here. All show a significant difference with a $p < 0.05$. However, the difference between the values at 0mm and 2.4mm is not visible in the plot for b. This is caused by the differences in values at $1 \cdot e^{-10}$. For making a distinction between two tissues in clinical practice, a high accuracy is desirable. Therefore, larger difference between values is superior to smaller differences.

De Boer et al. studied the differences in chromophore concentrations in pure adipose human tissue and pure muscle human tissue. [1] She points out three optical parameters as the best parameters for discrimination between benign and tumour tissue; fat-water ratio, StO_2 and Mie scattering with a p-value of $< 1.0\,x\,10^{-7}$, 0.004 and $1.3\,x\,10^{-7}$ respectively. De Boer does not describe a significant

difference for b and blood concentration in contrast with the results obtained in this thesis. In addition, she describes a significant difference for Mie scattering which had a p-value < 0.05 in this thesis. These differences can be due to the differences in tissue human versus pork), the treatment of the tissue (unknown versus multiple hours in the freezer), fiber distances (1.5mm versus 6.2mm) and number of measurements (169 versus 30). All data in parentheses contains information about the experiment of de Boer et al. on the left and information about the experiments in this thesis on the right. De Boer et al. performed another experiment on the change in chromophore concentrations in healthy and benign breast tumour tissue *in vivo* and *ex vivo*. [79] The included chromophore concentrations were fat-water ratio, StO_2, b, Mie scattering and blood. No significant difference between the values obtained *in vivo* and *ex vivo* was found. These results would imply the results obtained in this experiment would not change significant if obtained *in vivo*.

The plots of StO_2, Mie scattering, blood and α show a dip or a peak which deviates from the logical transition between muscle and adipose tissue. An explanation of this dip or peak could be the mix of muscle and adipose tissue in the sensing zone of the probe, compared to the pure muscle tissue at 0mm and the almost pure adipose tissue at 1.2mm.

Fiber distance

To be able to see the transition between muscle and adipose tissue, a large FD will provide the smoothest transition. Therefore, the FD of 6.2mm is used in further chapters to be able to provide the most information about the transition. However, there are some aspects that will influence the FD that will be chosen for clinical use. First, when the fibers are connected to the electrosurgical knife – as is currently done – the FD cannot deviate too much from the width of the knife. The knife which was used for the experiments in Chapter 8 and 11 had a width of 2.5mm. When using the same cutting blade, an FD of 6.2mm would mean the fiber is places 1.8mm next to the blade. A second aspect, is the margin of 2mm used for a clear margin in breast cancer. For a FD of 6mm, the tumour tissue cannot be detected after a depth of 0.8mm. A margin of 0.8mm would be designated as a positive margin and therefore lead to an extra surgery. Ideally, the muscle tissue can be detected from a decrease in fat-water-ratio at 2mm. Therefore, a probe with a FD of more than 6.2mm is needed.

Accuracy experiments

For these experiments, it was chosen to use layers of 0.4mm thickness to simulate the transition between muscle and adipose tissue in a controlled way. However, this advantage of having a controlled setting also involved some drawbacks. It was not possible to use pure adipose tissue, while this falls apart when it is cut this thin. Therefore, sowbelly was used while this had – similar to adipose tissue – a high fat percentage. However, it was observed that sowbelly layers react differently to electrosurgical cutting than pure adipose tissue. This can be due to the layer structure of the tissue and/or the difference in tissue. In addition, using layers of tissue made it possible that air can come between the layers. This was prevented as much as possible by using tissue forceps to push the air to the sides of the piece of tissue and then from under need the layers of sowbelly.

Two different probes where used for the experiments in this chapter. The first one, used for FDs of 3.25mm and 3.75mm, is a normal probe. The second one, used for creating FDs of 5mm and 6.2mm, where two probes taped together. There was no probe available with a FD larger than 3.75mm, therefore taping two probes together was an possibility to obtain a larger FD. However, this 'handmade' probe can

affect the accuracy of the measurement while the probes can move relative to each other and there is a possibility the fibers are not in one straight line. In addition, comparing the measurements for a FD of 3.25mm and 3.75mm and a FD of 5mm and 6.2mm can give a biased view while the accuracy of the latter – 'homemade' – probe is less compared to the former – real – probe. Looking back, it would have been better to also perform measurements with the 'homemade' probe with a FD of 3.25mm or 3.75mm to be able to compare these measurements to the ones made with the real probe.

10. Tissue interaction: cut tissue

In Chapter 9, the transition in DR spectra from pure muscle tissue to pure adipose tissue is described. The results are satisfying: the transition in DR spectra can be seen clearly and a significant difference in chromophore concentration is present for fat-water ratio, StO_2, blood and b. In this chapter, the experiment will be repeated, however now cut adipose tissue is used. This will provide a step forward towards the clinical setting. Similar to Chapter 9, adipose tissue layers will be used to be able to control the depth of the tissue layer.

In Paragraph 8.3.3 and 8.3.4, the changes in DR spectra for cut tissue are discussed. The overall shape of the graph did not change for cut adipose tissue compared to pure adipose tissue. Although another type of adipose tissue is used compared to Chapter 9, it is expected to see the changes for cut adipose tissue again in this experiment. Changes regarding the variation in adipose tissue type are discussed in Paragraph 13.4. The influence of electrosurgical cutting in adipose tissue – described in Paragraph 8.3.3 and 8.3.4 – are:

- the VIS region has a lower intensity for cut adipose tissue compared to pure adipose tissue; including the double oxygen peak between 500nm and 600nm and the plateau from 600nm until 700nm.
- The NIR region has a higher intensity for cut adipose tissue compared to pure adipose tissue; including the plateau from 700nm to 1100nm and the dip at 1200nm.
- The peak after 1400nm has a lower intensity for cut adipose tissue compared to pure adipose tissue.

10.1. Materials

Specimens

For this experiment porcine adipose and porcine muscle tissue was used. The porcine muscle tissue was received from LifeTech and the adipose tissue from 'Slagerij Lelieveld'. These specimens, Figure 43, will represent the clinical setting of a tumour within the breast, the porcine adipose tissue represents the human adipose tissue and the porcine muscle tissue represents the tumour tissue. The muscle tissue was cut into slices of 1.5 cm in the lab. The adipose tissue was cut in slices of 0.4mm when frozen at the butcher. Both specimen where frozen when not used. When used for measurements, the specimen was outside of the freezer for at least two hours to thaw.

Instruments

Three types of probes where used to achieve various fiber distances. The large probe was used for the fiber distances of 3.25mm and 3.75mm. To achieve a larger fiber distance, two small probes where

attached to each other, therefore fiber distances of 5mm and 6.2mm could be obtained. The large probe can be seen in Figure 44 and the combination of the probes is shown in Figure 45.

Equipment

After the tissue is being cut with an electrosurgical knife connected to an electrosurgical unit, the spectra can be measured. A setup for the cutting of tissue can be found in step 1 of Figure 34. In Figure 46, the setup used to obtain a DR spectrum is shown. Besides cutting in the adipose tissue layers, no changes were made in the setup compared to the setup described in Chapter 9.

10.2. Method

The dependent variable – the variable measured in this experiment – is the DRS signal. This signal will change due to variations in the independent variables, which can be seen in Table 9. The independent variables are the depth of the adipose tissue layer upon muscle tissue and the fiber distance of the probe. In addition, some of the variables will be controlled to secure they will not influence the results. The controlled variables in this experiment are the angle of the probe relative to the tissue, the muscle tissue and adipose tissue, which stay the same during the entire experiment. In this experiment, the chromophore concentrations are obtained in the same way as described in Chapter 9 as the calculation of the p-values.

To acquire the spectra as showed in this chapter, some steps were performed. A calibration was performed – as discussed in Paragraph 8.2 – and the integration time were set on 0.5 second for VIS and 1 second for NIR. After retrieving the spectra, they were normalized by setting the maximum value at one.

Table 9: Condition matrix with 24 different experimental conditions, 30 trials per condition and the independent variables fiber distance and depth of the fat layer (upon muscle tissue). The dependent variable is the measured DR spectra.

		Depth fat layer in mm (upon muscle tissue)					
Fiber distance	n = 30	**0**	**0.4**	**0.8**	**1.2**	**1.6**	**2.0**
	3.25mm	EC11	EC12	EC13	EC14	EC15	EC16
	3.75mm	EC21	EC22	EC23	EC24	EC25	EC26
	5mm	EC31	EC32	EC33	EC34	EC35	EC36
	6mm	EC41	EC42	EC43	EC44	EC45	EC46

10.3. Results

10.3.1. Raw spectra of cut tissue

Figure 50, shows the transition from muscle tissue (0mm) to cut adipose tissue (2.4mm). The measurements are obtained with a FD of 6.2mm. The transition is executed in steps of 0.4mm, with adipose tissue layers of the same thickness. A visualization of this setup can be seen in Figure 48. The red line represents the mean of the spectral measurements performed upon the muscle tissue. The blue line

represents the mean of the spectral measurements performed upon 2.4mm of adipose tissue layers. The other lines represent the transition from muscle to adipose tissue. All spectra in Figure 50 are the mean values of the 30 measurements performed per experimental condition. All measurements and their means values can be found in Appendix F.

The spectrum for muscle tissue (0mm) has the same characteristics as the muscle tissue described in Paragraph 8.3.3. When comparing it to the transition from pure muscle to pure adipose tissue – in Figure 47 – three differences can be seen in the spectra for muscle tissue. The double oxygen peak between 500 and 600nm and the peak between 1200 and 1400nm have a lower intensity. However, the small peak at 650nm has a higher intensity. Changes are present in the VIS spectrum comparing cut adipose tissue – in Figure 50 – to pure adipose tissue in Figure 47. All peaks and dips present in the spectrum of pure adipose tissue are flattened in the spectrum for cut adipose tissue. In the NIR region, a small peak at 1400nm is present which was not present for pure adipose tissue.

The steps of 0.4mm in between the graphs of 0mm and 2.4mm provide a gradually transition between the two extremes.

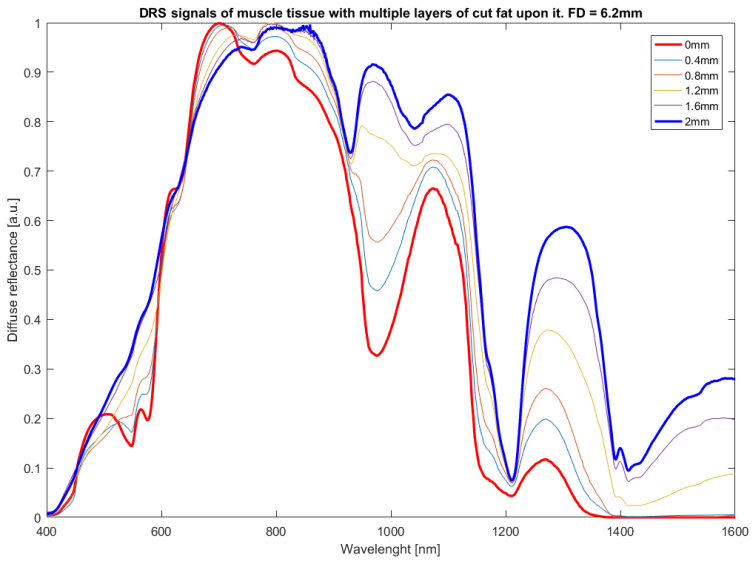

Figure 50: DR signal of the transition from muscle tissue (0mm) to cut adipose tissue (2.4mm) in steps of smaller layers of 0.4mm cut adipose tissue upon the muscle tissue. All spectra are mean values of 30 measurements, which can be found in Appendix F. A FD of 6.2mm was use to obtain these DR spectra.

For this experiment, measurements are performed using four different FDs: 3.25mm, 3.75mm, 5mm and 6.2mm. These measurements can be found in Appendix F. The observations for various FDs without cutting – described in Paragraph 9.3.2 – are listed below.

- All FD show a visible transition from muscle to adipose tissue from 0.4mm
- All FD show an increase in the height of the double oxygen peak when making the transition from muscle to adipose tissue
- Differences in transition for FDs are
  - Double peak between 500 and 600nm has a higher intensity for 3.25 and 3.75mm
  - Increase in intensity of the peaks between 900 and 1100nm, around 1300nm and after 1400nm for 5 and 6.2mm

Comparing the spectra of cut tissue to non-cut tissue, it can be noticed that the observations on all regions still hold, except for the oxygen peak between 400 and 600nm. The DRS plots of non-cut tissue for FD 5 and 6.2mm show less intensity in the 400 to 600nm region. However, for cut tissue the oxygen peaks in the same area totally disappear for FDs of 5 and 6.2mm.

The raw spectra of cut tissue make the following transitions from muscle to adipose tissue: all spectra start changing from 0.4mm. The plot regarding the FD of 3.25 and 3.75mm, transformed to adipose tissue at 0.8mm. The spectra measured with a FD of 5mm are stable at 1.6mm and the FD of 6.2mm still changed from 1.6mm to 2mm. The increase in the length of the transition for larger FD was already observed in Chapter 9.

10.3.2. Chromophore concentrations

In Paragraph 3.4.1, all chromophore concentrations available in PNSas are described. Three chromophore concentrations provided a significant difference between pure muscle and pure adipose tissue: fat-water ratio, StO_2, Mie scattering (f_{mie}) and blood percentage. These chromophore concentrations will be discussed again, however now for cut tissue.

In Figure 51 (upper left), the fat-water ratio can be seen for muscle tissue (0mm) and for every 0.4mm layer of adipose tissue added to come up to 2mm of adipose tissue. The transition from 10% at 0mm to 100% at 1.2mm can be seen clearly. After 1.2mm, the ratio reaches an equilibrium of 100%. The deviations in the plots are larger compared to non-cut tissue. A p-value of $3.32e^{-39}$ is calculated for the difference in fat-water ratio for muscle and adipose tissue. This p-value is < 0.05 and therefore called significant.

In addition, the percentage StO_2 is shown at various distances from the muscle tissue. Similar to the graph representing the StO_2 percentage for non-cut tissue, a clear distinction can be made between muscle tissue (30%) and adipose tissue (>60%). However, the graphs for cut and non-cut tissue look different. Both start around 30% for muscle tissue, but the graph for non-cut tissue ends at <10% for adipose tissue and the graph for cut tissue ends at >60%. The difference between muscle and adipose tissue is still significant with a p-value of $3.23e^{-27}$.

The percentage of Mie scattering (f_{mie}) for this experiment can also be seen in Figure 51 (bottom left). A distinction between muscle (0.825%) and adipose tissue (>0.9%) can be made on the mean values in this plot. However, the deviation of the measurements is large. Therefore, it is more difficult to clearly distinguish between muscle and adipose tissue, compared to the fat-water ratio plot. Comparing Figure 51 to Figure 49 – showing chromophore concentrations for pure tissue – a different shape of the plot representing Mie scattering is observed. For pure tissue, a dip between 0mm and 2.4mm is observed

though for cut tissue the curve has an ~-shape. The p-value of Mie scattering is $2.84e^{-8}$ and therefore significant.

The last significant difference between muscle and adipose tissue is found in the blood concentration. Again, the shape of the plot for blood concentration is different for cut tissue – in Figure 51 – compared to non-cut tissue in Figure 49. It starts at <0.2% at 0mm in muscle tissue and ends at >0.5% for 2mm in cut adipose tissue. The p-value of the change in blood concentration is $2.36e^{-9}$.

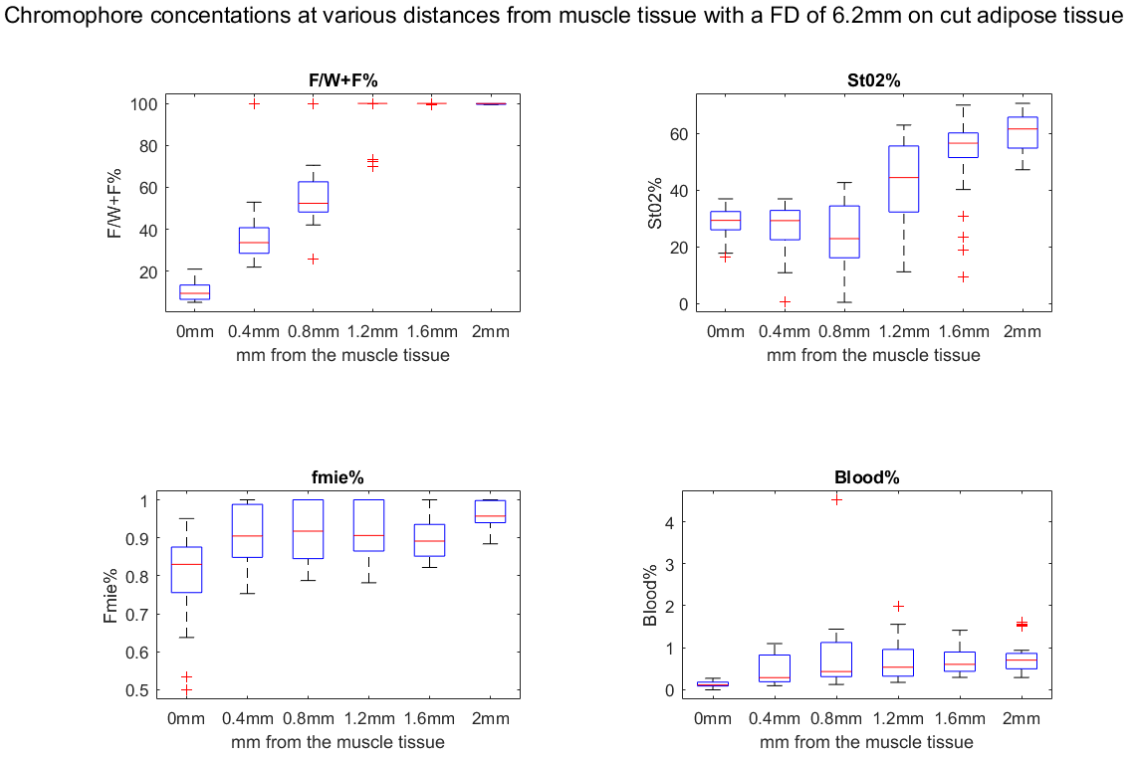

Figure 51: Chromophore concentrations obtained measuring the transition from muscle (0mm) to cut adipose tissue (2mm) in layers of 0.4mm. The transitions for fat-water ratio (upper left), StO2 (upper right), Mie scattering (bottom left) and blood (bottom right) concentrations are shown. The FD used to obtain these measurements is 6.2mm and all experimental conditions are performed 30 times.

The other chromophore concentrations present in PNSas did not provide a significant difference between muscle and cut-adipose tissue. This result is similar to the non-significant p-values described for pure tissue. The p-values for the fat-water ratio, StO_2, F_{mie} (Mie Scattering) and blood percentages are decreased relative to the p-values for the measurements on pure tissue in Chapter 9.

In Appendix G, the fat-water ratio can be seen for a FD of 3.25mm, 3.75mm, 5mm and 6.2mm. For 6.2mm, the graph reaches its equilibrium at 1.6mm for cut tissue. This is earlier than for non-cut tissue where it reaches its equilibrium at 2mm. For the other FD, this acceleration in reaching the equilibrium – compared to the Figure in Appendix E for pure tissue – is not present.

Table 10: P-value of the difference between muscle and cut adipose tissue for the chromophore concentrations: fat-water ratio, StO_2, F_{mie} and blood percentage.

Chromophore concentration	P value
Fat/water-ratio	$3.32e^{-39}$
$\boldsymbol{StO_2}$	$3.23e^{-27}$
$\boldsymbol{F_{mie}}$	$2.84e^{-8}$
Blood	$2.36e^{-9}$

10.4. Discussion

Raw DR spectra

For implementing DRS into an electrosurgical knife for better margin assessment, it is important to be able to distinguish between adipose and tumour tissue when cuts are made. In Chapter 8, the influence of electrosurgical cutting on muscle and adipose tissue is described. In Chapter 9, it was found it is possible to distinguish between muscle and adipose tissue with DRS. This chapter takes a step forward towards the real case by measuring DR spectra on cut tissue.

The DR spectra in this chapter still show the characteristics for muscle or adipose tissue, as they did for non-cut tissue. This makes it possible to distinguish between muscle and adipose tissue, which is needed for the 'smart electrosurgical knife'. The transition from muscle to adipose tissue starts (0.4mm) and ends at the same layer (1.6mm) as it did for non-cut tissue using a FD of 6.2mm. However, more deviation is present for cut tissue, especially between 1000 and 1200nm and between 1200 and 1400nm. This can be seen in Appendix F, where all measurements are shown. The largest visible dissimilarity is the disappearance of the oxygen peak between 400 and 600nm for cut tissue with a FD of 5 and 6.2mm.

Chromophore concentrations

All plots in Figure 51 show a difference between muscle (0mm) and cut adipose tissue (2mm). This is needed to distinguish between the two tissues for margin assessment. Comparable with the plots for non-cut tissue, the fat-water ratio shows the largest difference between muscle and adipose tissue. Therefore, this concentration seems the best option to look at in clinical practice. Besides examining the mean values of all plots, it is important to take into account the deviation of the measurements. Large deviations will make it difficult to achieve a high accuracy for tumour boundary detection.

When examining the StO_2 plot of non-cut tissue in contrast with the cut tissue, a non-expected observation is made. Both have the same values for muscle tissue (30%) however, for adipose tissue the non-cut plot gives <10% and the cut tissue >60%. While StO_2 represents the hemoglobin saturation by oxygen this would imply the haemoglobin is saturated by cutting the tissue with an electrosurgical knife. This result is counterintuitive with the known effect of cutting on blood, namely the conversion of haemoglobin to methaemoglobin. Haemoglobin has oxygen bind to it and this connection is lost after heating when the iron group – to which oxygen binds – changes and therefore cannot uptake oxygen anymore. [80]

A distinction between muscle (0.825%) and adipose tissue (>0.9%) can be made within the f_{mie} plot. For non-cut tissue, the difference between muscle and adipose tissue was not found relevant. In addition, the shape of the graph is different for cut tissue compared to non-cut tissue. A difference in outcome for cut and non-cut adipose tissue will decrease the accuracy when used in clinical practice.

Therefore, this chromophore concentration is found not satisfactory for margin assessment. In addition, the plot shows a large deviation in the measured values. For margin assessment, the difference between muscle and adipose tissue needs to be unmistakable.

The chromophore concentrations of StO_2, Mie scattering and blood have in common that they all are measured in the VIS region. Changes in this part of the spectrum can thus change these concentrations. As some charring can be present when cutting tissue – as can be seen in Figure 38 – this can affect the DR spectra in the VIS region.

The transition from muscle to cut-adipose tissue in fat-water ratio increases in length when a larger FD is used. This can be seen in Appendix G for cut tissue and in Appendix E for pure tissue. The observation seem logical while the sensing depth of the probe increases for larger FDs.

Accuracy experiments

Similar to the considerations described in Paragraph 9.4, the use of sowbelly and a 'homemade' probe will decrease the accuracy of the experiments. In addition to these considerations, a non-controllable aspect was used for the experiments in this chapter: electrosurgical cutting. As in Chapter 8, the cuts were made using a linear stage and the same setting and depth for every cut. However, while tissue is not entirely pure it can react differently to the same cut. In addition, electrosurgical cutting is not well visible in adipose tissue, which made it difficult to distinguish between cut and non-cut tissue. Another variable that changed – except for the tissue type – is its tissue form. Thin layers of 0.4mm where used instead of a thick layer. This could have affected the behaviour of the tissue during electrosurgical cutting.

11. Tissue interaction: while cutting

Chapter 8 and 9 describe the possibility to distinguish between muscle and adipose tissue for non-cut and cut tissue. Both confirm the feasibility of margin assessment with DRS. However, in practice the 'smart electrosurgical knife' is intended to distinguish between adipose and tumour tissue while cutting. Therefore, this chapter will simulate this action. Compared to Chapter 8 and 9, the experiments in this chapter are the least controlled, while electrosurgical cutting is a technique that entails uncertainties.

11.1. Materials

Specimens

Both specimen, muscle and adipose tissue of a pork, where obtained from LifeTech. The specimen where cut in slices of 3cm to be able to use them for the experiments. For cutting the specimen, a meat knife (Albert Heijn) was used. Both specimen where frozen when not used. When used for measurements, the specimen was outside of the freezer for at least two hours to thaw.

Instruments

To cut and obtain DRS measurements, an electrosurgical knife (Reliant) was used which can be seen in Figure 52. This knife is adjusted by Philips Research in order to obtain DRS. Two fibers are placed along the blade encapsulated in metal to protect them from the heat of the current. The tips of the fibers are exposed, as these need to emit or detect light.

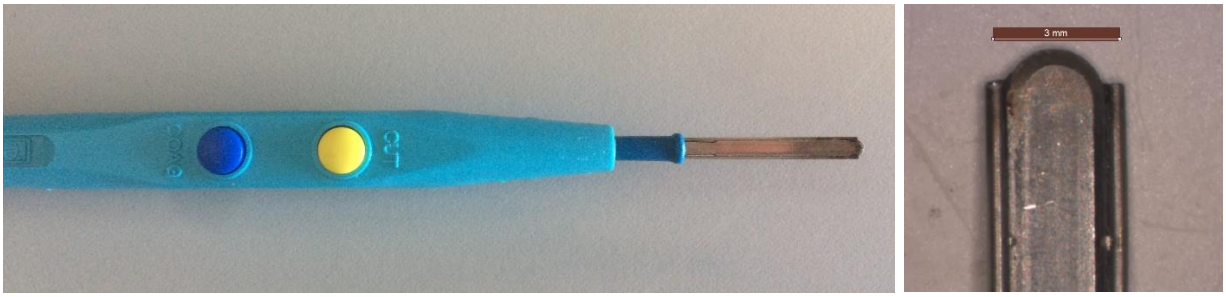

Figure 52: Electrosurgical knife (Reliant) including two fibers along the blade of the knife to be able to obtain DRS measurements. Left, the knife with two knobs to choose the setting. Right, a microscopic picture of the tip of the blade including the fibers.

Equipment

The setup in this experiment is a combination of the setups in Chapter 8, 9 and 10. The monopolar 'smart' electrosurgical knife is connected to an electrosurgical unit Force Fx (Valleylab, Boulder, United States). The electrical current flows from this unit, through the knife to the porcine tissue. The current leaves the tissue at the dispersive pad from where it returns to the electrosurgical unit. The power setting used is

80 Watt. To be able to cut and coagulate in a controlled setting, a linear stage actuator controlled by an ESP300 Universal motion controller (Newport, Irvine, United States) is used. During cutting, DR measurements are made. The 'smart' electrosurgical emits white light and detects light via a VIS and NIR spectrometer. Both transfer the detected light per wavelength to the PC with PNSas software. The PC stiches the spectra together to make it a continuous spectrum from 400 to 1600nm.

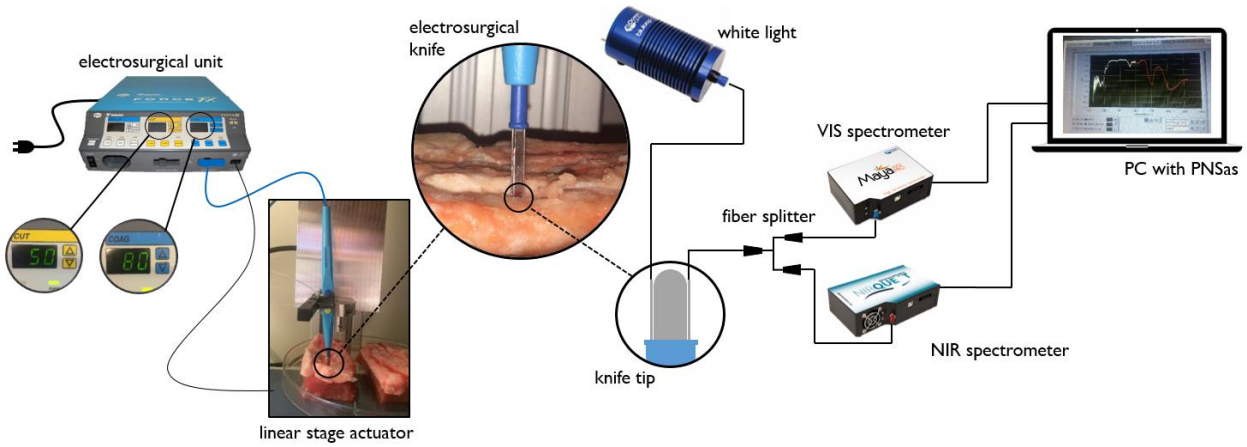

Figure 53: Experimental setup including an electrosurgical unit, dispersive pad, a linear stage actuator, an electrosurgical knife, white light, VIS spectrometer, NIR spectrometer and a PC including PNSas software.

11.2. Method

For this experiment, the independent variable is the depth of the knife while cutting. At 0mm, the knife is at the top of the muscle layer. All $> 0mm$ represent the knife being in adipose tissue, at the mentioned distance from the muscle tissue. All $< 0mm$ represent the knife being in the muscle tissue. This setup can be seen in Figure 48.

The 'smart' electrosurgical knife used to cut the tissue and obtain the DR spectra, can be seen in Figure 52. This instrument has a FD of 3mm. No other instruments were available to perform the same actions – electrosurgical cutting and measuring DR spectra – at ones. Therefore, no other FDs are used. The power used for electrosurgical cutting is set at 80Watt. The knife is placed in the adipose tissue at 3mm from the muscle tissue. A measurement is taken, after which the 'smart' electrosurgical knife cut for 1 second. Next, the knife moved 0.4mm downwards and the process was repeated. After 10 measurements – at -0.6mm in the muscle tissue – the measurements stops and the knife is brought to its starting position. The knife is cleaned with alcohol to remove the ablation on the cutting blade. Subsequently, the knife is placed at another spot in the tissue and the whole experiment is performed again. In total, 20 sets of measurements were made.

To acquire the spectra shown in this chapter, some additional steps are completed. A calibration is performed – as discussed in Paragraph 8.2 – and the VIS and NIR integration time are set on 0.1 second. After retrieving the spectra, they are normalized by setting the maximum value at one.

All spectra are examined on the correctness of the fit. A fit is 'bad' if a low or no signal is present, if the scattering coefficient is lower than the signal, or when the fit does not follow the measured spectrum. The conditions used to eliminate a spectrum are showed in Appendix I. All experimental conditions of Table 11 are measured 20 times. However, after examining the correctness of the fit, not all spectra were

considered correct. The amount of correct fits are: 17, 19, 18, 15, 12, 8, 8, 6, 1, 0 in order from EC11 to EC20. As EC19 and EC20 – both representing the measurements in muscle tissue – only provided one correct fit, no statistical relation could be calculated for the measurements in muscle tissue.

Table 11: Condition matrix with 10 different experimental conditions, 20 trials per condition and the independent variables fiber distance and depth of the fat layer (upon muscle tissue). The dependent variable is the measured DR spectrum.

			Depth adipose layer in mm (upon muscle tissue)								
Fiber distance	n = 20	**3.0**	**2.6**	**2.2**	**1.8**	**1.4**	**1.0**	**0.6**	**0.2**	**-0.2**	**-0.6**
	3mm	EC11	EC12	EC13	EC14	EC15	EC16	EC17	EC18	EC19	EC20

11.3. Results

11.3.1. Raw spectra obtained while cutting

Figure 54, shows two sets of spectra obtained while cutting with a 'smart' electrosurgical knife. The left figure presents spectra, which are considered 'good'. All spectra – except for '-0.2mm' and '-0.6mm' – show characteristics of adipose tissue as described in Paragraph 8.3.3. The spectra obtained in muscle tissue – named '-0.2mm' and '-0.6mm – have a lower signal compared to the other signals. In addition, the spectra do not show characteristic peaks for either muscle or adipose tissue. It can be observed that an increasing depth of the knife results in a lower signal measured.

The right plot in Figure 54 presents spectra, which are considered 'bad'. The fits of these spectra were correct for: '3mm', '2.6mm' and '2.2mm'. The other spectra were considered badly fitted. Examples of bad – or incorrect – fits are shown in Appendix I. Again, the intensity of the signal decreases as the depth of the 'smart' electrosurgical knife increases. The first four measurements – named '3mm', '2.6mm', '2.2mm' and '1.8mm' – show characteristics of adipose tissue as described in 8.3.3. The other six measurements do not show characteristics of muscle or adipose tissue.

Mean values DRS spectra

In Chapter 8 and 9, a clear distinction could be made between muscle tissue and adipose tissue when observing their characteristics. In Appendix H, all measured spectra – excluding and including the bad fits – can be found. Figure 55 shows the mean of measured spectra after elimination of bad fits for EC16 to EC19. One needs to keep in mind that EC19 represents one measured spectrum instead of the mean of multiple measured spectra. The mean spectra of EC16 to EC18 all show the characteristics for adipose tissue mentioned in Paragraph 8.3.3 in the NIR region. In the VIS region, the peaks are flattened, similar to the observations made for cut-adipose tissue in Paragraph 10.3. In the region between 1200 and 1400nm – which represents the fat-water ratio – the spectra decreases in intensity when coming closer to the muscle tissue. The spectrum of EC19 shows one measurement performed at -2mm, which had a 'good' fit. This spectrum shows the characteristics of cut muscle tissue – described in Paragraph 8.3.3 – in the NIR region. The lower double peak around 500nm – which is characteristic for pure and cut muscle tissue – is flattened out.

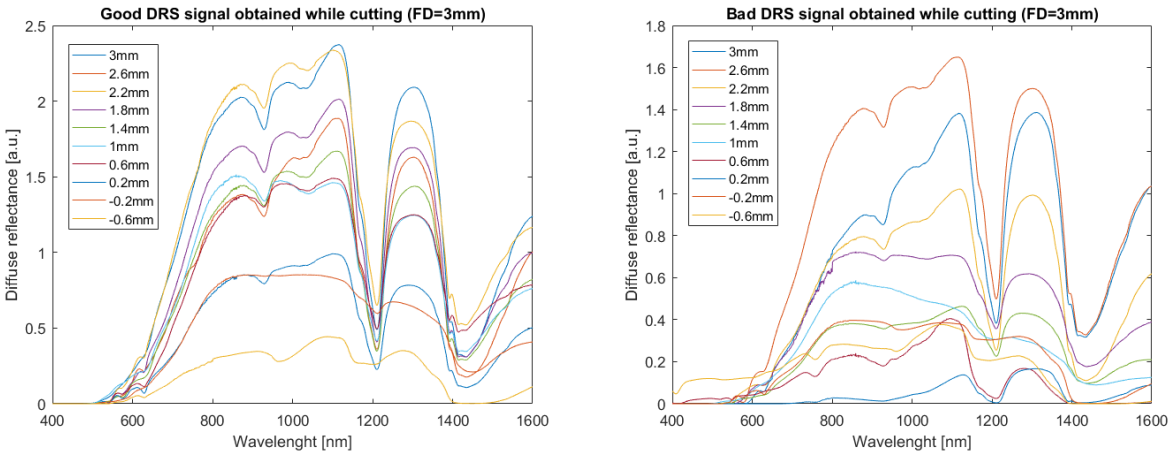

Figure 54: DR spectra obtained while cutting with a 'smart' electrosurgical knife. Left shows measurements of spectra, which could be fitted 'good'. Left shows measurements of spectra, which resulted in a 'bad' fit.

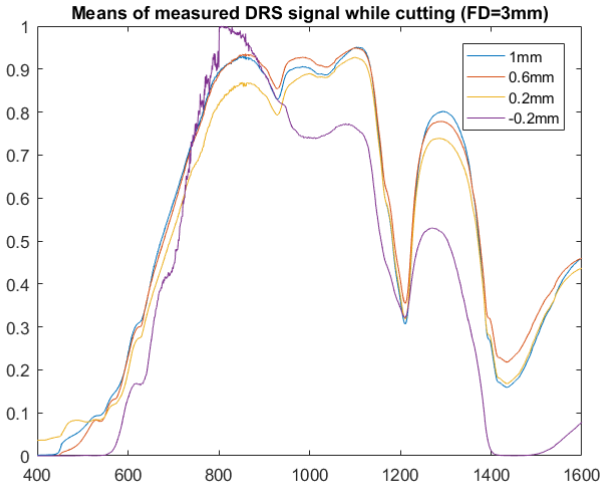

Figure 55: Means of DR spectra of the transition from adipose (>0mm) to muscle (<0mm) tissue during cutting with an electrosurgical knife. EC16 to EC19 are shown, excluding measurements with a 'bad' fit. The FD in this measurement is 3mm.

11.3.2. Chromophore concentrations

As in Chapter 8 and 9, there will be zoomed in on the relevant chromophore concentrations to distinguish between muscle and adipose tissue. For non-cut tissue, the chromophore concentrations which had a significant difference between muscle and cut adipose tissue were the fat-water ratio, StO_2, Mie scattering (f_{mie}) and blood percentage. The most promising chromophore concentration to discriminate between muscle and cut adipose tissue was found to be the fat-water ratio.

Comparing the chromophore concentrations described above for measurements during cutting, only the fat-water ratio showed a difference between cut adipose and muscle tissue. Figure 56, shows the

transition from adipose ($> 0mm$) to muscle ($< 0mm$). The measurements for adipose tissue ($> 0mm$) provide a ratio $> 83\%$. After examination of the fits, one measurement was found to have a good fit for muscle tissue ($> 0mm$). The fat-water ratio in this fit is $< 20\%$. Appendix J provides a plot with the fat-water ratio including the second best fit for muscle tissue ($< 0mm$) and one including the second and third best fit. Both show more deviation for the measurements in muscle tissue ($< 0mm$). The second and third best fit were considered bad fits and are therefore not included in Figure 56. When including these measurements, the means of these plots are 50% – for the second best fit – and 80% for the third best fit.

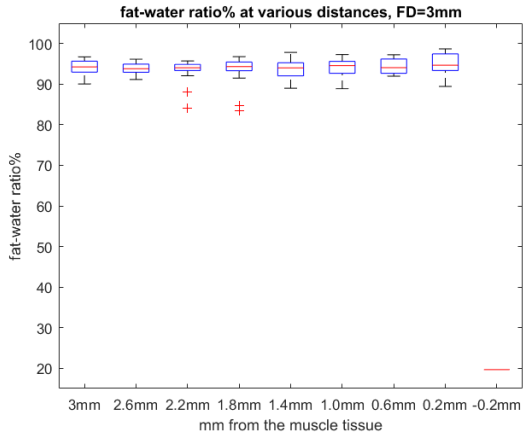

Figure 56: Fat-water ratio of the transition from adipose (>0mm) to muscle tissue (<0mm) during cutting. The FD is 6.2mm and all experimental conditions are performed 30 times.

Appendix K, shows the chromophore concentrations of StO_2, Mie scattering (f_{mie}) and blood for the transition from adipose ($> 0mm$) to muscle ($< 0mm$) tissue. For pure and cut tissue, a curve in StO_2 percentage was found for the transition from adipose tissue to muscle tissue in Figure 49 and Figure 51. The chromophore concentrations obtained while cutting showed no curve. The deviations are large, from 50 percent to 100 percent. There is no trend in the means of the measurements. This holds as well for the percentage Mie scattering (f_{mie}) for the transition from adipose ($> 0mm$) to muscle ($< 0mm$) tissue, also shown in Appendix K. The deviations are large, from 30 percent to 90 percent. Again, no trend is discovered when comparing the means of the chromophore concentrations. Finally, also for the percentage of blood no trend was found. The mean values of the boxplots do not show a curve and the deviation is large: 15 to 65%.

11.4. Discussion

The experiments in this chapter are the mostly related to the clinical practice compared to all experiments performed. In addition, these experiments are the least controlled as they include measurements during electrosurgical cutting.

Setup

In the setup, it was chosen to take steps of 0.4mm and use a power setting of 80 Watt. The former was chosen while the average cutting depth measured in Paragraph 8.3.1 is 0.6mm including 0.2mm knife depth. This results in an average cutting depth of 0.4mm. The power was set at 80 Watt as this is the highest power used in the experiments in Chapter 8. In addition, this power setting provided the most deviation in the DR plots compared to other power settings of 50, 60 and 70Watt.

The 'smart' electrosurgical knife used for the experiments showed ablation on the knife after the measurements. Figure 57 shows the cutting blade of the knife before (left) and after (middle) the measurements. The right picture in Figure 57 displays a zoom of the 'smart' electrosurgical knife after the measurements. Both knifes were cleaned with alcohol before the picture was taken however, still ablation is present on the knife after cutting. This ablation could be a reason for the decrease in signal intensity during cutting.

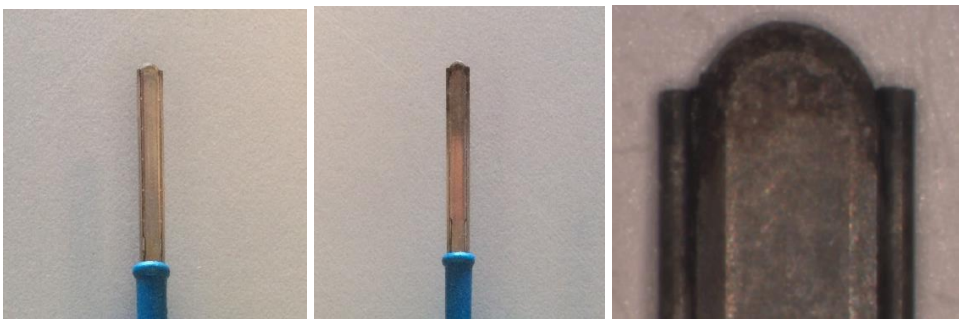

Figure 57: 'Smart' electrosurgical knife, before the measurements in Chapter 11 (left) and after the measurements in Chapter 11 (middle). Both were cleaned with alcohol. More ablation is found on the knife after the measurements. The right picture shows a zoom of the knife after cutting.

DRS

The spectra obtained during the experiment contain incorrect fits. The correct fits all showed characteristics for adipose tissue – described in Paragraph 8.3.3 – in the NIR region. In the VIS region, the peaks are flattened, similar to the observations made for cut-adipose tissue in Paragraph 10.3. These results are satisfying for measuring DR spectra during a margin assessment while cutting with an electrosurgical knife. In addition, the region between 1200 and 1400nm – which represents the fat-water ratio – showed a decrease in intensity when coming closer to the muscle tissue.

As a FD of 3mm is used it was expected, the spectra from $\leq 1.4mm$ would show the transition from adipose to muscle tissue. Nonetheless, no characteristics for muscle tissue or cut muscle tissue are observed in the spectra. When increasing the depth of the knife, a decrease in the signal strength is observed. This could be due to the ablation formed on the knife while cutting. When more ablation is present on the cutting blade and the fibers, less light can be emitted or detected through the fibers. This will result in a lower signal strength.

For the measurements in muscle tissue ($< 0mm$), only one spectra was fitted correctly. All other signals were too weak to fit to. The spectrum with a good fit – and a normal signal strength – showed characteristics of cut muscle tissue – described in Paragraph 8.3.3 – in the NIR region. The lower double peak around 500nm – which is characteristic for pure and cut muscle tissue – was flattened out. Although

the measurement in muscle tissue provides a satisfying result, it only relies on one measurement. Therefore, no conclusion can be drawn and more experiments should be performed on this topic to do so.

Chromophore concentrations

In Chapter 9, the fat-water ratio gave the impression to be the most accurate variable to make a distinction between adipose and muscle tissue. However, the StO_2, f_{mie} and blood percentage still provided significant p-values. In this chapter, the concentrations of StO_2, f_{mie} and blood do not provide a sufficient distinction between adipose and muscle tissue anymore in the plot. Due to the lack of multiple measurements in muscle tissue, no p-value could be calculated in this chapter.

It is possible to make a distinction between adipose and muscle tissue on the basis the fat-water ratio. When measuring in adipose tissue, the ratio is >83%. From this high ratio, it can be stated that it is possible to measure DR spectra while cutting adipose tissue. The fat-water ratio provides results for cut adipose tissue similar to ratio in pure adipose tissue. After the distance of 0.2mm, only one spectra was measured which had a good fit. This spectra provided a fat-water ratio of <20%. It was expected, the fat-water ratio would decrease from $\leq 1.4mm$ as a FD of 3mm was used. The results in Figure 56 do not show a transition from adipose to muscle tissue. The lack of transition in chromophore concentration corresponds to the measured DR spectra – in Figure 55 – were no transition is observed. A reason for the lack of transition could be the spectra containing a mixture of muscle and adipose tissue were considered as a 'bad' fit. More measurements should be performed to draw a conclusion on the feasibility to distinguish between adipose and muscle tissue while cutting with an electrosurgical knife.

Accuracy measurements and 'bad' fits

Multiple fits were found incorrect. These wrong fits were due to three reason: a minimum signal, a lower scattering coefficient compared to the signal and a fit that did not follow the measurement. All reasons can be found in Appendix I. By increasing the depth of the measurement, the amount of 'bad' fits increased as can be seen in Table 12. For the measurements in muscle tissue – at a depth of -0.2mm and -0.6mm – only one fit was correct. The bad fits in this experiment can have multiple reasons.

First, the measurements were made during electrosurgical cutting. This action causes ablation on the tissue, the blade and the fiber tips, which are placed next to the blade. Both ablation on the tissue and on the fibers can reduce or weaken the signal. If ablation is present on the tissue, the ablation instead of the tissue will be measured. If ablation is present on the fiber tip, less light is emitted to the fiber and less light can be detected. Second, to obtain spectra while cutting a short time was set to acquire the measurements. The VIS and NIR integration time were set on their minimum values of 0.1second. A higher integration time would have minimized the noise on the measurements, which could have led to better fits. Third, as is concluded in Chapter 8, electrosurgical cutting results in more deviation in muscle tissue compared to adipose tissue. This could have contributed to the high amount of 'bad' fits in muscle tissue compared to adipose tissue. At $\leq 1.4mm$ it was expected to see characteristics of muscle tissue – or see the transition from adipose to muscle tissue in the spectra – however, the number of correct fits decreases after that point. Fourth, it is possible the fiber was not always in contact with the tissue. The depth of the 'smart' electrosurgical knife was controlled by a linear stage. However, the cutting depth for electrosurgical cutting can variate. While the cuts and measurements where made in the adipose tissue, it

was not possible to check the depth of the cut and/or the measurement. Therefore, it is possible measurements are made when the fibers were not in contact with the tissue.

Table 12: Number of correct fits out of 20 measurements obtained while cutting with the electrosurgical knife.

Depth adipose layer [mm]	Experimental condition	No. correct fits*
3.0	EC11	17
2.6	EC12	19
2.2	EC13	18
1.8	EC14	15
1.4	EC15	12
1.0	EC16	8
0.6	EC17	8
0.2	EC18	6
-0.2	EC19	1
-0.6	EC20	0

After removing the 'bad' fits, only one measurement remained for measurements in muscle tissue. No conclusions can be drawn on one measurement. Therefore, more experiments should be performed on measuring DR spectra while cutting. In future experiments, the fibers should not be ablated during cutting. This could be done by inserting a probe next to the electrosurgical knife after cutting at each step. As the 'smart' electrosurgical knife is intended to be used intraoperative, tissue debris and blood tend to accumulate on the cutting blade. [81] This could also affect the measurements made by the 'smart' electrosurgical knife. A small study by Haj-Hosseini et al. showed a 500 µm thick blood layer alters the spectral measurements with a fiber distance of 0.9 mm. [82] No conclusion can be drawn on the effects of blood on the spectra from this small experiment. However, designing a prototype were the fibers are not placed next to the cutting blade would dissolve this issue.

In additional research, should obtain more measurements compared to the amount of measurements in this experiment. Therefore, more fits will be correct which could make a calculation on significance possible. A consideration on the fit of the spectra is, that the examination of the correctness of the fit is a subjective process. The tree types of errors in fits detected in this thesis are described in Appendix I. The measurements in adipose tissue yielded to 6 to 19 measurements out of 20 per experimental condition. The spectra all showed the characteristics of adipose tissue clearly. Therefore, it can be concluded that electrosurgical cutting does not affect DR measurements in adipose tissue.

IV
Validation

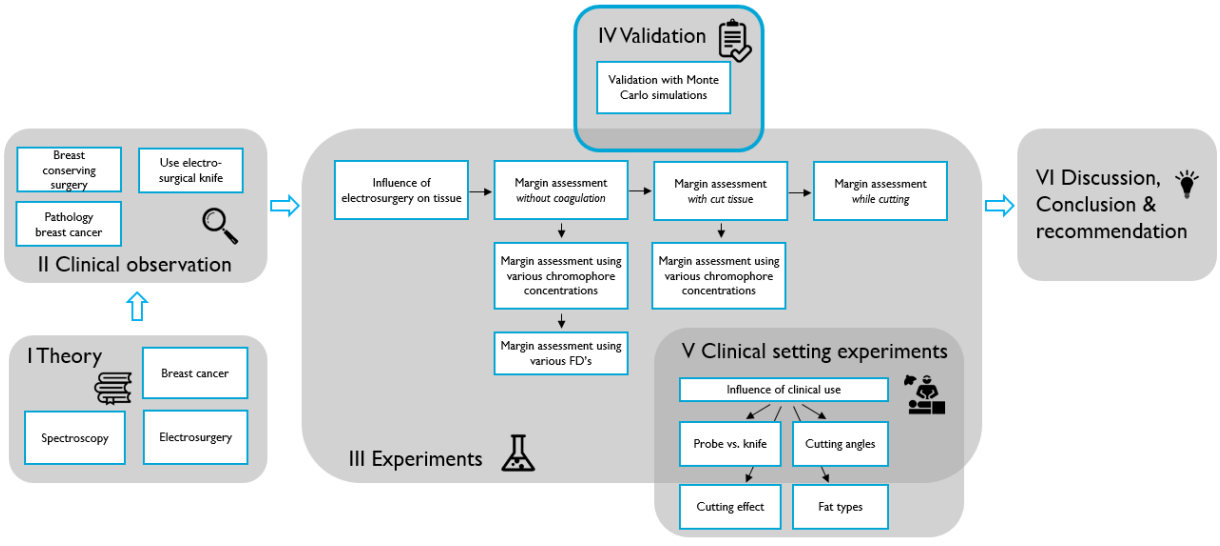

12. Validation: Monte Carlo simulation

Paragraph 3.3 presents the tissue properties required to characterize tissue with DRS. These properties can be described through analytical and empirical models. However, their reliance on mathematical assumptions and the exclusion of the effects of the shape and optical properties of the probe make them limited. [83] [84]

A Monte Carlo (MC) simulation is a method to describe the absorption of the light by tissue. It describes photon distribution within the tissue as probability distributions. In the case of moving photons through tissue, the randomness of photons being absorbed or scattered (photon propagation) is simulated. The advantage of this simulation – compared to experiments – is the possibility to vary the tissue geometry and characteristics in a controlled way. In addition, it provides a high accuracy of the outcomes for measurements taken near to a tissue boundary. Regular theories assume that tissue consists of one layer, which is obviously false and inaccurate for the outcome. [84] In this thesis, a MC simulation is performed to validate the experiments described. All tissues used are validated for pure tissue and for cut tissue.

12.1. Theory

The operation of the MC model will be described according to literature of Wang et al. and Landau et al. [85] [86] First the inputs and outputs of the model are described. Second, the grid that is used to describe the absorption at specific placed in the tissue is explained. Following, the probability density function used in the MC model is described. Finally, the simulation and boundary events that can occur are defined.

Inputs and outputs

To run the MCML model, four variables are needed, which can be seen in Figure 58. First, the absorption coefficient, which represents probability of photon absorption per unit infinitesimal path length. Second, the scattering coefficient, expressing the probability of photon scattering per unit infinitesimal path length. Third, the anisotropy factor g, being the average of the cosine value of the deflection angle θ. In addition, the refractive indices of the tissue, top ambient medium (air) and bottom ambient medium (if exiting) are needed. All values used as inputs during the experiment are described in Appendix L.

The MCML model then calculates the physical quantities of photon absorption: the fluence, reflectance and transmittance of the tissue. The absorption will be used to reconstruct a spectrum, which can be used to compare with the spectra measured in the experiments performed for this thesis.

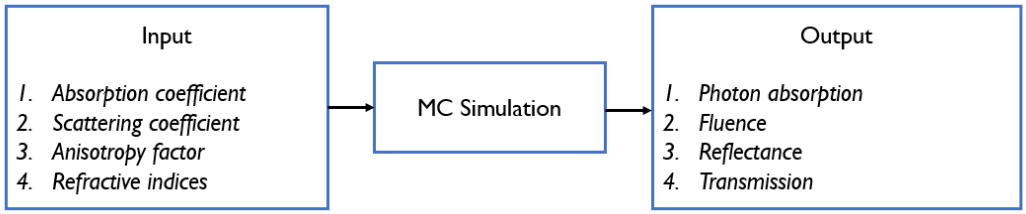

Figure 58: Visual representation of the inputs and outputs of the MC model.

Grid and coordinate systems

To simulate the photons' scattering path in three dimensions, a grid is used to describe absorption at specific places in the tissue. The absorption $[J/cm^3]$ is then described per local grid elements. A three-dimensional homogeneous grid is setup in directions z, r and a, as can be seen in Figure 59. The grid separations are d_z, d_r and d_a and the total number of elements in the z, r and a direction are N_z, N_r and N_a respectively. All measurements performed in this model are in cm. The simulation also records the escape of photons at the top (and bottom) surface as local reflectance (and transmittance).

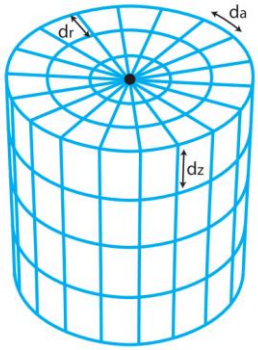

Figure 59: Cylindrical grid used at a MC simulation. Photons are launched into the tissue at the centre of the surface (black dot). The FD is described in multiple of d_r. [2]

Probability density function

A MC simulation relies on the random sampling of variables from well-defined probability distributions. Consider a random variable needed by MC, for example the angle of deflection. A probability density function defines the distribution of k over the interval (a, b). The probability density function is normalized such that

$$\int_a^b p(k)dk = 1 \tag{12}$$

To simulate the light propagation, the value of k is a – repeatedly – randomly chosen number. A computer provides a random variable p, which is uniformly distributed over the interval (0, 1). The probability density function for a photon tissue interaction is given as

$$p(s) = (\mu_a + \mu_s)e^{-(\mu_a + \mu_s)s} \tag{13}$$

Simulation events

Photons are launched as a packet simultaneously along a pathway. Each packet is assigned a weight and is launched orthogonally into the tissue at its origin. This is (0, 0, 0) in the Cartesian coordinate system. The probability of photons being specular reflected is expressed by

$$R_{sp} = \frac{(n1 - n2)^2}{(n1 + n2)^2} \tag{14}$$

Where $n1$ is the reflective index of the outside medium and $n2$ the reflective index of the tissue. The photon weight is decreased by R_{sp}.

$$W = 1 - R_{sp} \tag{15}$$

The step size of the photon packet (s) is based on the a sampling of the probability distribution for a photon's free path

$$s = \frac{-\ln(k)}{\mu_a + \mu_s} \tag{16}$$

Once the step size s is specified, the photon can move in the tissue. The position of the photon packet is described in the Cartesian coordinate system (x, y, z)

$$\begin{aligned} \mu_x &= \bar{r} \cdot \bar{x} \\ \mu_y &= \bar{r} \cdot \bar{y} \\ \mu_z &= \bar{r} \cdot \bar{z} \end{aligned} \tag{17}$$

This position is updated when moving through the tissue. The updated position is described by

$$x = x + \mu_x s$$
$$y = y + \mu_y s \quad (18)$$
$$z = z + \mu_z s$$

Once a step is taken by the photon, its weight will be weakened by absorption. A fraction of its weight will be saved in the local grid element. This saved weight is calculated by

$$\Delta W = W - W\frac{\mu_a}{\mu_a + \mu_s} \quad (19)$$

The total weight that is saved in a local grid element is accumulated after every photon passage. In addition, the total weight of the photon packet is updated by extracting the weight saved in the local grid element from the total weight described in Equation (15).

Once the photon is moved, the packet can be scattered. A deflection angle θ- and an azimuthal angle φ also depend on the random variable k. The deflection angle θ, is described as: [87]

$$\theta = cos^{-1}\left(\frac{1}{2g}\left(1 + g^2 - \left(\frac{1 - g^2}{1 - g + 2gk}\right)^2\right)\right) \quad (20)$$

And the azimuthal angle ψ by

$$\psi = 2\pi k \quad (21)$$

Boundary events

During a step, a photon can hit a boundary of the tissue. It can then either escape the tissue at the air/tissue interface or be internally reflected by the boundary. The step size s splits into two parts (i.e. the distance to the boundary surface s_1 and the remaining distance s_2). After traveling the distance s_1, the probability of internal reflection is calculated. The probability of internal reflection depends on the angle of incidence θ_1

$$\theta_1 = cos^{-1}(|\mu_z|) \quad (22)$$

The internal reflectance $R_{(\theta_1)}$ is calculated by Fresnel's formula

$$R_{(\theta_1)} = \frac{1}{2}\left(\frac{sin^2(\theta_1 - \theta_2)}{sin^2(\theta_1 + \theta_2)}\right) + \frac{tan^2(\theta_1 - \theta_2)}{tan^2(\theta_1 + \theta_2)} \quad (23)$$

Where θ_1 and θ_2 are the refractive indices of the media. If the photon reflects internally, the photon packet stays on the surface and its position must be updated by reversing the z component. At this point, the remaining step size has to be checked to see whether it is large enough to hit the other boundary. If so, the described process can be repeated. If not, the photon package will move with an updated step size Δs

$$\Delta s = s\frac{\mu_{a1} + \mu_{s1}}{\mu_{a2} + \mu_{s2}} \quad (24)$$

When photon weight is under a specified threshold, it goes into a roulette process. This roulette process has a pre-defined chance for selection to end propagation.

If the photon packet escapes the tissue, the tracing of the packet ends. The reflectance or transmittance is updated by the amount of escaped photon weight. Figure 60, shows flowchart visualizing the process described above. A more comprehensive explanation of Monte Carlo can be found in [84], [85] and [86].

12.2. Method

The model used for the MC simulation is the MCML model, a Monte Carlo model of steady-state light transport in Multi-Layered tissue. The model was provided by Philips Research and the MATLAB code was adjusted by Julie Fleischer and Akash Swamy. The model was used to validate the DR spectra of the pure and cut tissues used for the experiments performed for this thesis. The input of the parameters used by the model can be found in Table 13. In Appendix L, the input values for the parameters can be found.

Table 13: Overview of the input parameters for the MC model and the source used to find the correct value.

Input parameter	Sources
Refractive Index	Literature
Anisotropy	Literature
Absorbtion coefficient ($\boldsymbol{\mu_a}$)	Fit software
Scattering coefficient ($\boldsymbol{\mu_s}$)	Fit software
Number of photons	By choice
Depth layer	By choice
Grid elements ($\boldsymbol{d_z}$, $\boldsymbol{d_r}$ and $\boldsymbol{d_a}$)	By choice

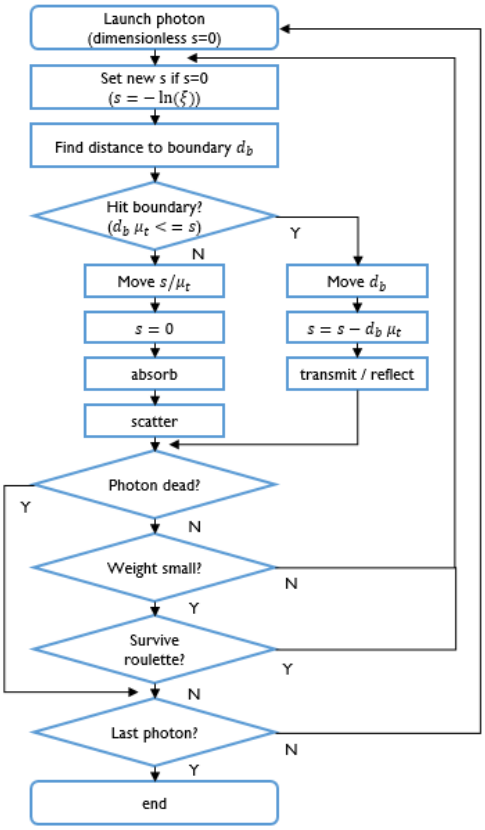

Figure 60: Flowchart for tracing photons in multi-layered tissues with the Monte Carlo simulation [85].

The Monte Carlo validation is performed for all types of tissue used in the experiments performed for this master thesis. In addition, a validation is performed for the tissue types with electrosurgical cutting effects. The tissue types are: muscle, muscle with cutting, pork belly, pork belly with cutting, adipose pork, adipose pork with cutting, sowbelly layers and sowbelly layers with cutting. The influence of the various types of adipose tissue on DR spectra are also described in Paragraph 13.4.

The measured signal – to which the simulated signal is compared – was the spectra most similar to the mean spectra of all measured spectra for one condition.

To perform an adequate validation, the measured spectra and the simulated spectra need to be compared. This is performed by using the Variance Accounted For (VAF). The VAF, is normally used to verify the correctness of a model. However, in this case it is used to quantify the variance of the graphs. When two signals are the same, the VAF will be 100%.

$$VAF = \left(1 - \frac{var(y_i - \hat{y}_i)}{var(y_i)}\right) \cdot 100\% \tag{25}$$

The VAF was calculated in MATLAB by using the 'var' function. In this function, y_i is the measured signal and $\hat{y}_i$ is the simulated signal. When the VAF percentage is higher than 95%, the model – and in this case simulated signal – is classified as 'good'.

12.3. Results

In this Paragraph, the Monte Carlo simulation of all tissues used in this thesis can be found. All are plotted next to the mean of the DR spectrum measured for the same tissue. The simulated spectra for pure muscle tissue – using a FD of 3mm – can be seen in Figure 61 (left). The overall shape of the simulated muscle spectra is similar to the measured muscle spectra. The largest deviation can be seen in the VIS region between 500 and 600nm. The VAF for this simulation is 97%. ($var(y) = 0.1093$ and $var(\hat{y}) = 0.1093$) Figure 61 (right) shows the simulated spectra for cut muscle tissue. Again, the shape of the simulated spectra is similar to the measured spectra. It seems, larger deviation is present between the measured and simulated spectra. The double peak around 500nm is flattened out in the simulated spectrum. The VAF for this simulation is 99.85%. ($var(y) = 0.1322$ and $var(\hat{y}) = 0.1374$)

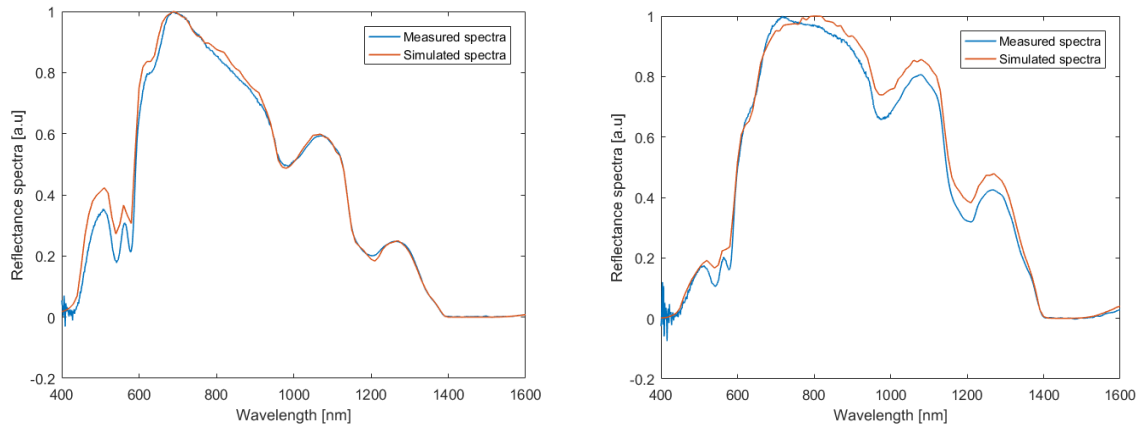

Figure 61: DR spectra of muscle tissue (left) and cut muscle tissue (right). FD = 3mm. The blue spectrum is the measured spectrum and the orang spectrum is the simulated spectrum by a Monte Carlo model.

The simulated plots for pork belly tissue and cut pork belly tissue can be seen in Figure 62. Both the simulated spectra have a similar shape compared to the measured for the same tissue. Figure 62 (left) deviates a bit for all wavelengths. The VAF of the simulation for pork belly tissue is 99.38%. ($var(y) = 0.0848$ and $var(\hat{y}) = 0.0781$) Figure 62 (right) deviates from 700nm onwards; the most deviation is found in the NIR region. The VAF of the simulation for cut pork belly tissue is 99.87%. ($var(y) = 0.1172$ and $var(\hat{y}) = 0.1129$)

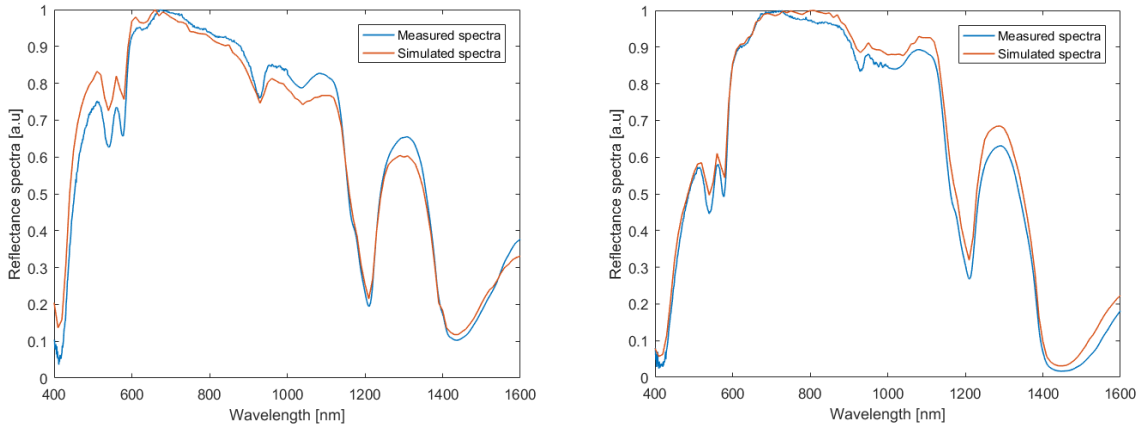

Figure 62: DR spectra of pork belly tissue (left) and cut pork belly tissue (right). FD = 3mm. The blue spectrum is the measured spectrum and the orang spectrum is the simulated spectrum by a Monte Carlo model.

Figure 63 show the Monte Carlo simulation for adipose pork tissue and cut adipose pork tissue. Both simulated spectra show some deviation at all wavelengths. However, the overall shape of the spectra of the simulation corresponds to its measured spectra for the same tissue. The VAF of the simulation for adipose pork tissue is 99.88%. ($var(y) = 0.1197$ and $var(\hat{y}) = 0.1156$) For cut adipose pork tissue, the simulation has a VAF of 99.97%. ($var(y) = 0.1097$ and $var(\hat{y}) = 0.1078$)

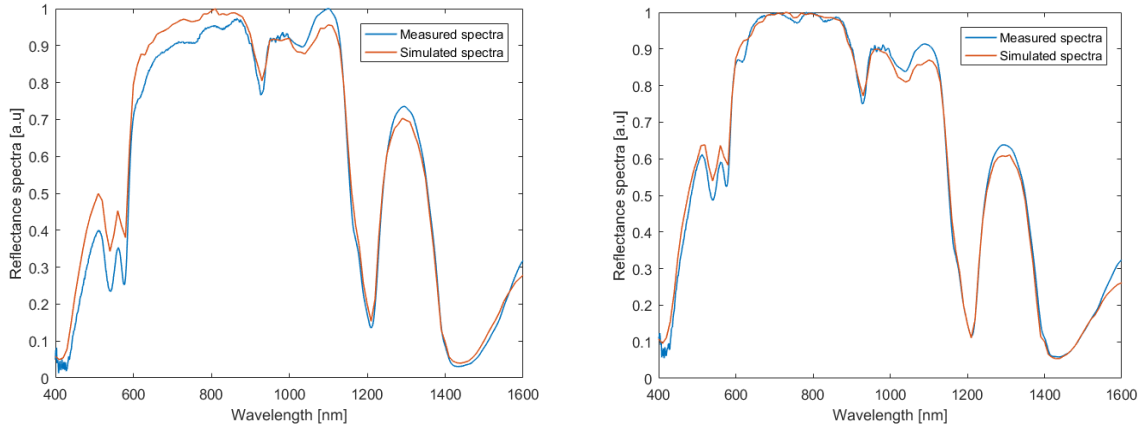

Figure 63: DR spectra of adipose pork tissue (left) and cut adipose pork tissue (right). FD = 3.25mm. The blue spectrum is the measured spectrum and the orang spectrum is the simulated spectrum by a Monte Carlo model.

In Figure 64, the Monte Carlo simulation for sowbelly pork tissue and cut sowbelly pork tissue can be seen. The deviation in these plots is present in the whole spectrum. In the left plot, the measured data has a higher intensity compared to the simulated data in the NIR region. In the right plot, this is the other way around. The VAF of the simulation for sowbelly tissue is 99.43%. ($var(y) = 0.0992$ and $var(\hat{y}) = 0.1066$) For cut sowbelly tissue, the simulation has a VAF of 99.9%. ($var(y) = 0.1071$ and $var(\hat{y}) = 0.1037$)

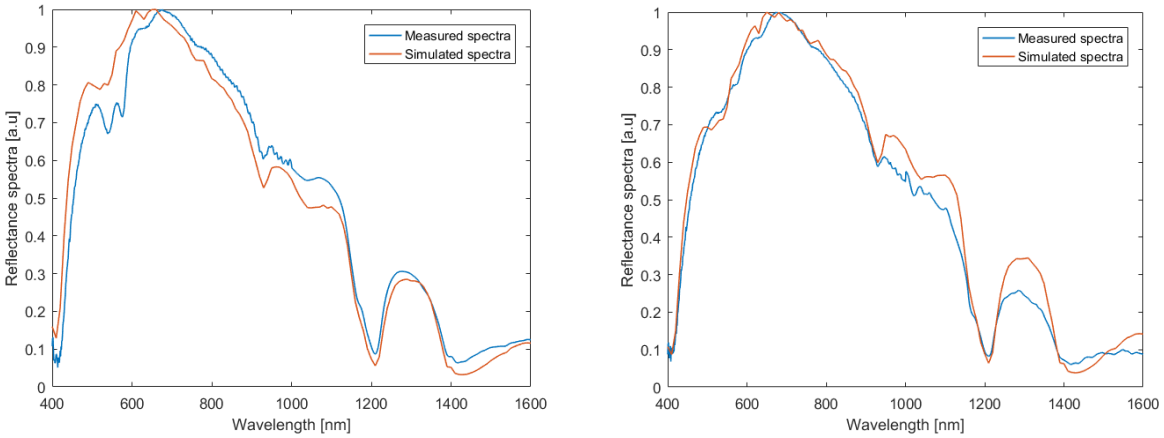

Figure 64: DR spectra of sowbelly layers (left) and cut sowbelly layers (right). FD = 3.25mm. The blue spectrum is the measured spectrum and the orang spectrum is the simulated spectrum by a Monte Carlo model.

12.4. Discussion

This validation is performed to detect flaws in the measurements performed for this thesis. Normally, simulations are run first and when the outcome provides accurate results, experiments are performed. This is while experiments typically are most time consuming. Another example of using a simulation is to test – or compare – two or more variables. In a simulation, the influence of specific variables can often be tested in a more controlled way compared to an experiment.

MC Model

It needs to be considered that a MC simulation is an attempt to approach the reality. This model is created by making some assumptions, which can be untrue. Therefore, small deviations between the measured and simulated spectrum are acknowledged.

- Absorption (μ_a) is modeled as a continuous linear decrease of photon weight. After each step, some of the weight is left behind. However, in tissue, absorption happens in one step. As a result of this model, it is possible to track photon paths and therefore also the maximum photon penetration depth. Nonetheless, the maximum photon depth should be considered as an approximation as it is based on a linear decrease of absorption.
- In the model, tissue is modelled as totally homogeneous however this is never true for human or animal tissue.
- The incident light beam is considered infinitely small and the photons all parallel to each other. Nonetheless, when optical fibers are used the light beam has a circular surface. In addition, it will emit the photons in various directions.

Simulated spectra and VAF values

While all simulations correspond to the measured spectra with a VAF value ≥ 97% the fits are considered good enough. Accordingly, it can be concluded no major mistakes are made during the experiments and

the measured spectra are good enough to draw conclusions on. In addition, the peak between 1200 and 1400nm for adipose tissue is clearly visible in all measured and simulated spectra. This peak influences the fat-water ratio, which is considered the most relevant chromophore concentration to be able to distinguish between adipose and muscle tissue.

Deviations between the measured and the simulated spectra are most likely due the inhomogeneous tissue. The model assumes a homogeneous tissue; however, animal tissue is never homogeneous. In addition, cutting tissue with an electrosurgical knife will change the tissue. However, it is not certain the measured spectra of the cut tissue contains only information about the cut tissue and not a mixture of both cut and non-cut tissue. The measured and simulated spectra for sowbelly were assumed to show more deviation due to the tissue formation. The model considers an infinite tissue layer while the sowbelly used in the experiment exists of 0.4mm layers. All other tissue types existed of a thick layer of at least 2cm. Another aspect that could have affected the results is the possibility that air was present between the layers.

The spectra in Figure 61 (left) seem to show less deviation compared to the spectra in Figure 61 (right). However, the VAF value is higher (2.85%) for the spectra in the right figure. The difference in the VAF values could be due to rounding numbers in the var formula. In addition, not all deviation between spectra is clearly visible in the plots.

Recommendations

More simulations would have been made when more time was available. First, the validation would be performed for multiple layers. Then the transition between adipose and muscle tissue – as is measured in the experiments – could have been validated. In a simulation, the depths of the adipose tissue layer(s) could be adjusted in smaller amounts than for the experiments. As a result of that, the fat-water ratio per 0.1mm – or smaller – distance from the tissue could be described.

Second, multiple simulations would have been done instead of one per tissue type. While the basis of the Monte Carlo simulation is a probability distribution, the outcome of the simulation will never be exactly the same. When multiple simulations would be performed, the accuracy of the model will increase.

V

Clinical setting

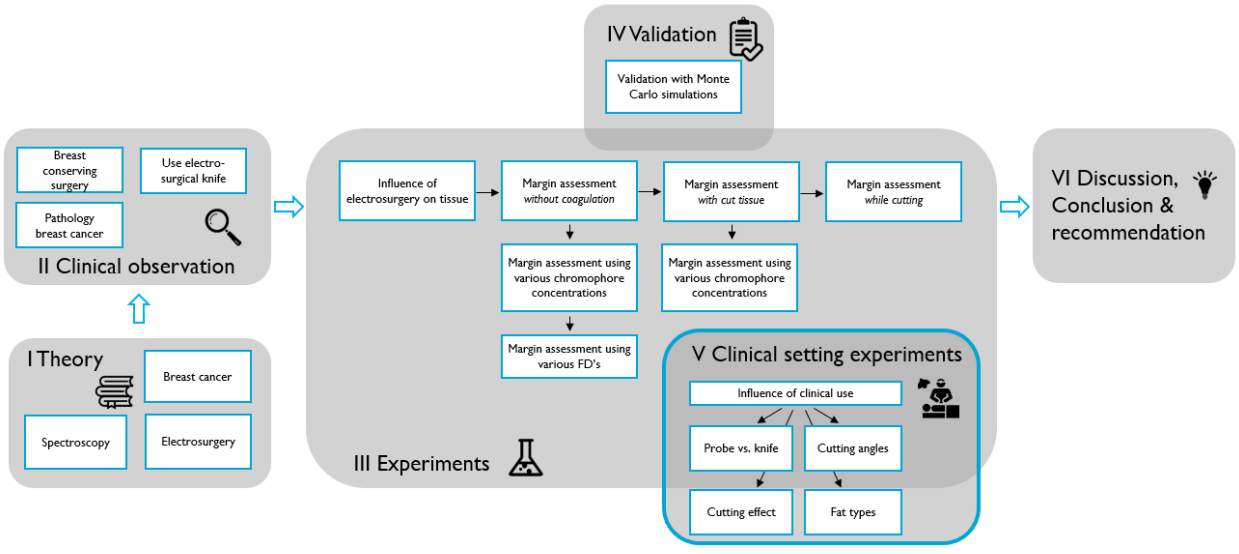

13. Influence of clinical use

For this master thesis, experiments are performed regarding the characterization of tissue. To be able to provide the most valuable output of the measurements, the experimental setup(s) are made constant. However, when a 'smart' electrosurgical knife would be used in clinical practice, the setup and variables regarding the experiment will change. These changes could influence the outcome of the measurements. In this chapter, the differences between the experimental and clinical setting will be discussed. In addition, the influence of these differences on the outcome of the measurements in Chapter 8, 9, 10 and 11 will be examined. In the discussion, some recommendations for the design of the device will be given according to the results found in the experiments performed in this chapter.

All experiments in this master thesis are performed under these conditions: the surrounding light was minimalized, the electrosurgical knife or probe was held perpendicular to the tissue, pure muscle or adipose tissue was used and when possible, a probe was used to measure the DR spectrum. Comparing these experimental conditions to the clinical setting, some observations can be made. First, in the OR surrounding light is always present. Often, spots are pointing at the place where the surgeon is dissecting. Second, surgeons have different ways of holding the electrosurgical knife. Accordingly, it cannot be assumed the electrosurgical knife will always be perpendicular to the tissue when cutting. Third, human tissue is not always pure, as assumed in these experiments and the validation of the experiments. Test on human tissue need to be performed to prove the accuracy of the knife in non-pure tissue. And fourth, the fibers on the electrosurgical knife with sensing capabilities are affected by the coagulation and charring of the tissue. Fibers that are affected by coagulation and charring can influence the outcome of the measurements.

13.1. Surrounding light: darkness vs. light

One of the differences between the experimental setup in the lab and the clinical setting of the operating room is the surrounding light. The experiments are performed in 'complete darkness', except for the light of the two laptops used in the setup. Generally, in a clinical setting, the lighting is on and often a lamp is focused on the operating site. The surrounding light is one of the variables that could affect the light detection by the probe.

When performing an experiment, first a calibration is performed. This is a measurement with a spectral response of a white reflectance standard (Spectralon) with known reflectivity. The measurement is followed by a background measurement. The background measurement is extracted from all 'real' measurement performed after the calibration to minimize the impact of the surrounding light. This step allows correcting for the system response (e.g. spectral shape of the light source and wavelength-dependent sensitivity in the optics and gratings and the detectors). The white reference measurement is used to divide each spectral measurement on the tissue samples for which a background measurement is subtracted yielding to the final reflectance measurement. [88]

Nachabe et al. describes the same setup as used to obtain DR spectra in the experiments for this thesis. [88] He states the surrounding does not influence the measurements when a calibration is performed a priori to the measurements. The PNSas software will use the calibration for correction of

the surrounding light. As the PNSas software will use the calibration for correction of the surrounding light, no experiments evaluating the surrounding light are performed.

13.2. Cutting angles

The second difference that is examined, is the use of the electrosurgical knife by the surgeon. As described in my literature study there are no clear rules of the use of electrosurgical instruments and so the use can differ per surgeon. [29] In Chapter 6, it can be seen, the electrosurgical knife is held in the same way as a pencil. Just like people hold there pencil differently, every surgeon holds the electrosurgical knife in its own way. In the previous experiments, the probes where always held perpendicular to the tissue. Therefore, the influence of a changing cutting angle on the outcome of the measurements is not examined yet.

In this experiment, the outcomes of measurements taken in different cutting angles will be compared. The perpendicular measurements where taken as a reference and compared to measurements at a cutting angle of 30 degrees and 60 degrees.

Materials & methods

The specimen used for this experiment is similar to Chapter 9 and 10 where layers of adipose tissue (Slagerij Lelieveld) are placed on muscle tissue (LifeTech). This setup can be seen in Figure 43. Three layers of 0.4mm adipose tissue where placed on the muscle tissue for this experiment.

The instruments and equipment used are similar to Chapter 9. In addition, a protractor was used to measure the angles and a coupling piece was put on the linear stage to hold the probe in the right position. The angles used can be seen in Figure 65.

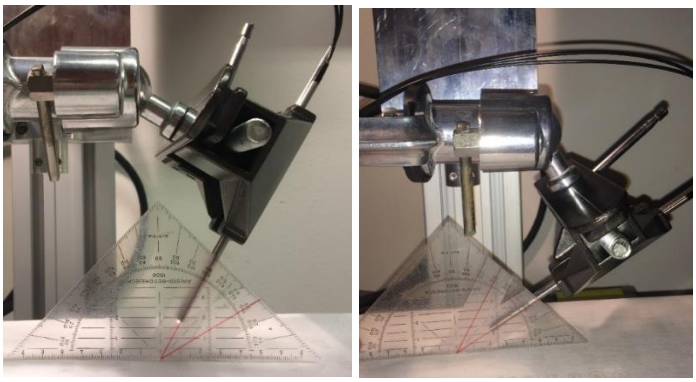

Figure 65: Variation in cutting angles. Left, a cutting angle of 60 degrees. Right, a cutting angle of 30 degrees.

The independent variables in this experiment are the cutting angles (90˚, 60˚ and 30˚) and the FD of the probe. Each experimental condition is performed 30 times. The controlled variable is the tissue, which is not changed during this experiment. The DR spectrum is the dependent variable, which was measured to identify trends for the independent variables. The condition matrix for this experiment can be found in Table 14.

Table 14: Condition matrix with two independent variables: cutting angle (90˚, 60˚ and 30˚) and the fiber distance (6.2mm). All experimental conditions were performed 30 times.

		Cutting angle (degrees)		
Fiber distance (mm)	n = 30	90˚	60˚	30˚
	6.2mm	EC11	EC12	EC13

Results

In Figure 66, the DR spectra can be seen of a layer of adipose tissue (1.2mm) upon muscle tissue using three different measurement angles. The reference plot – Figure 66a – shows clear characteristics of adipose tissue that are described in Paragraph 8.3.3. From 800 nm, all spectra in Figure 66 show approximately the same spectrum. However, before 800nm, the spectrum of the condition of 60 degrees – Figure 66b – varies from Figure 66a,c. Figure 66a,c show double peaks around 500nm and around 600nm. However, these peaks are flattened in Figure 66b. In addition, the spectrum of Figure 66b shows less deviation compared to the spectra in Figure 66a and c.

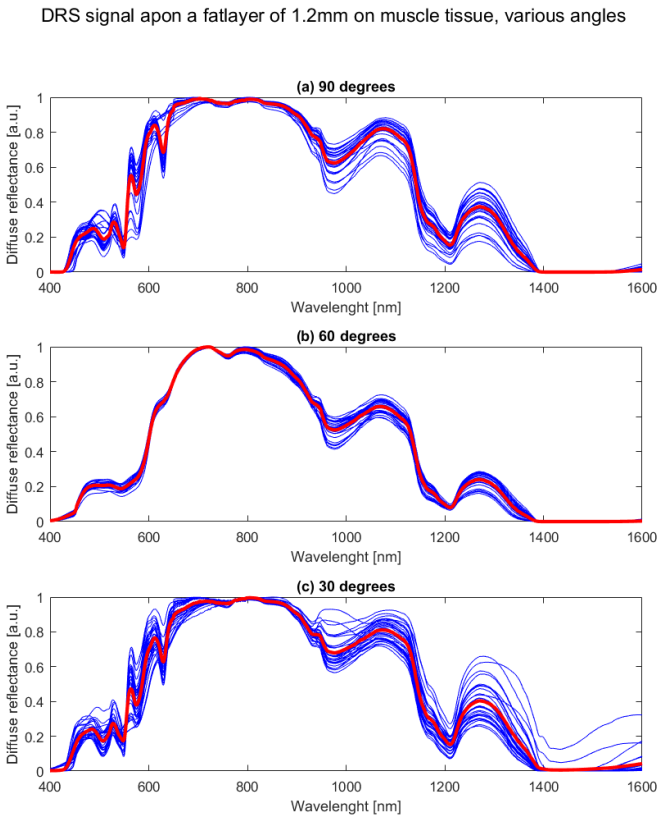

Figure 66: DRS signal of 1.2mm adipose tissue upon muscle tissue, FD=6.2. The probe was held in different angles: 30˚, 60˚ and 90˚. All conditions are performed 30 times.

Discussion

It was expected the outcome of the measurement would change for different angles, as the sensing zone will detect a different zone when the angle is changed. This is visualized in Figure 67. For the experiment it was chosen to use three layers of adipose tissue on top of muscle tissue. If only one type of tissue was used, the sensing zone would only measure this type of tissue. When looking at Figure 67, it is expected the DR spectra would change – if it would change – gradually from Figure 66a to Figure 66c. Figure 66b, would be then be in the middle within this transition. However, this is not the case. Figure 66a and Figure 66c are similar to each other and Figure 66b differs, especially in the VIS region. Around 500nm and 600nm double peaks are visible in the spectra in Figure 66a and Figure 66c. These peaks are flattened out in Figure 66b. In addition, less deviation is present in Figure 66b compared to the other spectra.

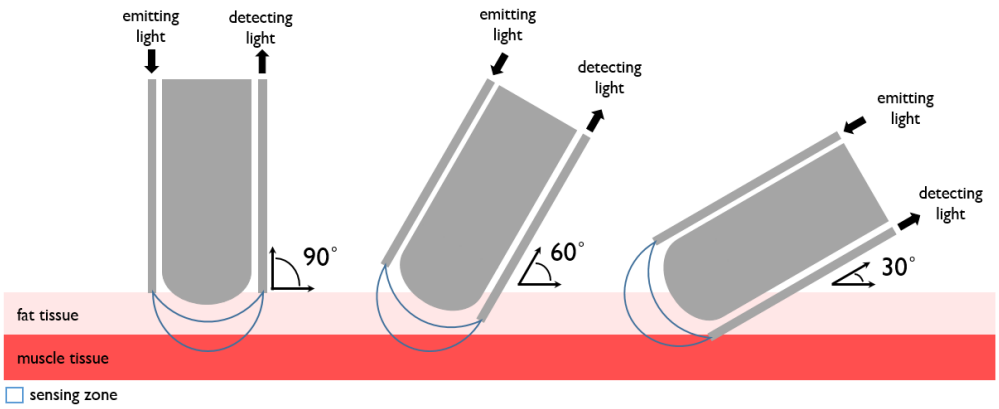

Figure 67: Visualization of the sensing zone of probes in different angles (90°, 60° and 30°). The sensed zone will change for various angles.

The differences between Figure 66a, Figure 66c and Figure 66b are particularly present in the VIS region. This implicates changes in the chromophore concentration of – oxygenated – blood (Hb and $Hb02$) or scattering coefficients (b, $s800$, f_{mie} and α). In addition, the change surface contact of the probe could have effected the results. It is possible, the probe was not fully in contact with the tissue for the cutting angle of 30° and 60°. This will affect the diffusion of the light in the tissue and can therefore effect the measured spectra.

In the Chapters 9, 10 and 11, it was concluded that the fat-water ratio is the most valuable variable for making a distinction between muscle and adipose tissue. This ratio is extracted from the DR spectrum at the peak between 1200 and 1400nm. In this region, all plots of Figure 66 are similar. Therefore, the change in spectrum will not influence the outcome of the measurements for the fat-water ration in this thesis much.

When more experiments could be performed, they should be repeated for one type of tissue. Than the influence of a changing angle could be examined without the potential influence of a double layer of tissue for the DR spectra.

13.3. Probe vs. knife

Another variable that could have influenced the outcomes of the measurements in this thesis is the use of a probe compared to a 'smart' electrosurgical knife for obtaining DR spectra. The 'smart' electrosurgical knife – which can be seen in Figure 52 – has integrated fibers next to the cutting blade. While these fibers are close to the cutting blade, coagulation can be formed on the tip of the fiber(s). This is not the case for the probe, as this instrument is not used to cut tissue with. Therefore, it is expected using a knife to obtain measurements will give more noise and/or a less clear signal compared to a probe. To test this hypothesis, the differences in spectra obtained by a probe and a 'smart' electrosurgical knife are examined.

Materials & methods

The specimen used for this experiment is similar to Chapter 8 where pork belly (Albert Heijn) was used. The specimen – both muscle tissue and adipose tissue – were coagulated with 80 Watt. A probe and a 'smart' electrosurgical knife where used to obtain DR spectra. The probe – which can be seen in Figure 33 – has a FD of 3.25mm and the 'smart' electrosurgical knife – which can be seen in Figure 52 – has a FD of 3mm.

The independent variables in this experiment are the instrument used to obtain the DR spectrum ('smart' electrosurgical knife and probe) and the tissue type examined (muscle and adipose pork belly tissue). The coagulation setting was held constant on 80 Watt. In Table 15, the condition matrix of this experiment can be seen.

*Table 15: Condition matrix with two independent variables: instrument used for measuring the DR spectra ('smart' electrosurgical knife and probe) and the tissue type (muscle and adipose tissue). All experimental conditions were performed 24 times. * Both tissue types were coagulated with a power of 80 Watt.*

		Instrument	
Tissue type	n = 24	**Knife**	**Probe**
	Muscle*	EC11	EC12
	Adipose*	EC12	EC22

Results

In Figure 68 (upper left and right), the spectra of coagulated muscle tissue obtained with a 'smart' electrosurgical knife with a FD of 3mm and a probe with a FD of 3.25mm can be seen. The median of both plots shows many similarities. The peaks around 500nm have a higher intensity for the probe and the peak and dip around 1100nm show a higher intensity for the knife. Both plots show relative large variations in spectra.

Figure 68 (bottom left and right) shows the spectra of coagulated adipose tissue obtained with a 'smart' electrosurgical knife with a FD of 3mm and a probe with a FD of 3.25mm. Similar to Figure 68, both plots obtained by using a probe and a 'smart' knife show many similarities. In addition, the same regions dominate as in Figure 68. The peaks around 500nm have a higher intensity for the measurements

obtained by the probe while high intensity in the region from 1000nm to 1200nm is present for the measurements obtained by the 'smart' knife.

Discussion

The results obtained in this experiment – for a 'smart' knife and a probe – do not show a major difference in outcome. It was expected that the results obtained by the 'smart' electrosurgical knife would show more deviation. This was not true for the results in this experiment. Nonetheless, for this experiment a cleaned 'smart' electrosurgical knife is used. Little ablation or charring can be found on this knife. While the measurements do not contain electrosurgical cutting, no ablation or charring is formed on the knife during the measurements. The outcomes of this experiment can therefore not be compared to experiments where the 'smart' electrosurgical knife is used to cut and obtain DR spectra.

All plots in Figure 68 show large variations between the trials. This is could be due to coagulation among other things. However, the spectra clearly show the characteristics of muscle tissue and adipose tissue in Figure 68 respectively. When there would be more time for experiments, a setup with a clean and a dirty 'smart' electrosurgical knife could be used. The influence of dirty fibers could then be examined. More experiments should be performed on how ablation on the fibers influences the spectrum measurements to draw a conclusion.

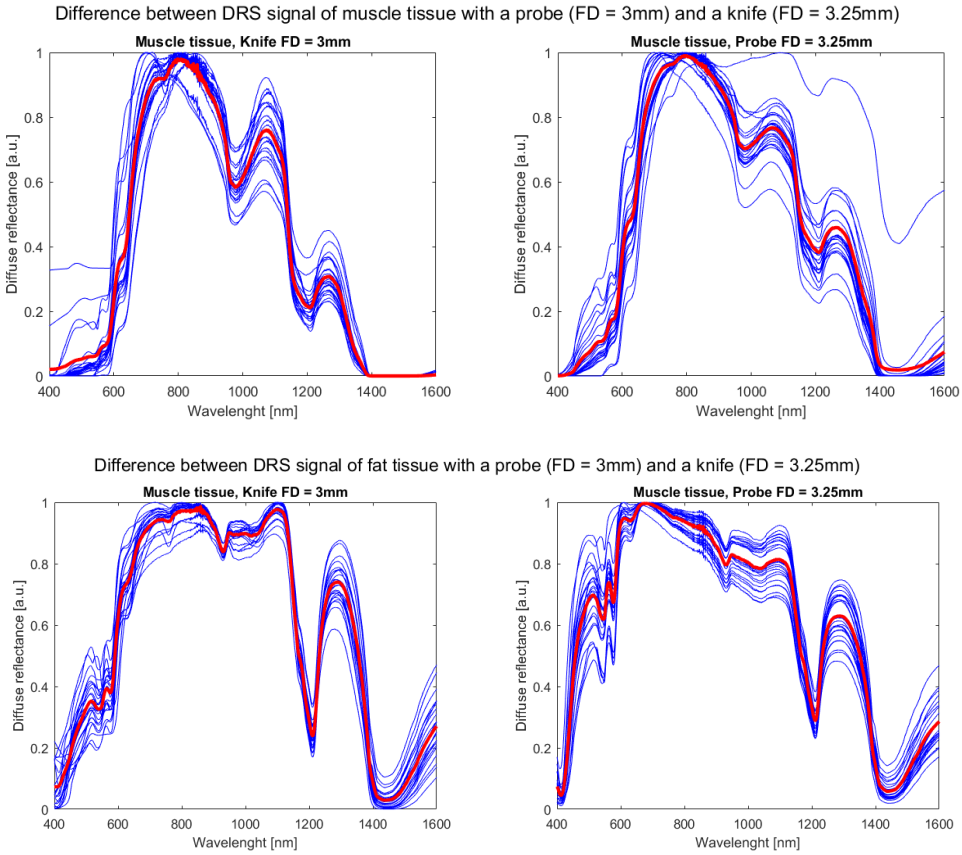

Figure 68: DR spectrum of muscle tissue (upper left and right) and adipose tissue (bottom left and right) measured with a knife (FD=3mm) and a probe (FD=3.25mm). All conditions are measured 24 times, all in blue. The red line is the median of the graph.

13.4. Types of fat

In the various experiments performed for this master thesis, three different types of adipose tissue are used. To examine the influence of electrosurgical cutting and coagulation, pork belly was used. This is a cheap type of muscle which can be obtained in the supermarket and contains both adipose and muscle tissue. The adipose pork tissue – which is most comparable to human adipose tissue – was obtained at LifeTech. To examine the precise transition from muscle to adipose tissue, layers of <1mm were needed. A type of adipose tissue, which could be cut this thin, was frozen sowbelly. Therefore, sowbelly was used for the experiments described in Chapter 9 and 10. All types of adipose tissue can be seen in Figure 69.

Materials & methods

The three types of adipose tissue used for this experiment can be seen in Figure 69, from left to right: adipose pork tissue, sowbelly tissue layers and pork belly tissue. In Figure 44, the probe – which was used to obtain the DR spectra – can be seen. The FD used is 3.25mm. All measurements were taken from non-cut and non-coagulated adipose tissue.

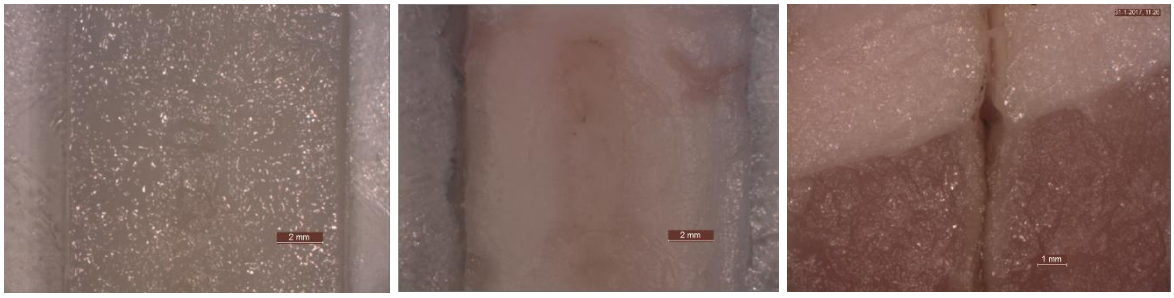

Figure 69: Types of adipose tissue used. From left to right: adipose pork tissue, sowbelly tissue layers and pork belly tissue. Pork belly tissue contains of both muscle tissue (red) and adipose tissue (white).

The independent variables in this experiment are the different types of adipose tissue that are used. The fiber distance and the instrument used to obtain the DR spectra were controlled and the DR spectra itself is the dependent variable which is 'measured'. All variables can be seen in the condition matrix in Table 16.

*Table 16: Condition matrix with two independent variables: types of adipose tissue (pork fat, fat layers and pork belly) and the fiber distance of 3.25mm. All experimental conditions were performed 20 times. * Pork belly tissue was measured 5 times.*

		Tissue type		
Fiber distance	n = 20	**Adipose pork tissue**	**Sowbelly tissue layers**	**Pork belly tissue**
	3.25mm	EC11	EC12	EC 13*

Results

In Figure 70, the different spectra for adipose pork tissue (a), sowbelly tissue layers (b) and pork belly tissue (c) can be seen. All show the characteristics of adipose tissue, described in Paragraph 8.3.3. However, some regions dominate more in one plot compared to the other. In Figure 70a, the region between 900 and 1100nm and the peak around 1300nm dominate more whilst the double peak at 500nm has a lower intensity compared to the other plots. The plot in Figure 70b is weaker for the region between 900 and 1100nm and the peak around 1300nm. Around 500nm, the graph rises however; the double peak is flattened out. The DR spectra obtained from pork belly tissue, seems the average between Figure 70a and c. The region between 900 and 1100nm and the peak around 1300nm dominate less than in Figure 70a but more than in Figure 70c. The region around 500nm dominates more than in Figure 70a, in addition it has a clear double peak.

Discussion

In all three spectra of Figure 70 the characteristics of adipose tissue can be found. Nonetheless, differences in the spectra can be seen. These differences are most likely because of the difference in tissue composition while besides the change of tissue all variables are the same for the experiments. The most important region – between 1200 and 1400nm – shows a peak for all spectra. This region represents the fat lipids, and is crucial for the measurement of fat-water ratio. In Chapter 9, 10 and 11, it is concluded that the fat-water ratio is the best variable to distinguish between adipose and muscle tissue. Therefore, the changes in other parts of the spectra are less important. In addition, the measurements in Chapter 9 and 10 in fat-water ratio could potentially have better outcomes if adipose or pork belly tissue were used while both have a higher intensity between 1200 and 1400nm. Human adipose tissue is most similar to adipose pork tissue when comparing it to the used adipose tissues visually. Therefore, it is expected that, the spectra of human adipose tissue will correspond the most to the spectra of adipose pork tissue. In addition, the characteristics described in Paragraph 8.3.3 for adipose pork tissue correspond to landmarks for adipose tissue described by Schols et al. [78]

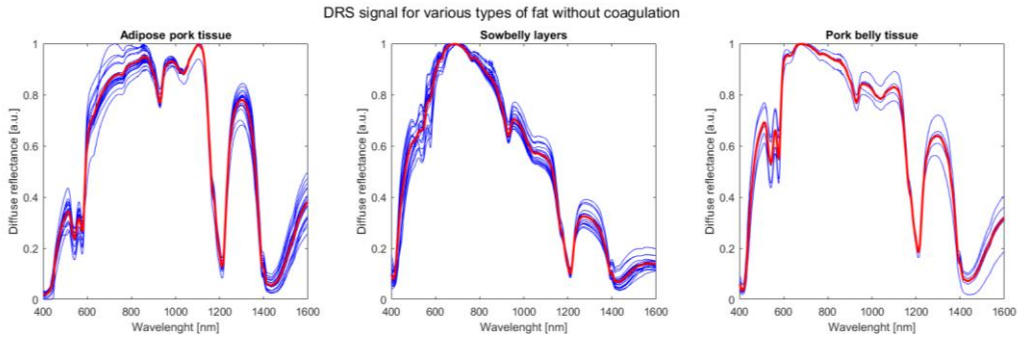

Figure 70: DR spectra of three types of fat. From left to right: adipose pork tissue (a), sowbelly tissue layers (b) and pork belly tissue (c). All conditions are performed 20 times, except for pork belly tissue. This type was measured 5 times.

13.5. While cutting

The intention of this research is to evaluate the possibility to assess margins in a BCS with a 'smart' electrosurgical knife. Assessing margins could then be performed with the same tool as the tissue is cut

with. Measuring DR spectra is a very delicate process with fibers that need to be handled with care. Electrosurgical cutting produces a current with a high voltage from the knife to the dispersive pad. It is expected electrosurgical cutting can disturb the signal measured to obtain a DR spectra. Appendix H shows high peaks between 1000 and 1200nm and between 1200 and 1400nm.

In this experiment, electrosurgical cutting and the measurement of DR spectra are performed at the same time to examine the influence of electrosurgical cutting on the outcome of the measurements in Chapter 11.

Materials & method

For the experiment, a setup similar to the setup in Chapter 11 was used. A layer of 2cm adipose tissue (LifeTech) was placed upon a layer of 2cm muscle tissue (LifeTech). The electrosurgical knife – which is showed in Figure 52 – was used for electrosurgical cutting and obtaining the DR spectra. The knife was placed in the adipose tissue at a depth of 5mm measured from the surface. The timing settings in the PNSas software were set on 0.1 second for both VIS and NIR integration. Therefore, the DR spectra were obtained as fast as possible during cutting.

There are no independent variables present in this experiment. The cutting time, measurement time, tissue, cutting angles and fiber distance are controlled. The DR spectrum is the dependent variable that is measured. The measurement was performed 40 times.

Results

Figure 71 shows 40 measurements of DR spectra obtained while cutting with an electrosurgical knife. The spectra are not normalized in order to show any change in signal strength. Deviation is present throughout the whole spectrum and is largest in the VIS region. Except for the decreased plateau between 800 and 1100nm, all characteristics for adipose tissue – described in Paragraph 8.3.3 – are present in the mean graph of Figure 71. However, some plots have no or less signal before 600nm in the VIS region.

Discussion

The most striking observation in Figure 71 is the large deviation of the measurements. The deviations can be due to multiple causes. First, the VIS and NIR integration time was set as low as possible – on 0.1 second – which will increase the noise on the measurements. Second, it is thought electrosurgical cutting will add noise to the signal by disturbing it with its current and heat production. To be able to distinguish as accurate as possible between adipose and tumour tissue for tumour margin assessment, it is not recommended to measure during cutting. Cutting will increase the noise on your measured signal and therefore provide a less accurate estimate of the chromophore concentrations on which the distinction between tissues is made.

In the VIS region, two extra effects are observed. First, even more deviation is present. This could be due to the visual changes in the tissue caused by electrosurgical cutting. Second, some measurements do not have a signal – or a very small signal – before 600nm. It is assumed the detection of light was too early for these measurements, which leads to the detection of the emitting light from the source. None of this light is absorbed, while it did not enter the tissue yet. Therefore, no signal is present in the spectrum.

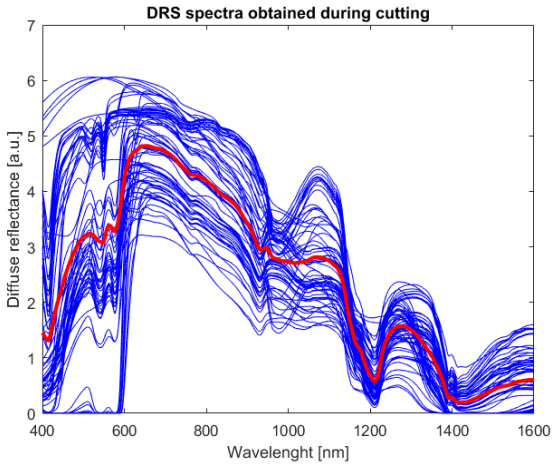

Figure 71: DR spectrum of adipose tissue on top of muscle tissue obtained while cutting. The blue lines represent all 40 measurements and the red – thicker – line represents the mean of all spectra. The spectra are not normalized in order to show any change in signal strength.

Appendix H shows measurements obtained by while cutting, described in Ch12. High peaks between 1000 and 1200nm and between 1200 and 1400nm are observed in these plots. It was thought, these peaks were present due to cutting. Therefore, it was expected to observe the same peaks for this experiment, however this is not true.

13.6. Discussion

In this discussion, the influence of the surrounding light, cutting angles, types of adipose tissue and cutting during measurements will be discussed. The focus will be on the region between 1200 and 1400nm in the spectrum while the peak in this region corresponds to the fat-water ratio. The fat-water ratio is the chromophore concentration concluded to be the most important when making a distinction between adipose tissue and muscle tissue according to the experiments in Chapter 9, 10 and 11.

No experiments are performed on the influence of surrounding light to the measurements. However, Nachabe et al. stated PNSas corrects for surrounding light when a calibration measurements is performed. [88] Nachabe et al. used the same setup as used for the experiments in this thesis. Therefore, it can be assumed surrounding light did not influence the measurements performed in this thesis and will not influence the outcome in clinical practice.

Differences in DR spectra are observed for changing cutting angles. Especially the measurements for 60˚ varied from the other measurements – 30˚ and 90˚ – in the VIS region. To draw a conclusion on the influence of the cutting angle for DR measurements, more experiments for different angles should be performed. Nonetheless, when observing the region between 1200 and 1400nm, all spectra show a peak. This indicates the chromophore concentration of fat-water ratio will be present for all measured spectra. The influence of a changing cutting angle – on the measurements and conclusions drawn in this thesis – will therefore not be major. In addition, changing the cutting angle will not change the possibility of using the 'smart' electrosurgical knife to distinguish between muscle and adipose tissue focusing on the fat-water ratio.

There was no major difference in the DR spectra obtained using a 'smart' knife and a probe. It was expected that the results obtained by the 'smart' electrosurgical knife would show more deviation. However, this was not true observing the DR spectra. A reason for the lack of deviation could be the little ablation and/or charring on the knife. More experiments should be performed on how ablation on the fibers influences the spectrum measurements to be able to draw a conclusion.

The influence of a variation in adipose tissue is minimal for the region between 1200 and 1400nm in DR spectra. In all spectra, a peak is observed which corresponds to the fat-water ratio. Therefore, the difference in adipose tissue will not influence the conclusions made (e.g. fat-water ratio is the best chromophore concentration to focus on for discrimination between adipose and muscle tissue). However, the DR spectra of pork belly tissue were used as a reference to the other adipose spectra. The characteristics for adipose tissue described in Paragraph 8.3.3, are made on the basis of the DR spectra from pork belly tissue. Therefore, when DR spectra of adipose pork tissue and sowbelly layers were observed, they were compared to pork belly. In clinical setting, human adipose tissue will be used. This will – again – be slightly different in DR spectra compared to the other tissues. However, it is expected human adipose tissue will include a peak between 1200 and 1400nm, which makes it possible to distinguish between muscle and adipose tissue.

DR spectra obtained while cutting contained large deviations. This can be due to the electrosurgical cutting itself and/or the minimization of the VIS and NIR integration time in PNSas. Both can increase the noise on the measured signal, which makes it less accurate. Therefore, it is not recommended to measure DR spectra during cutting. In the experiments in this thesis, no DR spectra are measured during cutting. In clinical practice, the tool could be designed in such a way that performing measurements during cutting is not possible.

Design requirements

This chapter describes the influence of a clinical setting on the outcomes of the measurements on the basis of some small experiments. Besides the outcomes of the experiments, the experiments led to some ideas about the design of a 'smart' electrosurgical knife.

Currently, the fibers to emit and detect light are designed next to the cutting blade of the smart electrosurgical knife. To design a sustainable solution that should not be replaced often, it would be better to place the fibers apart from the cutting blade. In this way, they will not be exposed to ablation or charring and the fiber tips will stay clean. An interview with F.J. van Duijnhoven and A.A. Hellingman (both surgeons at The Netherlands Cancer Institute) indicated there is no wish to measure the spectra during cutting but only detect the tumour from <2mm distance. The detection of a tumour should be marked by a sound so the surgeon does not have to change their sight. Perhaps it is possible to design a tool that could slide the fibers forward to the tissue when wanting to measure the spectra and slide them backwards when cutting. In addition, a design could include the restriction of measuring DR spectra when cutting.

When designing the 'smart' electrosurgical knife, it would be an advantage if the fibers were made into an individual tool that could be placed on all – or most – electrosurgical knifes available. Then the tool, including the fibers – which are delicate but not that expensive – could be a single-use object. Therefore, the fiber-tool does not have to be sterilize proof and can be placed upon the electrosurgical knife which is used multiple times.

VI

Discussion, conclusion and recommendations

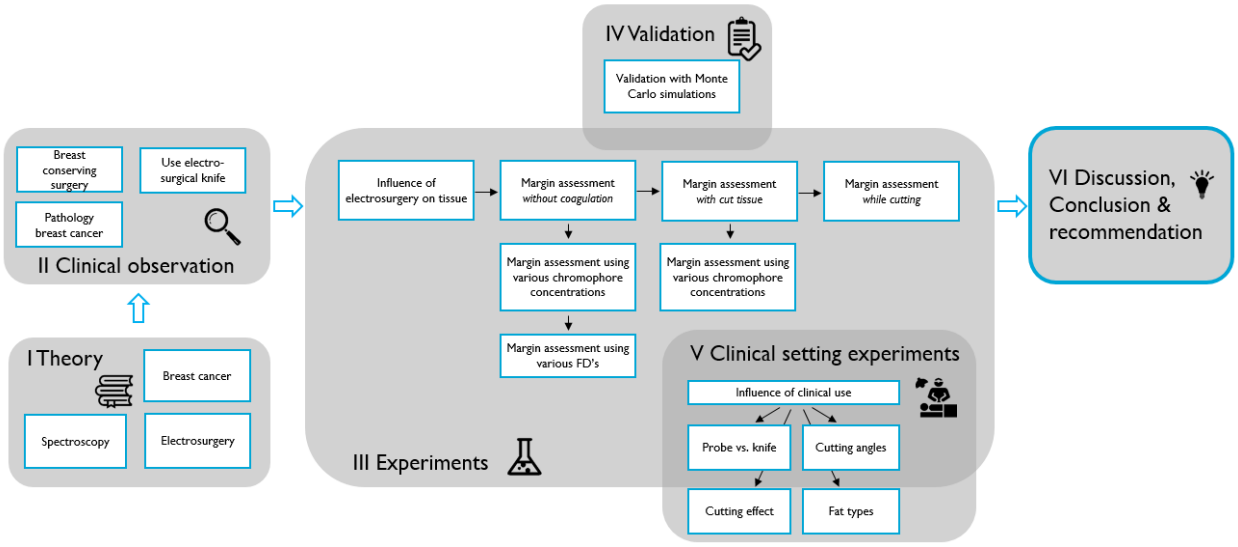

14. Overall discussion

This discussion is a summary of all discussions described per chapter. In addition, links between these discussions are established and an outlook regarding the development of the 'smart' electrosurgical knife is presented.

Influence of electrosurgical cutting and coagulation on tissue

In Chapter 6, the use of the ES knife is described. It is observed that, there are no clear rules on how- and when to use the ES knife for either cutting or coagulation during a BCS. Besides using coagulation for closing blood vessels and cutting tissue close to the surface, surgeons use the setting they prefer at that moment.

From the results of Chapter 8, no clear relation is observed between the increasing power setting and an increasing depth or width of the cut for both cutting and coagulation. According to these results, electrosurgical cutting and coagulation can be called an uncontrollable action of which the precise depth and width of the cut cannot be predicted. A maximum and minimum cutting depth of 1.5mm and 0.27mm respectively, are found for electrosurgical cutting with 50 to 80 Watt. Currently a guideline for margin assessment is to keep a margin of 5 to 10mm. However, the size of the tumour-free resection margin (>1mm) is unrelated to local recurrence. When a 'smart' electrosurgical knife would be able to detect a tumour from a distance of 2mm, this could be insufficient when a maximum cutting depth of 1.5mm is considered. For example, a situation where the ES knife fails to identify a tumour at 2.1mm could occur. When a new cut with a maximum depth of 1.5mm would be made, the clear margin is only 0.6mm. Therefore, using a margin of 2mm could also jeopardize the resection margin of >1mm.

A relation between the increasing power setting and the coagulation zone in muscle tissue is present, according to the results of Chapter 8. For adipose tissue, no coagulation zone is observed. In addition, increasing the power setting increases the deviation of the DR spectrum from pure tissue for both muscle and adipose tissue. The differences between electrosurgical cutting and coagulation and the increase in deviation in DR spectrum would imply a distinction should be made on when to use which setting. Additional research should be performed on the relationship between the settings of the electrosurgical knife and its influence on the tissue. Guidelines on which setting should be used for BCS could prevent a coagulation zone or too much deviation in DR spectra.

DR spectra for tissue transition

The experiments in Chapter 9, 10 and 11 examine the transition from muscle tissue to adipose tissue in pure tissue, cut adipose tissue and while cutting respectively. The transition is described on the basis of the characteristics of muscle tissue and adipose tissue are described in Paragraph 8.3.3. The experiments in Chapter 9 and 10 provide a clear transition from muscle tissue to adipose tissue in Figure 47 and Figure 50.

It was expected, the measurements obtained while cutting would provide a similar transition in DR spectra. However, the spectra obtained while cutting, showed characteristics of adipose tissue while cutting in adipose tissue. Cutting in muscle tissue provided one correct measurement which showed

characteristics of muscle. No transition from muscle and adipose tissue was visible in the DR spectra. The reason of this lack in transition is not known. However, two aspects could have influenced the results. First, when increasing the depth of the knife, a decrease in the signal strength is observed. This could be due to the ablation formed on the knife while cutting. When more ablation is present on the cutting blade and the fibers, less light is emitted or detected by the fibers. This will result in a lower signal strength. Second, the DR spectra in cut muscle tissue – described in Chapter 8 – showed more deviation in the spectra compared to cut adipose tissue.

Not all measured spectra are considered correct. Appendix I, shows three examples of errors observed in measured spectra which are considered as a 'bad' fit. A fit is 'bad' if a low or no signal is present, if the scattering coefficient is lower than the signal, or when the fit does not follow the measured spectrum. Reasons for a bad fit could be the following: ablation on the knife reduces the signal, a – too – short integration time was used, the probe or knife was not in contact with the tissue, the probe or knife moved during the measurement or the surrounding light changed during the measurement.

Fiber distance

The results in Chapter 9, 10 and 11 show a deeper sensing depth when a larger FD is used. Therefore, the transition from adipose to muscle tissue runs smoother for larger FDs in both DR spectra as well as chromophore concentrations.

A significant difference in fat-water ratio was measured when comparing muscle to adipose tissue. For a FD of 6.2mm, the detection of muscle tissue under an adipose tissue layer is possible from 1.2mm – for non-cut tissue – and from 0.8mm for cut tissue. When cutting – with a FD of 3mm – a significant change in spectra was obtained from 2mm distance. More research should be performed on the specific sensing depth at certain FD's to choose the right FD for the 'smart' electrosurgical knife, taking into consideration the clear margin needed for BSC. In addition, the FD cannot be set too large as a large FD will decrease the obtained signal strength. The design of the ES knife should also be taken into consideration when choosing a FD.

Chromophore concentrations

For this master thesis, all chromophores available in the PNSas model were observed for changes in measurements comparing muscle to adipose tissue. The fat-water ratio is concluded to be the most valuable variable to focus on when making a distinction between muscle and adipose tissue. This variable provided a significant outcome for non-cut tissue ($p = 1.28e^{-39}$) and cut tissue ($p = 3.32e^{-39}$). De Boer – who examined the difference in chromophore concentrations for non-cut tissue – also came up with these conclusions. [1] The small p-values show a significant difference for muscle and adipose tissue. A significant difference is important in order to have a high accuracy of your measurements in clinical setting.

The measurements obtained while cutting did not provide a significant outcome as there was only one correct measurement obtained in muscle tissue. The fat-water ratio for the measurements in adipose tissue while cutting showed values similar to the concentrations for pure and cut adipose tissue. However, no transition in fat-water ratio is present. The only correct measurement in muscle tissue while cutting, did provide a fat-water ratio similar to the ratios for pure and cut muscle tissue.

The conclusions in this master thesis are based on muscle and adipose tissue. A next step would be to examine the same test on human adipose tissue and tumour tissue. A difference in tissue can change the chromophore concentrations, and therefore the outcome of the results.

Margin assessment

An argument to discontinue this research could be that the focus is too much on the secondary aim of BCS namely the cosmetic outcome by minimizing the clear margin. Instead, large margins could be made to minimizing the reoccurrence of the disease. In my opinion, this is not true because of the following arguments. First, instead of locating the tumour, ion seeds or a guidewire are currently localized. In addition, the relative distance is measured instead of the absolute distance. A 'smart' electrosurgical knife would provide the absolute distance to the actual tumour. Another advantage is the minimization of ablating the tumour as ablation on the tumour encumber the detection of it by a pathologist.

Second, a study of Krekel [28] reports a margin >10mm for 98.8% of all patients receiving a BCS. Although the guidelines of a clear margin are 5 to 10mm. In addition, the tumour was located non-central and close to the nearest margin in most cases. This indicates – despite the use of localization tools as a guidewire or a gamma probe – that it is difficult to perform margin assessments. An additional problem is the negative cosmetic outcome for at least 33.6% of the patients in the study of Krekel.

Third, increasing the amount of dissected tissue will increase the wound and therefore increase the healing time for the patient. Therefore, dissecting with a smaller margin will also stimulate the healing process.

Validation

All simulations performed with the MC model correspond to the measured spectra with a VAF value ≥ 97%. Accordingly, it can be concluded no major mistakes are made during the experiments and the measured spectra are good enough to draw conclusions on. In addition, the peak between 1200 and 1400nm for adipose tissue is clearly visible in all measured and simulated spectra. This peak influences the fat-water ratio, which is considered the most relevant chromophore concentration to be able to distinguish between adipose and muscle tissue.

More simulations would have been made when more time was available. First, the validation would be performed for multiple layers. Then the transition between adipose and muscle tissue – as is measured in the experiments – could have been validated. In a simulation, the depths of the adipose tissue layer(s) could be adjusted in smaller amounts than for the experiments. As a result of that, the fat-water ratio per 0.1mm – or smaller – distance from the tissue could be described.

Future development of the 'smart' electrosurgical knife

In order to evaluate the 'smart' electrosurgical knife, the benefits and considerations of this new technology will be discussed.

First of all, the 'smart' electrosurgical knife will impact the current workflow of a BCS. Making it possible to assess margins while holding the knife will minimize the alterations between the knife and a localization instrument. This will decrease the surgical time and also making it easier to measure and cut at the same location as the surgeon does not have to move his/her hand. Currently ion seeds or a

guidewire are used for tumour detection. Both can be misplaced and therefore not lead to detection of the tumour. In addition, a 'smart' electrosurgical knife will provide the absolute distance instead of a relative distance as is provided when using ion seeds. The distance can be quantified by looking at the chromophore concentrations instead of the spectra. The possibility of ablating the tumour, as shown in Chapter 7, will decrease when it is possible to measure the absolute distance to the tumour.

While the results for making a distinction between muscle and adipose tissue are promising, the 'smart' electrosurgical knife cannot be used in clinical practice yet. The measurements performed during cutting did not provide satisfying results yet. More experiments should be performed on measuring DR spectra during cutting, without the influence of ablation on the fibers. Additional research on signal processing filters can potentially address this issue. In addition, changing the tissue from pork to human tissue could have an effect on the outcome of the measurements. It needs to be taken into account that global localization is still needed as a 'smart' electrosurgical knife cannot guide the surgeon towards the tumour from a distance >2mm.

The advantages described above, the promising results and the positive feedback from practitioners should be an encouragement to continue the development process of the 'smart' electrosurgical knife. The next step would be to repeat the measurements of DR spectra during cutting however, without the influence of ablation on the fibers.

Design

During this project, the design of the 'smart' electrosurgical instrument was omitted. However, the insights obtained in the course of this project are valuable to the subsequent design process. In the current design, fibers to emit and detect light are placed next to the cutting blade of the smart electrosurgical knife. Because of ablation or charring in the vicinity of the electrosurgical knife, the fibers can be damaged. Damaged fibers will provide a signal with more noise. The design could be improved when placing the fibers apart to make sure the fibers will not be damaged due to electrosurgical cutting.

In an interview with F.J. van Duijnhoven and A.A. Hellingman (both surgeons at The Netherlands Cancer Institute), both woman indicated they do not wish to measure the spectra during cutting. Perhaps it is possible to design a tool that could slide the fibers forward in order to measure the spectra, and slide them backwards when cutting. In addition, a design could include the restriction of measuring DR spectra when cutting. When detecting a tumour, the 'smart' electrosurgical knife should provide signal, e.g. a sound or vibration to make sure the surgeon does not have look away from the operating site.

When designing the 'smart' electrosurgical knife, it would be an advantage if the fibers were made into a separate tool that could be placed on the electrosurgical knife. Then the separate fiber tool could be a single-use object. Therefore, the fiber-tool does not have to be sterilisable and can be placed upon the electrosurgical knife which is used multiple times.

15. Conclusion

To conclude this master thesis, the research question described in the Introduction will be answered.

1. What changes in adipose and muscle tissue can be identified when cutting or coagulating with an electrosurgical knife at various (50, 60, 70, 80 Watt) settings?

Electrosurgical cutting and/or coagulation affects tissue. No relationship was observed between the cutting depth or width and an increasing power. The width of the cut is larger than the depth of the cut for both cutting and coagulation in muscle- and adipose tissue. An average depth of 0.72mm and 0.65mm was measured for cutting muscle tissue and adipose tissue respectively. For coagulation, the average depth measured was 0.43mm for muscle tissue and 0.71mm for adipose tissue. A coagulation zone was only observed in muscle tissue after coagulating. The coagulation zone has an average depth of 0.43mm. All values can be found in Table 17.

Electrosurgical cutting and coagulation does not only influence the tissue visually, but also affects the composition of the tissue. Change in composition can be seen in DR spectra where measurements on pure tissue are compared to measurements on cut or coagulated tissue. According to the results in this Chapter 8, cutting and coagulation in muscle and adipose tissue does not change the overall shape of the spectrum. However, cutting decreases the intensity of the peaks in the visual region between 500 and 600nm and at 700nm for muscle tissue. These peaks decrease in intensity when cutting with higher power settings. Coagulation also decreases the intensity of the peaks in the visual region for muscle tissue. The peak at 700nm has a lower intensity and the double peak between 500 and 600nm disappears when increasing the coagulation power. For adipose tissue, less deviation is observed for both cutting and coagulation compared to muscle tissue. The small deviation present is not limited to specific regions but is present in the whole spectrum. The deviation increases for an increasing power in electrosurgical cutting, for coagulation, no trend is observed.

Table 17: Cutting and coagulation depth and width for muscle and adipose tissue, measured in the experiment described in Chapter 8. A coagulation zone is only observed in muscle tissue.

		Cutting		Coagulation	
		Muscle tissue	Adipose tissue	Muscle tissue	Adipose tissue
Depth	Min.	0.27mm	0.28mm	0.20mm	0.23mm
	Avg.	0.72mm	0.65mm	0.43mm	0.71mm
	Max.	1.5mm	1.4mm	1.16mm	1.56mm
Width	Min.	0.31mm	0.29mm	0.40mm	0.41mm
	Avg.	0.82mm	1.16mm	0.88mm	1.12mm
	Max.	1.52mm	2.27mm	1.67mm	2.03mm
Depth Zone	Min.	-	-	0.20mm	0mm
	Avg.	-	-	0.43mm	0mm
	Max.	-	-	1.05mm	0mm

II. Is it possible to observe the transition from healthy to tumour tissue in the DR spectrum when no electrosurgical cutting is used?

The DR spectra measured in Chapter 8 are used to describe characteristic peaks for pure adipose and pure muscle tissue. In pure adipose tissue, five characteristics can be found in the DR spectrum:

1. A double peak between 500 and 600nm with a higher intensity compared to muscle tissue.*
2. A plateau from 600 to 1100nm.*
3. A double peak at 1000nm.
4. A large peak between 1200 and 1400nm.
5. A new peak starting from 1400nm.

Pure muscle tissue can also be recognized by five characteristics in the DR spectrum:

1. A low double peak between 500 and 600nm.
2. A peak at 700nm with a small dip just before this peak.
3. A gradually decreasing slope after 700nm.*
4. A peak and dip at 1000 and 1100nm.*
5. A second peak and dip at 1200 and 1300nm.*

The characteristics marked by an asterisk indicate qualitative landmarks for haemoglobin – in muscle tissue – and for adipose tissue. [78] The difference between a DR spectrum for pure adipose and pure muscle tissue are apparent by comparing the aforementioned characteristics. In this thesis, the differences between the two spectra are not quantified. However, when looking at the chromophore concentrations, a quantified difference between pure muscle and pure adipose tissue can be seen. The difference between pure muscle and pure adipose tissue is significant for the fat-water ratio ($p = 1.28e^{-39}$), StO_2 percentage ($p = 4.81e^{-15}$), blood percentage ($p = 9.93e^{-7}$) and b percentage ($p = 0.014$). The other chromophores in PNSas do not provide a significant difference between pure muscle and pure adipose tissue.

Changes in fiber distances influence the measured spectra. First, the transition between muscle and adipose tissue – which can be seen for all fiber distances – elapses faster for small fiber distances compared to large fiber distances. The transition is elapsed at 1.2mm for an FD of 3.25mm, at 1.6 for a FD of 3.75mm, at 2mm for a FD of 5mm and at 1.6mm for a FD of 6.2mm. Second, the results in this thesis show some changes in the spectra for different fiber distances. For the smaller FDs – 3.25mm and 3.75mm – the double peak between 500 and 600nm has a higher intensity. For a FD of 5mm and 6.2mm an increase in intensity for the region between 500 and 700nm, around 900nm and between 1000 and 1200nm was observed. Changes in the obtained spectra due to a change in FD need to be considered when designing a 'smart' electrosurgical knife.

III. Is it possible to observe the transition from healthy to tumour tissue in the DR spectrum during cutting with an electrosurgical knife?

Cutting does not change the overall shape of the DR spectra for both muscle and adipose tissue according to the results in Chapter 8. However, changes that can be seen are:

1. A decrease in intensity in the regions between 500 and 600nm and at 700nm for muscle tissue.
2. An increase in intensity in the region between 900 and 1100nm.
3. More deviation in the regions between 1000 and 1200nm and between 1200 and 1400nm.

When observing the transition from muscle to adipose tissue, the elapse of the transition begins and ends at the same distance from muscle tissue for both cut and non-cut tissue.

The difference between a DR spectrum for cut adipose and pure muscle tissue are apparent by comparing the aforementioned characteristics, similar as for pure muscle- and adipose tissue. This difference can be quantified looking at the difference in chromophore concentrations when comparing pure muscle and cut adipose tissue. The difference can be seen best in the fat-water ratio ($p = 3.32e^{-39}$), StO_2 percentage ($p = 3.23e^{-27}$), blood percentage ($p = 2.36e^{-9}$) and F_{mie} percentage ($p = 2.84e^{-8}$). The other chromophores in PNSas do not provide a significant difference between pure muscle and pure adipose tissue.

The spectra obtained while cutting did not provide a clear transition from adipose to muscle tissue as observed for pure and cut tissue. Measurements in adipose tissue ($> 0mm$) provided spectra containing characteristics of adipose tissue and measurements in muscle tissue ($< 0mm$) provided spectra containing characteristics of muscle tissue. Additionally, all spectra obtained in muscle tissue – except for one – were rejected due to 'bad' fits. As no transition between muscle and adipose tissue can be seen and only one measurement was obtained in muscle tissue, no conclusion can be drawn on the possibility to discriminate between muscle and adipose tissue while cutting.

16. Recommendations

While writing this master thesis, some gaps of knowledge were identified. In addition, – if the research on 'smart' electrosurgical knifes is continued – some ideas for further research are determined.

It is concluded it is possible to distinguish between muscle and adipose tissue for non-cut tissue and cut tissue. The focus for further research should be on the fat-water ratio as this chromophore concentration discriminates between muscle and adipose tissue with the highest accuracy compared to the other variables. The DR measurements obtained while cutting did not provide a significant distinction between muscle and adipose tissue. Further research should be conducted to address the transition from muscle to adipose tissue while cutting. The experiments in Chapter 11 should be repeated excluding the influence of ablation on the fibers. This could be done using a 'smart' needle to measure the DR spectra after the cuts are made. The results obtained for pure and cut tissue, together with advantages of the 'smart' electrosurgical knife described in Chapter 14 make me believe this research should be continued.

Some uncertainties – which came to thought during this master thesis – should be examined when continuing the research. Do changing cutting angles influence the DR spectrum? How does blood effect the DR spectrum in the region between 1200 and 1400nm? Is it possible to distinguish between adipose and muscle tissue for coagulated tissue or during coagulation? Does tension affects DR spectra?

Another step in further research is the design of a prototype, integrating the requirements for a 'smart' electrosurgical knife. More interviews should be conducted asking the users all requirements. In addition, the suggestions for a design made in Chapter 14 could be integrated. After a prototype is made, the experiments described in this thesis could be repeated. The results obtained in this thesis can then serve as reference values for the prototype. If these results are satisfactory, a next step could be taken by performing measurements on a phantom breast of adipose tissue including a 'tumour' made of muscle tissue.

A future step – when the 'smart' electrosurgical knife has proven its feasibility and accuracy to detect a tumour in adipose tissue – could be to use the knife for other applications. Experiments using DRS for the detection of lung and colon cancer are already performed and provide promising results. [89] [90] [91]

Bibliography

[1] L. L. de Boer, B. G. Molenkamp, T. M. Bydlon, B. H. W. Hendriks, J. Wesseling, H. J. C. M. Sterenborg, and T. J. M. Ruers, "Fat/water ratios measured with diffuse reflectance spectroscopy to detect breast tumour boundaries.," *Breast Cancer Res. Treat.*, vol. 152, no. 3, pp. 509–518, 2015.

[2] J. Fleischer, B. H. W. Hendriks, and J. Dankelman, "Diffuse Reflectance Spectroscopy for Intraoperative Tumour Margin Assessment - Workflow Analysis and Effect of Coagulation on Tissue Sensing," 2015.

[3] IARC and I. A. for R. on Cancer, "World Cancer Report 2014," 2014.

[4] A. M. Mohs, M. C. Mancini, S. Singhal, J. M. Provenzale, B. Leyland-Jones, M. D. Wang, and S. Nie, "Hand-held spectroscopic device for in vivo and intraoperative tumour detection: Contrast enhancement, detection sensitivity, and tissue penetration," *Anal. Chem.*, vol. 82, no. 21, pp. 9058–9065, 2010.

[5] A. Manuscript, "Stereotactic Mass Spec Surgery," vol. 68, no. 2, pp. 280–290, 2013.

[6] A. M. De Grand and J. V Frangioni, "An operational near-infrared fluorescence imaging system prototype for large animal surgery.," *Technol. Cancer Res. Treat.*, vol. 2, no. 6, pp. 553–62, Dec. 2003.

[7] J. Balog, L. Sasi-szabó, J. Kinross, M. R. Lewis, L. J. Muirhead, K. Veselkov, R. Mirnezami, B. Dezs, L. Damjanovich, A. Darzi, J. K. Nicholson, and Z. Takáts, "Intraoperative Tissue Identification Using Rapid Evaporative Ionization Mass Spectrometry," vol. 5, no. 194, 2013.

[8] D. Evers, B. Hendriks, G. Lucassen, and T. Ruers, "Optical spectroscopy: current advances and future applications in cancer diagnostics and therapy," *Futur. Med.*, vol. 8, pp. 1–14, 2012.

[9] A. Westgaard, S. Tafjord, I. N. Farstad, M. Cvancarova, T. J. Eide, O. Mathisen, O. P. F. Clausen, and I. P. Gladhaug, "Resectable adenocarcinomas in the pancreatic head: the retroperitoneal resection margin is an independent prognostic factor," *BMC Cancer*, vol. 8, no. 1, p. 5, Dec. 2008.

[10] A. Wibe, P. R. Rendedal, E. Svensson, J. Norstein, T. J. Eide, H. E. Myrvold, and O. Soreide, "Prognostic significance of the circumferential resection margin following total mesorectal excision for rectal cancer," *Br. J. Surg.*, vol. 89, no. 3, pp. 327–334, Mar. 2002.

[11] R. Jeevan, D. A. Cromwell, M. Trivella, G. Lawrence, O. Kearins, J. Pereira, C. Sheppard, C. M. Caddy, and J. H. P. van der Meulen, "Reoperation rates after breast conserving surgery for breast cancer among women in England: retrospective study of hospital episode statistics," *BMJ*, vol. 345, 2012.

[12] A. S. Haka, Z. Volynskaya, J. A. Gardecki, J. Nazemi, J. Lyons, D. Hicks, M. Fitzmaurice, R. R. Dasari, J. P. Crowe, and M. S. Feld, "In vivo Margin Assessment during Partial Mastectomy Breast Surgery Using Raman Spectroscopy," *Cancer Res.*, vol. 66, no. 6, 2006.

[13] F. Meric, N. Q. Mirza, G. Vlastos, T. A. Buchholz, H. M. Kuerer, G. V. Babiera, S. E. Singletary, M. I. Ross, F. C. Ames, B. W. Feig, S. Krishnamurthy, G. H. Perkins, M. D. McNeese, E. A. Strom, V. Valero, and K. K. Hunt, "Positive surgical margins and ipsilateral breast tumour recurrence predict disease-specific survival after breast-conserving therapy," *Cancer*, vol. 97, no. 4, pp. 926–933, Feb. 2003.

[14] P. I. Karakiewicz, J. A. Eastham, M. Graefen, I. Cagiannos, P. D. Stricker, E. Klein, T. Cangiano, F. H. Schröder, P. T. Scardino, and M. W. Kattan, "Prognostic impact of positive surgical margins in surgically treated prostate cancer: Multi-institutional assessment of 5831 patients," *Urology*, vol. 66, no. 6, pp. 1245–1250, 2005.

[15] B. Kuvshinoff, I. Maghfoor, B. Miedema, M. Bryer, S. Westgate, J. Wilkes, and D. Ota, "Distal Margin Requirements After Preoperative Chemoradiotherapy for Distal Rectal Carcinomas: Are ? 1 cm Distal Margins Sufficient?," *Ann. Surg. Oncol.*, vol. 8, no. 2, pp. 163–169, Mar. 2001.

[16] T. Karni, I. Pappo, J. Sandbank, O. Lavon, V. Kent, R. Spector, S. Morgenstern, and S. Lelcuk, "A device for real-time, intraoperative margin assessment in breast-conservation surgery," *Am. J. Surg.*, vol. 194, no. 4, pp. 467–473, 2007.

[17] M. R. Grootendorst, M. Cariati, A. Kothari, D. S. Tuch, and A. Purushotham, "Cerenkov luminescence imaging (CLI) for image-guided cancer surgery," *Clin. Transl. Imaging*, vol. 4, no. Cli, pp. 353–366, 2016.

[18] J. F. Waljee, E. S. Hu, L. A. Newman, and A. K. Alderman, "Predictors of Re-excision among Women Undergoing Breast-

Conserving Surgery for Cancer."

[19] K. A. Iczkowski, M. S. Lucia, K. A. Iczkowski, and M. S. Lucia, "Frequency of positive surgical margin at prostatectomy and its effect on patient outcome.," *Prostate Cancer*, vol. 2011, p. 673021, 2011.

[20] T. S. Menes, P. I. Tartter, I. Bleiweiss, J. H. Godbold, A. Estabrook, and S. R. Smith, "The Consequence of Multiple Re-Excisions to Obtain Clear Lumpectomy Margins in Breast Cancer Patients," *Ann. Surg. Oncol.*, vol. 12, no. 11, pp. 881–885, Nov. 2005.

[21] H. R. Raziee, R. Cardoso, R. Seevaratnam, A. Mahar, L. Helyer, C. Law, and N. Coburn, "Systematic review of the predictors of positive margins in gastric cancer surgery and the effect on survival," *Gastric Cancer*, vol. 15, no. S1, pp. 116–124, Sep. 2012.

[22] P. B. A. A. van Driel, M. van de Giessen, M. C. Boonstra, T. J. A. Snoeks, S. Keereweer, S. Oliveira, C. J. H. van de Velde, B. P. F. Lelieveldt, A. L. Vahrmeijer, C. W. G. M. Löwik, and J. Dijkstra, "Characterization and Evaluation of the Artemis Camera for Fluorescence-Guided Cancer Surgery," *Mol. Imaging Biol.*, vol. 17, no. 3, pp. 413–423, 2015.

[23] M. Kauer, V. Vuskovic, J. Dual, G. Szekely, and M. Bajka, "Inverse finite element characterization of soft tissues," *Lect. Notes Comput. Sci. (including Subser. Lect. Notes Artif. Intell. Lect. Notes Bioinformatics)*, vol. 2208, pp. 128–136, 2001.

[24] A. Munshi, S. Kakkar, R. Bhutani, R. Jalali, A. Budrukkar, and K. A. Dinshaw, "Factors Influencing Cosmetic Outcome in Breast Conservation," *Clin. Oncol.*, vol. 21, pp. 285–293, 2009.

[25] M. F. E B Hanlon, R Manoharan, T-WKoo, K E Shafer, J T Motz, MFitzmaurice, J R Kramer, I Itzkan, R R Dasari, "Prospects for in vivo Raman spectroscopy Evaluation of texture parameters for the quantitative description of multimodal NLO images Compton scattering from breast tissue Prospects for in vivo Raman spectroscopy," *Phys. Med. Biol.*, vol. 45, no. 1–59, 2000.

[26] J. C. Fleischer, J. Dankelman, and H. W. Hendriks, "Effect of coagulation on tissue sensing with diffuse reflectance spectroscopy – towards real-time surgical guidance in cancer surgery," pp. 7–10.

[27] K. D. Miller, R. L. Siegel, C. C. Lin, A. B. Mariotto, J. L. Kramer, J. H. Rowland, K. D. Stein, R. Alteri, and A. Jemal, "Cancer treatment and survivorship statistics, 2016.," *CA. Cancer J. Clin.*, vol. 66, no. 4, pp. 271–89, 2016.

[28] N. M. Krekel, B. M. Zonderhuis, H. W. Schreurs, A. M. Lopes Cardozo, H. Rijna, H. van der Veen, S. Muller, P. Poortman, L. de Widt, W. K. de Roos, A. M. Bosch, A. H. Taets van Amerongen, E. Bergers, M. H. van der Linden, E. S. de Lange de Klerk, H. A. Winters, S. Meijer, and P. M. van den Tol, "Ultrasound-guided breast-sparing surgery to improve cosmetic outcomes and quality of life. A prospective multicentre randomised controlled clinical trial comparing ultrasound-guided surgery to traditional palpation-guided surgery (COBALT trial)," *BMC Surg.*, vol. 11, no. 1, p. 8, Dec. 2011.

[29] M. W. Adank, H. W. Hendriks, and J. Dankelman, "Assessing the added value of diffuse reflectance spectroscopy in electrosurgery."

[30] American Cancer Society, "Cancer Facts & Figures 2016," *Cancer Facts Fig. 2016*, pp. 1–9, 2016.

[31] B. S. Nichols, C. E. Schindler, J. Q. Brown, L. G. Wilke, C. S. Mulvey, M. S. Krieger, J. Gallagher, J. Geradts, R. A. Greenup, J. A. Von Windheim, and N. Ramanujam, "A Quantitative Diffuse Reflectance Imaging (QDRI) system for comprehensive surveillance of the morphological landscape in breast tumour margins," *PLoS One*, vol. 10, no. 6, pp. 1–25, 2015.

[32] F. Sheikh, A. Rebecca, B. Pockaj, N. Wasif, A. E. McCullough, W. Casey, P. Kreymerman, and R. J. Gray, "Inadequate margins of excision when undergoing mastectomy for breast cancer: which patients are at risk?," *Ann. Surg. Oncol.*, vol. 18, no. 4, pp. 952–6, 2011.

[33] J. Carlander, K. Johansson, S. Lindström, A. K. Velin, C. H. Jiang, and C. Nordborg, "Comparison of experimental nerve injury caused by ultrasonically activated scalpel and electrosurgery," *Br. J. Surg.*, vol. 92, no. 6, pp. 772–777, 2005.

[34] J. P. Holland, G. Normand, A. Ruggiero, J. S. Lewis, and J. Grimm, "Intraoperative imaging of positron emission tomographic radiotracers using cerenkov luminescence emissions," *Mol. Imaging*, vol. 10, no. 3, pp. 177–186, 2011.

[35] M. E. M. van der Noordaa, K. E. Pengel, E. Groen, E. van Werkhoven, E. J. T. Rutgers, C. E. Loo, W. Vogel, and M. J. T. F. D. Vrancken Peeters, "The use of radioactive iodine-125 seed localization in patients with non-palpable breast cancer: A comparison with the radioguided occult lesion localization with 99m technetium," *Eur. J. Surg. Oncol.*, vol. 41, no. 4, pp. 553–558, 2015.

[36] H. C. Snider and D. G. Morrison, "Intraoperative Ultrasound Localization of Nonpalpable Breast Lesions," *Ann. Surg. Oncol.*, vol. 6, no. 3, pp. 308–314, Apr. 1999.

[37] D. L. Pavia, G. M. Lampman, G. S. Kriz, and J. R. Vyvyan, *Introduction to Spectroscopy*, vol. 121, no. 1. 2015.

[38] M. E. James, *Physics for Radiation Protection: A Handbook*, 1st ed. Wiley, 2013.

[39] S. Keereweer, P. B. A. A. Van Driel, T. J. A. Snoeks, J. D. F. Kerrebijn, R. J. B. De Jong, A. L. Vahrmeijer, H. J. C. M. Sterenborg, and C. W. G. M. Löwik, "Optical image-guided cancer surgery: Challenges and limitations," *Clin. Cancer Res.*, vol. 19, no. 14, pp. 3745–3754, 2013.

[40] R. Choe, "Diffuse optical tomography and spectroscopy of breast cancer and fetal brain," *Med. Phys.*, vol. 32, no. 10, p. 3230, 2005.

[41] Y. Garini, I. Young, and G. McNamara, "Spectral imaging: principles and applications," *Cytom. Part A*, vol. 747, pp. 735–747, 2006.

[42] G. Lu and B. Fei, "Medical hyperspectral imaging: a review.," *J. Biomed. Opt.*, vol. 19, no. 1, p. 10901, 2014.

[43] E. A. Genina, A. N. Bashkatov, Y. P. Sinichkin, I. Y. Yanina, and V. V Tuchin, "Optical clearing of biological tissues : prospects of application in medical diagnostics and phototherapy," vol. 247, no. March, pp. 2838–2842, 2015.

[44] S. L. Jacques, "Optical Properties of Biological Tissues: A Review," *Phys. Med. Biol.*, vol. 58, no. 11, pp. R37-61, 2013.

[45] V. Sharma, D. Kashyap, A. Mathker, S. Narvenkar, K. Bensalah, W. Kabbani, A. Tuncel, J. a Cadeddu, and H. Liu, "Optical reflectance spectroscopy for detection of human prostate cancer.," *Conf. Proc. IEEE Eng. Med. Biol. Soc.*, vol. 2009, pp. 118–21, 2009.

[46] A. T. M. H. Van Keersop, R. Nachabe, B. H. W. Hendriks, M. Mueller, and T. Bydlon, "PhotonicNeedle Spectral Analysis User manual," 2011.

[47] T. M. Bydlon, R. Nachabé, N. Ramanujam, H. J. C. M. Sterenborg, and B. H. W. Hendriks, "Chromophore based analyses of steady-state diffuse reflectance spectroscopy: Current status and perspectives for clinical adoption," *J. Biophotonics*, vol. 8, no. 1–2, pp. 9–24, 2015.

[48] V. G. Prabitha, S. Suchetha, J. L. Jayanthi, K. V. Baiju, P. Rema, K. Anuraj, A. Mathews, P. Sebastian, and N. Subhash, "Detection of cervical lesions by multivariate analysis of diffuse reflectance spectra: a clinical study," *Lasers Med. Sci.*, vol. 31, no. 1, pp. 67–75, 2016.

[49] R. M. P. Doornbos, R. Lang, M. C. Aalders, F. W. Cross, and H. J. C. M. Sterenborg, "The determination of in vivo human tissue optical properties and absolute chromophore concentrations using spatially resolved steady-state diffuse reflectance spectroscopy," *Phys. Med. Biol.*, vol. 44, no. 4, pp. 967–981, 1999.

[50] I. Georgakoudi, E. E. Sheets, M. G. Müller, V. Backman, C. P. Crum, K. Badizadegan, R. R. Dasari, and M. S. Feld, "Trimodal spectroscopy for the detection and characterization of cervical precancers in vivo," *Am. J. Obstet. Gynecol.*, vol. 186, no. 3, pp. 374–382, 2002.

[51] L. Yang and S. J. Miklavcic, "Revised Kubelka-Munk theory. III. A general theory of light propagation in scattering and absorptive media.," *J. Opt. Soc. Am. A. Opt. Image Sci. Vis.*, vol. 22, no. 9, pp. 1866–1873, 2005.

[52] A. Escobedo Morales, E. Sánchez Mora, and U. Pal, "Use of diffuse reflectance spectroscopy for optical characterization of un-supported nanostructures," *Rev. Mex. Física S*, vol. 53, no. 5, pp. 18–22, 2007.

[53] T. J. Farrell, M. S. Patterson, and B. Wilson, "A diffusion theory model of spatially resolved, steady-state diffuse reflectance for non invasive determination of tissue optical properties in vivo," *Med. Physics1*, vol. 19, pp. 879–888, 1992.

[54] A. Jewel, R. Nachabe, and B. H. W. Hendriks, "Applicability of diffusion theory for different fiber distances separations in determination of phantoms and tissue properties," *Tech. Note - Philips*, 2010.

[55] R. Hafez, O. Hamadah, and W. Bachir, "Mapping of healthy oral mucosal tissue using diffuse reflectance spectroscopy: ratiometric-based total hemoglobin comparative study," *Lasers Med. Sci.*, vol. 30, no. 8, pp. 2135–2141, 2015.

[56] N. Lue, J. W. Kang, C. Yu, I. Barman, N. C. Dingari, S. Michael, R. R. Dasari, and M. Fitzmaurice, "Portable Optical Fiber Probe-Based Spectroscopic Scanner for Rapid Cancer Diagnosis : A New Tool for Intraoperative Margin Assessment," vol. 7, no. 1, 2012.

[57] K. Wang and A. P. Advincula, "'Current thoughts' in electrosurgery," *Int. J. Gynecol. Obstet.*, vol. 97, no. 3, pp. 245–250, 2007.

[58] G. Sankaranarayanan, R. R. Resapu, D. B. Jones, S. Schwaitzberg, and S. De, "Common uses and cited complications of energy in surgery," *Surg. Endosc. Other Interv. Tech.*, vol. 27, no. 9, pp. 3056–3072, 2013.

[59] World Health Organization, "Core Medical Equipment Core medical equipment - Information," p. 5, 2011.

[60] I. Alkatout, T. Schollmeyer, N. a. Hawaldar, N. Sharma, and L. Mettler, "Principles and Safety Measures of Electrosurgery in Laparoscopy," *JSLS, J. Soc. Laparoendosc. Surg.*, vol. 16, no. 1, pp. 130–139, 2012.

[61] L. S. Feldman, P. R. Fuchshuber, and D. B. J. Editors, *The SAGES Manual on the Fundamental Use of Surgical Energy (FUSE)*. 2012.

[62] C. W. Van Way, "Electrosurgery 101.," *Curr. Surg.*, vol. 57, no. 2, pp. 172–7, 2000.

[63] K. Gallagher, B. Dhinsa, and J. Miles, "Electrosurgery," *Surg.*, vol. 29, no. 2, pp. 70–72, 2011.

[64] Erbe Elektromedizin GmbH, "Electrosurgery," *Electrosurgery, use Pract. tips*, 2015.

[65] A. Taheri, P. Mansoori, L. F. Sandoval, S. R. Feldman, D. Pearce, and P. M. Williford, "Electrosurgery: part II. Technology, applications, and safety of electrosurgical devices.," *J. Am. Acad. Dermatol.*, vol. 70, no. 4, p. 607.e1-12; quiz 619-20, Apr. 2014.

[66] D. L. Carr-Locke and J. Day, "Principles of Electrosurgery," *Success. Train. Gastrointest. Endosc.*, pp. 125–134, 2011.

[67] A. Taheri, P. Mansoori, L. F. Sandoval, S. R. Feldman, D. Pearce, and P. M. Williford, "Electrosurgery: Part I. Basics and principles," *J. Am. Acad. Dermatol.*, vol. 70, no. 4, pp. 1–14, 2014.

[68] N. N. Massarweh, N. Cosgriff, and D. P. Slakey, "Electrosurgery: History, principles, and current and future uses," *J. Am. Coll. Surg.*, vol. 202, no. 3, pp. 520–530, 2006.

[69] K. M. Group, "Electrosurgery," *KLS Martin Group*. [Online]. Available: http://www.klsmartin.com/fileadmin/Inhalte/Downloads_Prospekte/HF-Geraete/90-604-02-04_09_06_Handbuch_HF.pdf. [Accessed: 23-Oct-2016].

[70] A. S. Technologies, "Aesculap ® BipoJet ®."

[71] B. Braun, *Aesculap ® Electrosurgical Instruments and Devices*. Tuttlingen, 2016.

[72] M. P. Wu, C. S. Ou, S. L. Chen, E. Y. T. Yen, and R. Rowbotham, "Complications and recommended practices for electrosurgery in laparoscopy," *Am. J. Surg.*, vol. 179, no. 1, pp. 67–73, 2000.

[73] T. L. Smith and J. M. Smith, "Electrosurgery in otolaryngology-head and neck surgery: principles, advances, and complications.," *Laryngoscope*, vol. 111, no. 5, pp. 769–80, 2001.

[74] A. Madani, Y. Watanabe, M. C. Vassiliou, P. Fuchshuber, D. B. Jones, S. D. Schwaitzberg, G. M. Fried, and L. S. Feldman, "Impact of a hands-on component on learning in the Fundamental Use of Surgical Energy™ (FUSE) curriculum: a randomized-controlled trial in surgical trainees," *Surg. Endosc. Other Interv. Tech.*, vol. 28, no. 10, pp. 2772–2782, 2014.

[75] H.-C. Hur, I. Green, A. M. Modest, M. Milad, E. Huang, and H. Ricciotti, "Needs Assessment for Electrosurgery Training of Residents and Faculty in Obstetrics and Gynecology," *JSLS J. Soc. Laparoendosc. Surg.*, vol. 18, no. 3, p. e2014.00293, 2014.

[76] B. Cugmas, M. Bregar, M. Bürmen, F. Pernuš, and B. Likar, "Impact of contact pressure–induced spectral changes on soft-tissue classification in diffuse reflectance spectroscopy: problems and solutions," *J. Biomed. Opt.*, vol. 19, no. 3, p. 37002, Mar. 2014.

[77] W. C. Vogt, A. Izquierdo-Román, B. Nichols, L. Lim, J. W. Tunnell, and C. G. Rylander, "Effects of mechanical indentation on diffuse reflectance spectra, light transmission, and intrinsic optical properties in ex vivo porcine skin," *Lasers Surg. Med.*, vol. 44, no. 4, pp. 303–309, Apr. 2012.

[78] R. M. Schols, L. Alic, G. L. Beets, S. O. Breukink, F. P. Wieringa, and L. P. S. Stassen, "Automated Spectroscopic Tissue Classification in Colorectal Surgery.," *Surg. Innov.*, vol. 22, no. 6, pp. 557–67, 2015.

[79] L. L. de Boer, B. H. W. Hendriks, F. van Duijnhoven, M.-J. T. F. D. V. Peeters-Baas, K. Van de Vijver, C. E. Loo, K. Jóźwiak, H. J. C. M. Sterenborg, and T. J. M. Ruers, "Using DRS during breast conserving surgery: identifying robust optical parameters and influence of inter-patient variation," *Biomed. Opt. Express*, vol. 7, no. 12, p. 5188, 2016.

[80] K. Farahani, R. E. Saxton, H. Yoon, A. A. F. De Salles, K. L. Black, and R. B. Lufkin, "MRI of thermally denatured blood:

Methemoglobin formation and relaxation effects," *Magn. Reson. Imaging*, vol. 17, no. 10, pp. 1489–1494, 1999.

[81] L. N. Deden, T. Ruers, T. M. Bydlon, and B. H. W. Hendriks, "Development of an optical device for intra - operative tumour margin detection," *Tech. Note - Philips*, 2014.

[82] N. Haj-Hosseini, S. Lowndes, G. Salerud, and K. Wårdell, "Blood interference in fiber-optical based fluorescence guided resection of glioma using 5-aminolevulinic acid," 2011, p. 78833R.

[83] J. Fleischer, B. H. W. Hendriks, and J. Dankelman, "Integration of tissue-sensing into electrosurgical instruments," no. may, 2015.

[84] H. Arimoto, M. Egawa, and Y. Yamada, "Depth profile of diffuse reflectance near-infrared spectroscopy for measurement of water content in skin," *Ski. Res. Technol.*, vol. 11, no. 1, pp. 27–35, Feb. 2005.

[85] L. Wang, S. L. Jacques, and L. Zheng, "MCML - Monte Carlo modeling of light transport in multi-layered tissues," *Comput. Methods Programs Biomed.*, vol. 47, pp. 131–146, 1995.

[86] D. P. Landau and K. Binder, *A guide to Monte Carlo Simulations in Statistical Physics*. Cambridge: Cambridge University Press, 2013.

[87] L. Henyey and J. Greenstein, "Diffuse radiation in the galaxy," *Astrophys. J.*, 1941.

[88] R. Nachabé, *Diagnosis with near infrared spectroscopy during minimally invasive procedures*. 2012.

[89] J. W. Spliethoff, W. Prevoo, M. A. J. Meier, J. de Jong, H. M. Klomp, D. J. Evers, H. J. C. M. Sterenborg, G. W. Lucassen, B. H. W. Hendriks, and T. J. M. Ruers, "Real-time In Vivo Tissue Characterization with Diffuse Reflectance Spectroscopy during Transthoracic Lung Biopsy: A Clinical Feasibility Study," *Clin. Cancer Res.*, vol. 22, no. 2, 2016.

[90] J. W. Spliethoff, D. J. Evers, H. M. Klomp, J. W. van Sandick, M. W. Wouters, R. Nachabe, G. W. Lucassen, B. H. W. Hendriks, J. Wesseling, and T. J. M. Ruers, "Improved identification of peripheral lung tumours by using diffuse reflectance and fluorescence spectroscopy," *Lung Cancer*, vol. 80, no. 2, pp. 165–171, 2013.

[91] E. Tanis, J. W. Spliethoff, D. J. Evers, G. C. Langhout, P. Snaebjornsson, W. Prevoo, B. H. W. Hendriks, and T. J. M. Ruers, "Real-time in vivo assessment of radiofrequency ablation of human colorectal liver metastases using diffuse reflectance spectroscopy," *Eur. J. Surg. Oncol.*, vol. 42, no. 2, pp. 251–259, 2015.

[92] I. S. Saidi, S. L. Jacques, and F. K. Tittel, "Mie and Rayleigh modeling of visible-light scattering in neonatal skin," *Appl. Opt.*, vol. 34, no. 31, p. 7410, Nov. 1995.

Appendices

Appendix	Reference	Description
A	§3.3	Description on tissue properties relevant for optical imaging
B	§3.5	Definition of all variables used in Equation (8)
C	§8.5	DR spectra of pure, cut and coagulated muscle tissue and pure, cut and coagulated adipose tissue.
D	§9.3	DR spectra of the transition from pure muscle to adipose tissue with FD's: 3.25, 3.75, 5 and 6.2mm.
E	§9.5	Chromophore concentrations of the transition from pure muscle to adipose tissue for α, $s800$ and F_{mie}. The fat-water ratio for FD's of 3.25, 3.75, 5 and 6.2mm.
F	§10.3	All DR spectra obtained for the transition from muscle to cut adipose tissue for FD's of 3.25, 3.75, 5 and 6.2mm.
G	§10.4	The fat-water ratio for the transition from pure muscle to cut adipose tissue for FD's of 3.25, 3.75, 5 and 6.2mm.
H	§11.3	All DR spectra obtained while measuring during cutting with and without removing the 'bad' fits. The mean values of all measured spectra during cutting excluded the 'bad' fits in one plot.
I	§11.4	Examples of 'bad' fits: a low signal, low scattering, a bad fit.
J	§11.4	Chromophore concentrations (fat-water ratio, StO_2 and F_{mie}) measured for the transition from muscle to adipose tissue while cutting including the second best and third best fit.
K	§11.4	Chromophore concentrations (StO_2 and F_{mie}) measured for the transition from muscle to adipose tissue while cutting including the one 'good' fit.
L	§ 12.1	Values used as inputs for the Monte Carlo model

Appendix A

Referred to in Paragraph 3.3. A more elaborate description of tissue properties relevant for optical imaging: the absorption coefficient, μ_a [cm^{-1}], the scattering coefficient μ_s [cm^{-1}], the scattering function $p(\theta, \psi)$ [sr^{-1}], anisotropy coefficient g, refractive index of the tissue n' and the reduced scattering coefficient $\mu_s{}'$.

Reduced scattering coefficient

For prediction of tissue scattering and the behaviour of light diffusion in the wavelength range of 400 to 1300 nm, two equations are used which are equally good according Jacques. [44] One description of the reduced scattering coefficient is given by

$$\mu_s' = a\left(\frac{\lambda}{500\ (nm)}\right)^{-b} \tag{26}$$

where λ is the wavelength, normalized by a reference wavelength of 500 nm. The b characterizes the wavelength dependence of μ_s' which is called the scattering power. Alternatively, the reduced scattering coefficient can be described by

$$\mu_s'\ (\lambda) = a'\left(f_{ray}\left(\frac{\lambda}{500\ (nm)}\right)^{-4} + (1 - f_{ray})\left(\frac{\lambda}{500\ (nm)}\right)^{-b_{Mie}}\right)^{-b} \tag{27}$$

where the coefficient is dependent on the separated contributions of the Rayleigh and Mie scattering at the reference wavelength. Mie scattering describes the scattering of light meeting objects with a similar size to the wavelength whereas Rayleigh scattering describes the elastic scattering of light by particles much smaller than the wavelength. More information about Rayleigh and Mie scattering can be found in [92].

Scattering and anisotropy

The scattering coefficient is usually measured by a collimated transmission measurement (T_c). It is described by the formula

$$\mu_s = -\frac{\ln(T_c)}{L}, \tag{28}$$

where L is the thickness of the tissue. To be able to measure μ_s a thin sample, of approximately 100 µm (the scale of one mean free path: $meanfreepath = 1/\mu_s$), is required. An underestimation of μ_s can

occur when the tissue sample is desiccated or the tissue is non-heterogenic. In addition a too large angle of collection of the light will lead to an underestimation of μ_s.

The same complications can occur when preparing a sample for measuring g, of which the sample needs to be thin. The measurement of $p(\theta)$ using goniometry concerns measuring the angular scattering of light of a thin sample.

Tissue scattering properties can be controlled by compressing, stretching, dehydration, coagulation of the tissue and by immersion with biocompatible chemical agents and photochemical and –thermal clearing. [43] Controlling these properties can be important when wishing to decrease the light scattering of the tissue to improve the imaging depth and quality. It can also increase the precision of spectroscopic information of deep tissue layers and blood. [43]

Refractive index

To describe the complex refractive index n,

$$n = n' + jn'' \tag{29}$$

the real refraction index n', the imaginary refractive index n'' and the absorption coefficient $\mu_a = 4\pi n''/\lambda$ are required. The real refraction index describes energy storage and hence affects the speed of light in a medium. The imaginary refraction index describes energy dissipation and specifies the absorption coefficient.

Absorption coefficient

The absorption coefficient μ_a is described by T, the transmitted or surviving fraction of the incident light after the incremental path length ∂L [cm]. In addition, ∂T/T per ∂L yields an exponential decrease in the intensity of the light as a function of increasing path length L. The relation between μ_a and T is given by

$$\mu_a = -\frac{1}{T}\frac{\partial T}{\partial L} \tag{30}$$

where T can be described as

$$T = e^{-\mu_a L} = 10^{-\varepsilon C L} = e^{-4\pi n'' L/\lambda}\,. \tag{31}$$

Appendix B

Referred to in 3.5. Definition of all variables used in Equation (8)

Farrel described the measured diffuse reflectance intensity distribution $I(r)$ as

$$I(r) = \alpha \frac{a'}{4\pi}\left[\frac{1}{\mu_t{}'}\left(\mu_{eff} + \frac{1}{\widetilde{r_1}}\right)\frac{e^{-\mu_{eff}\widetilde{r_1}}}{\widetilde{r_1}^2} + \left(\frac{1}{\mu_t{}'} + 2z_b\right)\left(\mu_{eff} + \frac{1}{\widetilde{r_2}}\right)\frac{e^{-\mu_{eff}\widetilde{r_2}}}{\widetilde{r_2}^2}\right].$$

Where

$$r^2 = x^2 + y^2$$

$$\mu_s' = \mu_s(1 - g)$$

$$\mu_t' = \mu_a + \mu_s'$$

$$z_b = \frac{2}{3\mu_t'}$$

$$\widetilde{r_1} = \left[r^2 + \left(\frac{1}{\mu_t'}\right)^2\right]^{1/2}$$

$$\widetilde{r_2} = \left[r^2 + \left(\frac{1}{\mu_t'} + 2z_b\right)^2\right]^{1/2}$$

$$\mu_{eff} = \sqrt{3\mu_a\mu_t'}$$

$$a' = \frac{\mu_s'}{\mu_t'}$$

Appendix C

Referred to in Paragraph 8.5. DR signals of pure muscle tissue, cut muscle tissue, pure adipose tissue, cut adipose tissue, coagulated muscle tissue and coagulated adipose tissue. All measurements performed are showed in these plots including a plot of the mean in red.

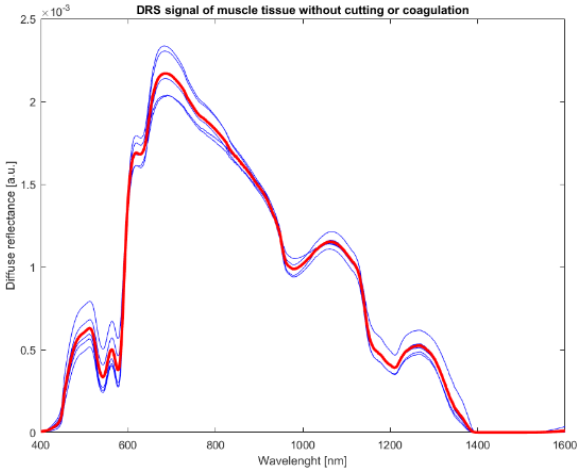

Figure 72: DRS signal of muscle tissue without cutting or coagulation. Five measurements are performed which are plotted in blue. The average of all measurements is plotted in red.

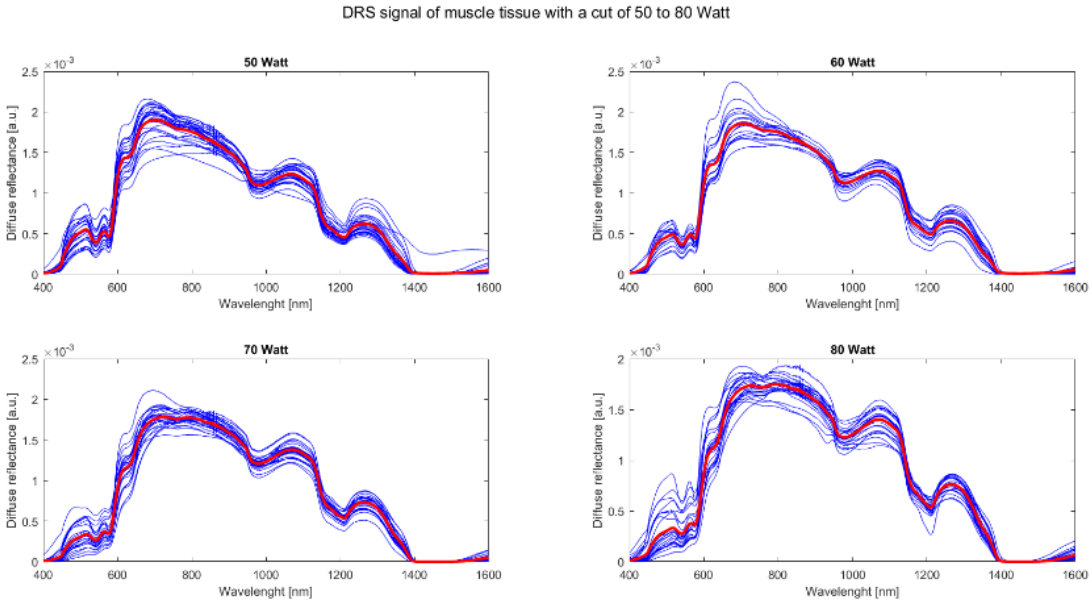

Figure 73: DRS signal of muscle tissue with a cut performed at 50 Watt (top left), 60 Watt (top right), 70 Watt (bottom left) and 80 Watt (bottom right). All experimental conditions are performed 30 times, plotted in blue. The average is plotted in red.

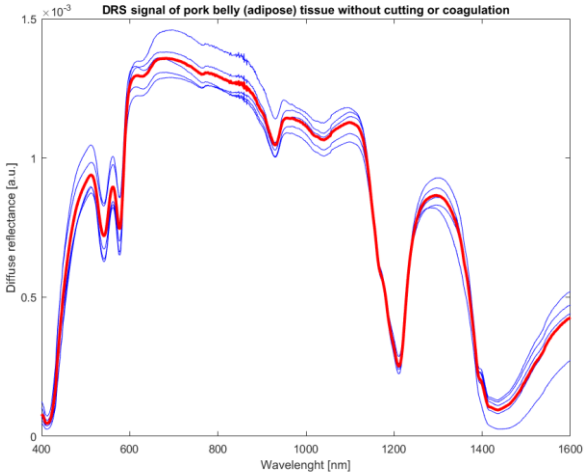

Figure 74: DRS signal of adipose tissue without cutting or coagulation. Five measurements are performed, plotted in blue. The average is plotted in red.

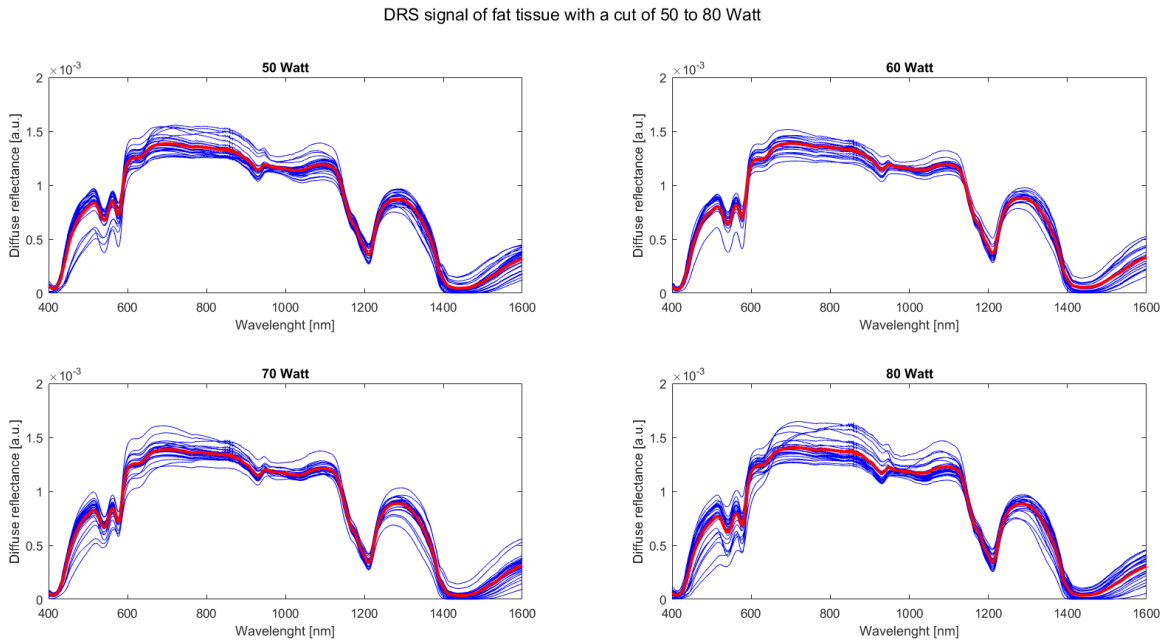

Figure 75: DRS signal of adipose tissue with a cut performed at 50 Watt (top left), 60 Watt (top right), 70 Watt (bottom left) and 80 Watt (bottom right). All experimental conditions are performed 30 times.

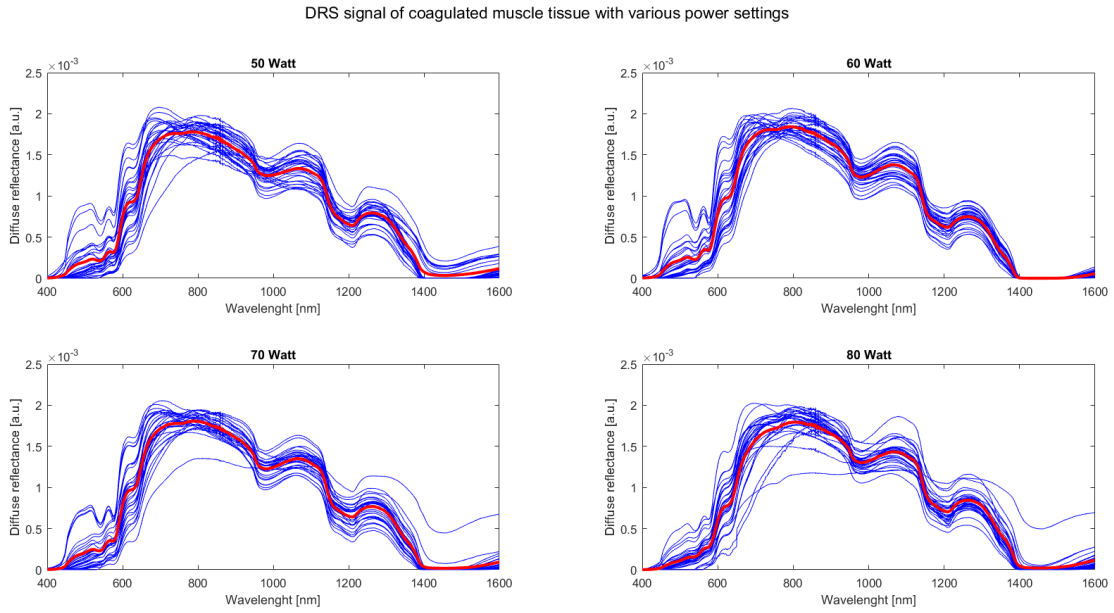

Figure 76: DRS signal of coagulated muscle tissue performed at 50 Watt (top left), 60 Watt (top right), 70 Watt (bottom left) and 80 Watt (bottom right). All experimental conditions are performed 30 times.

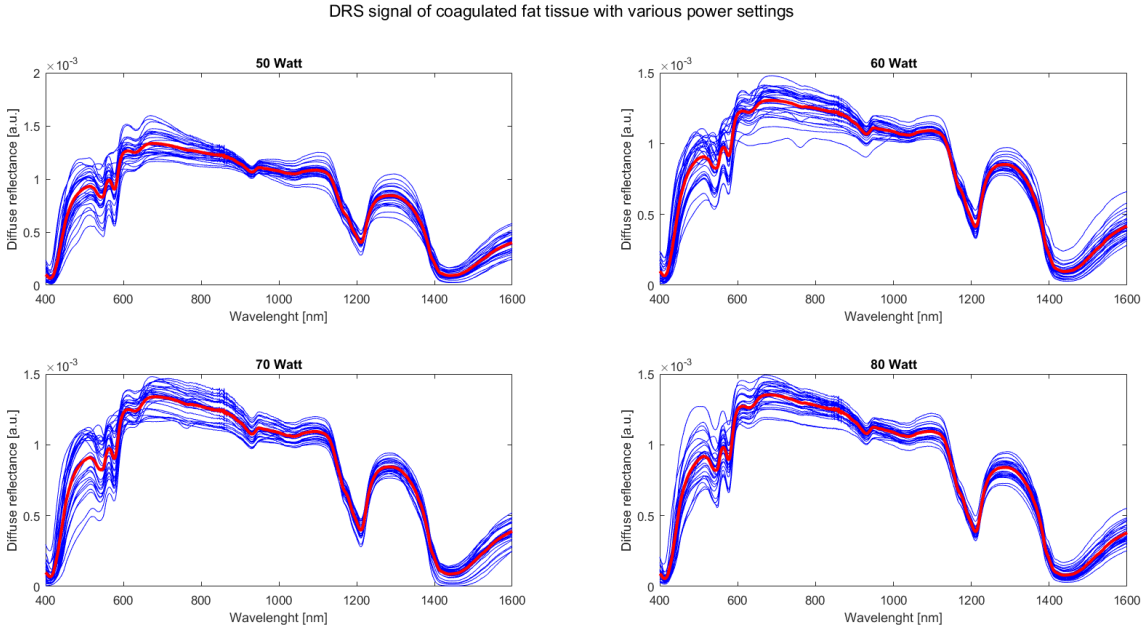

Figure 77: DRS signal of coagulated adipose tissue performed at 50 Watt (top left), 60 Watt (top right), 70 Watt (bottom left) and 80 Watt (bottom right). All experimental conditions are performed 30 times.

Appendix D

Referred to in Paragraph 9.3 DR spectra of the transition from pure muscle to pure adipose tissue with FD's: 3.25, 3.75mm, 5mm and 6.2mm.

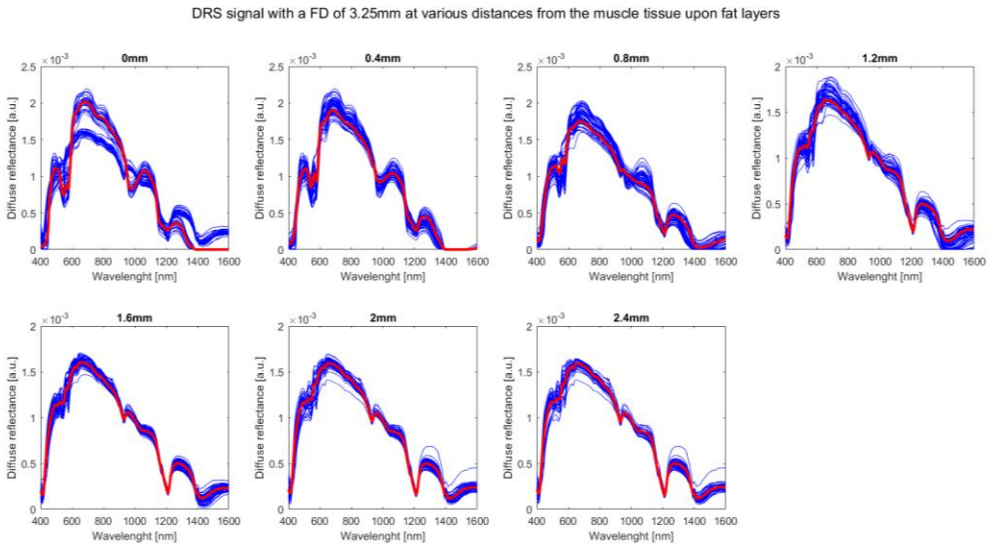

Figure 78: DRS signal of muscle tissue with layers of fat upon it, a probe with a fiber distance of 3.25mm is used. The title of every plot represents the thickness of the fat layer upon the muscle tissue for that measurement. All experimental conditions are performed 30 times, plotted in blue. The average is plotted in red.

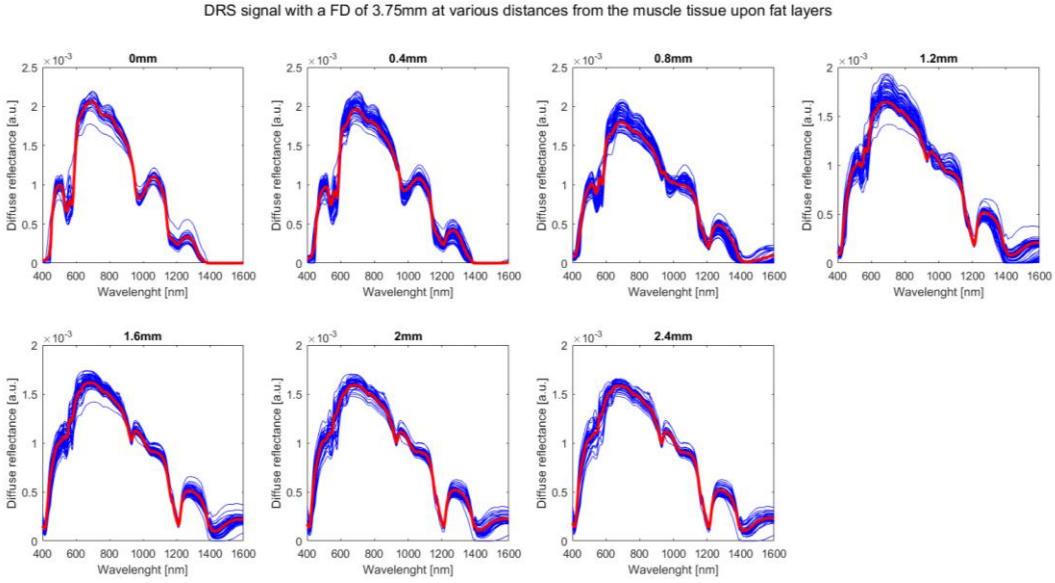

Figure 79: DRS signal of muscle tissue with layers of fat upon it, a probe with a fiber distance of 3.25mm is used. The title of every plot represents the thickness of the fat layer upon the muscle tissue for that measurement. All experimental conditions are performed 30 times, plotted in blue. The average is plotted in red.

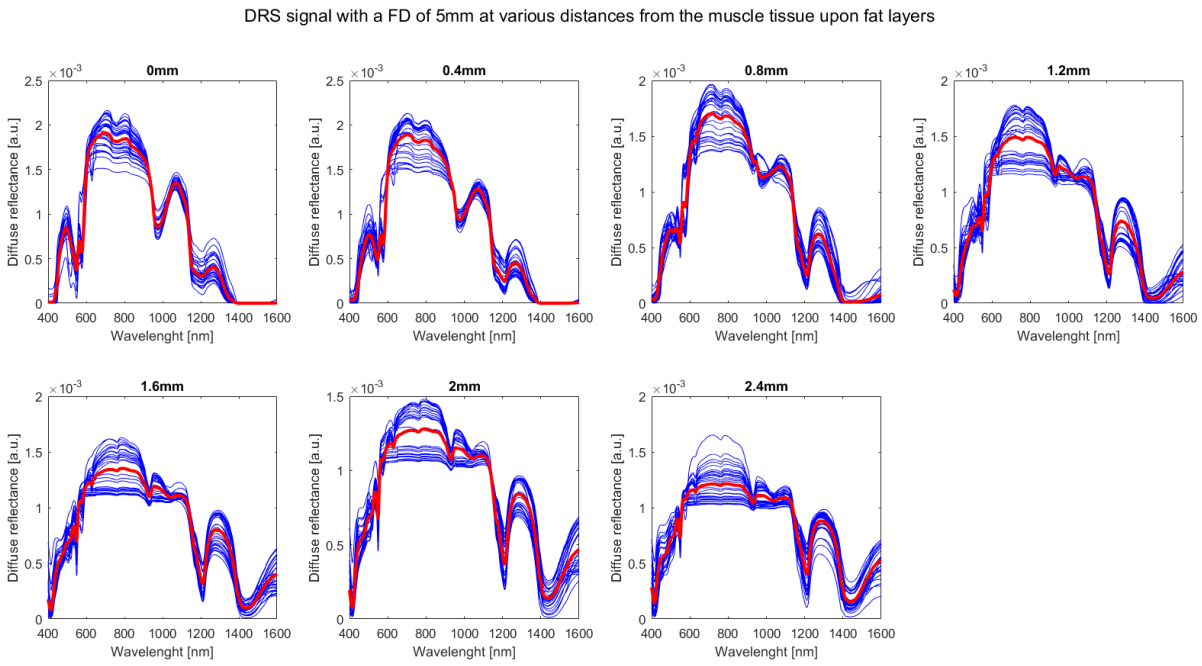

Figure 80: DRS signal of muscle tissue with layers of fat upon it, a probe with a fiber distance of 5mm is used. The title of every plot represents the thickness of the fat layer upon the muscle tissue for that measurement. All experimental conditions are performed 30 times, plotted in blue. The average is plotted in red.

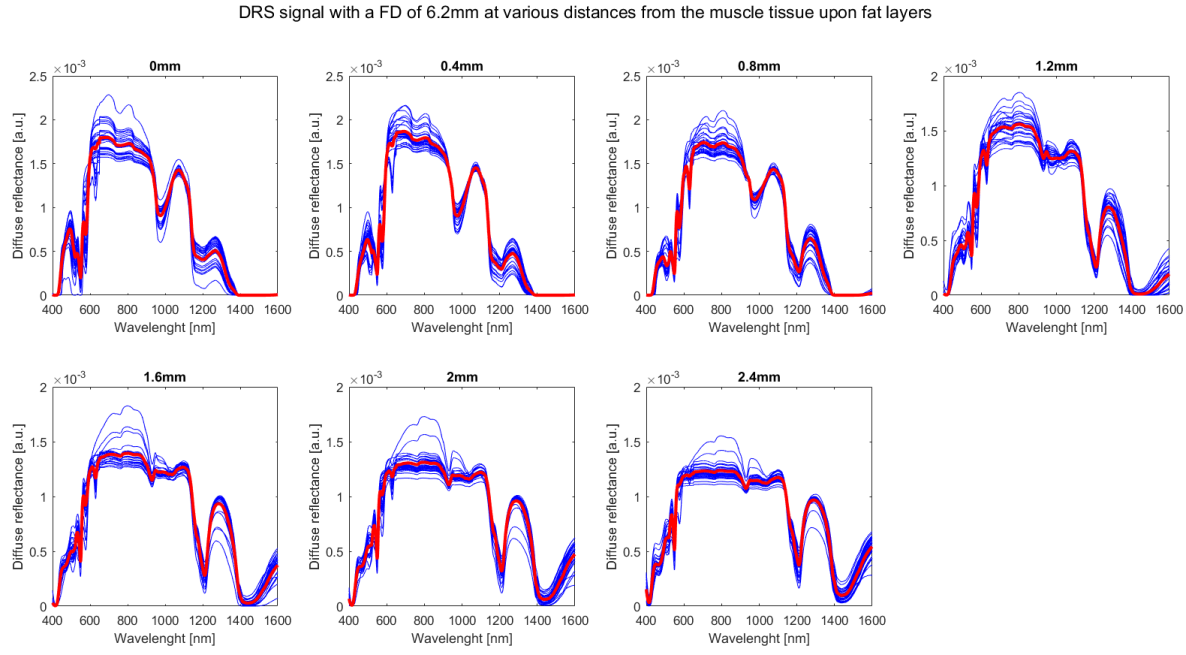

Figure 81: DRS signal of muscle tissue with layers of fat upon it, a probe with a fiber distance of 6.2mm is used. The title of every plot represents the thickness of the fat layer upon the muscle tissue for that measurement. All experimental conditions are performed 30 times, plotted in blue. The average is plotted in red.

Appendix E

Referred to in Paragraph 9.5. The first plot shows the fat-water ratio of the transition from pure muscle tissue to pure adipose tissue for multiple fiber distances: 3.25, 3.75, 5 and 6.2mm. The transition in concentration runs more smoothly for increasing fiber distances. The second plot represents chromophore concentrations from coefficients not providing a significant difference between muscle and adipose tissue: α, S_{800} and F_{mie}

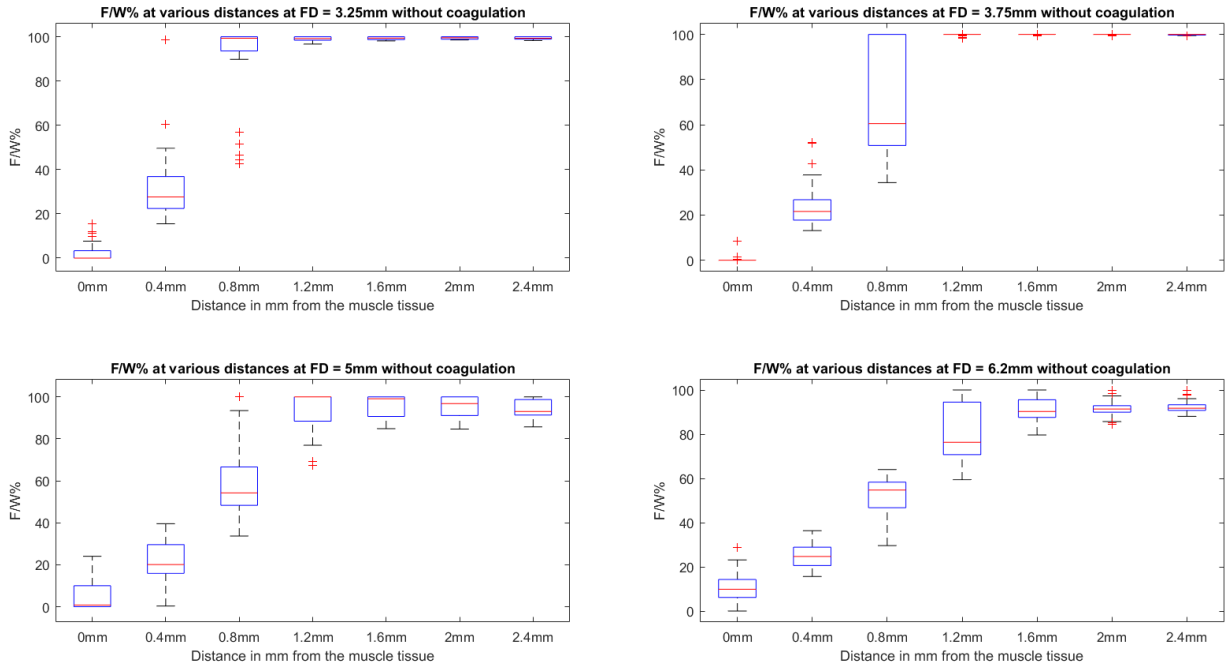

Figure 82: Chromophore concentrations for Fat/Water ratio at various distances from the muscle tissue. The different FDs used are 3.25mm (upper left), 3.75mm (upper right), 5mm (bottom left) and 6.2mm (bottom right). All conditions include 30 measurements.

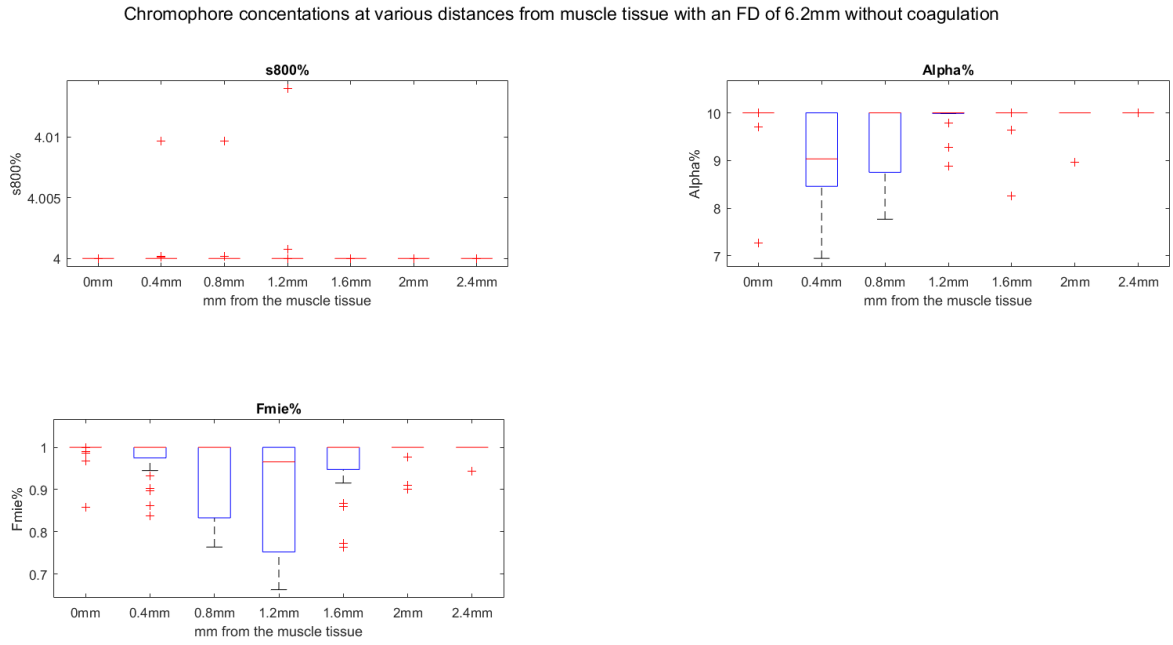

Figure 83: Chromophore concentrations of scattering variables b, alpha and s800 at various distances, 0mm, 0.4mm, 0.8mm, 1.2mm, 1.6mm, 2mm and 2.4mm from muscle tissue with a FD of 6.2mm. All conditions include 15 measurements.

Appendix F

Referred to in Paragraph 10.3. All DR spectra obtained for the transition from muscle to cut adipose tissue for FD's of 3.25, 3.75, 5 and 6.2mm.

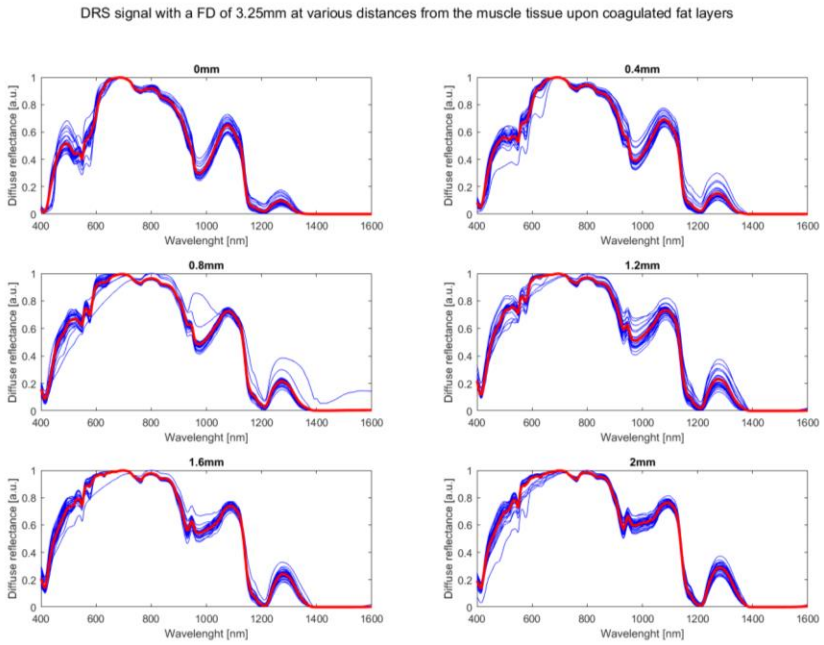

Figure 84: DR spectra of the transition between muscle tissue (0mm) and adipose tissue layers (from 0.4mm). The title represents the depth of the adipose layers. The FD used is 3.25mm. All experimental conditions are performed 30 times.

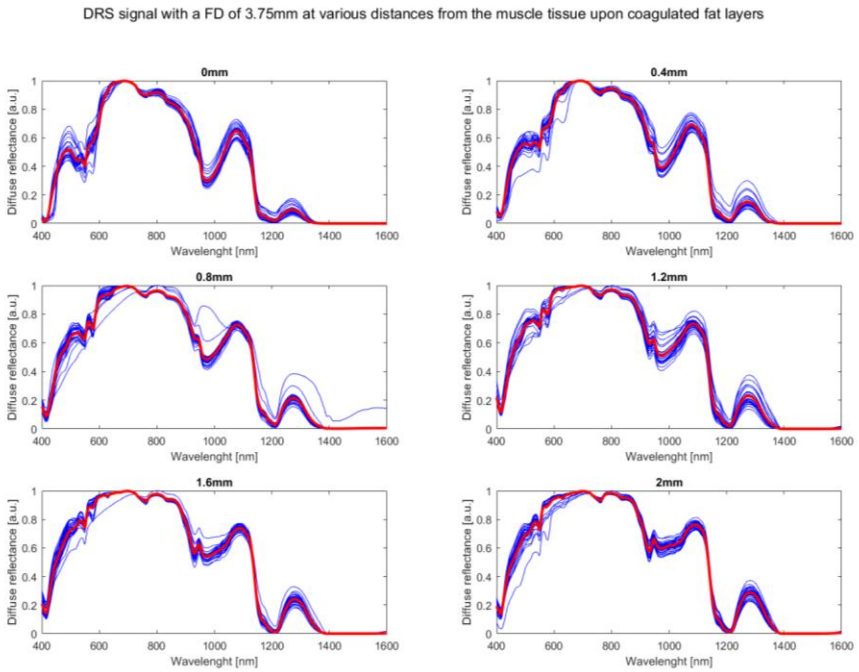

Figure 85: DR spectra of the transition between muscle tissue (0mm) and adipose tissue layers (from 0.4mm). The title represents the depth of the adipose layers. The FD used is 3.75mm. All experimental conditions are performed 30 times.

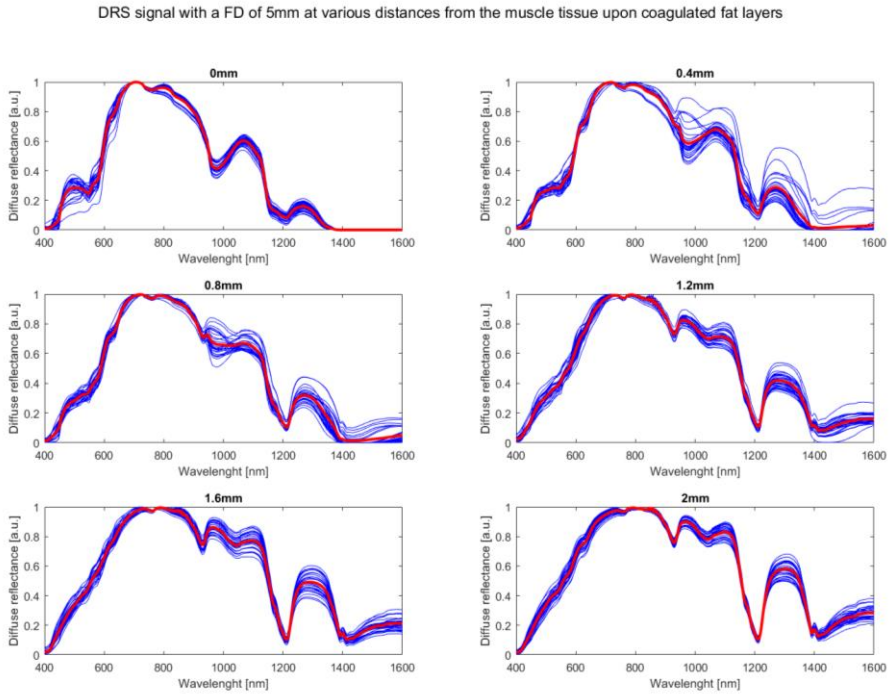

Figure 86: DR spectra of the transition between muscle tissue (0mm) and adipose tissue layers (from 0.4mm). The title represents the depth of the adipose layers. The FD used is 5mm. All experimental conditions are performed 30 times.

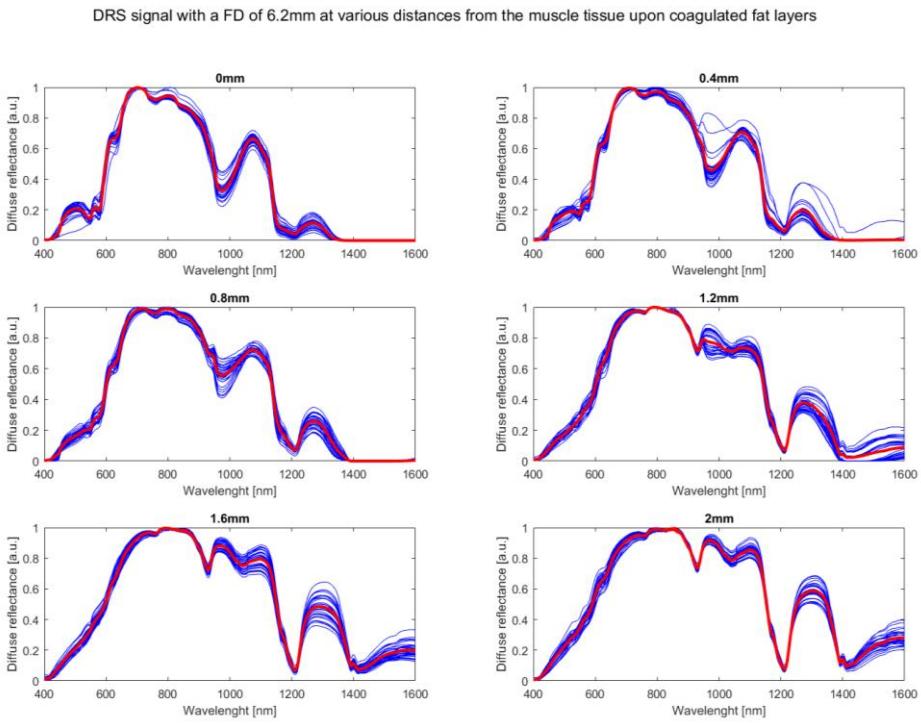

Figure 87: DR spectra of the transition between muscle tissue (0mm) and adipose tissue layers (from 0.4mm). The title represents the depth of the adipose layers. The FD used is 6.2mm. All experimental conditions are performed 30 times.

Appendix G

Referred to in Paragraph 10.4. The fat-water ratio for the transition from pure muscle to cut adipose tissue for FD's of 3.25, 3.75, 5 and 6.2mm.

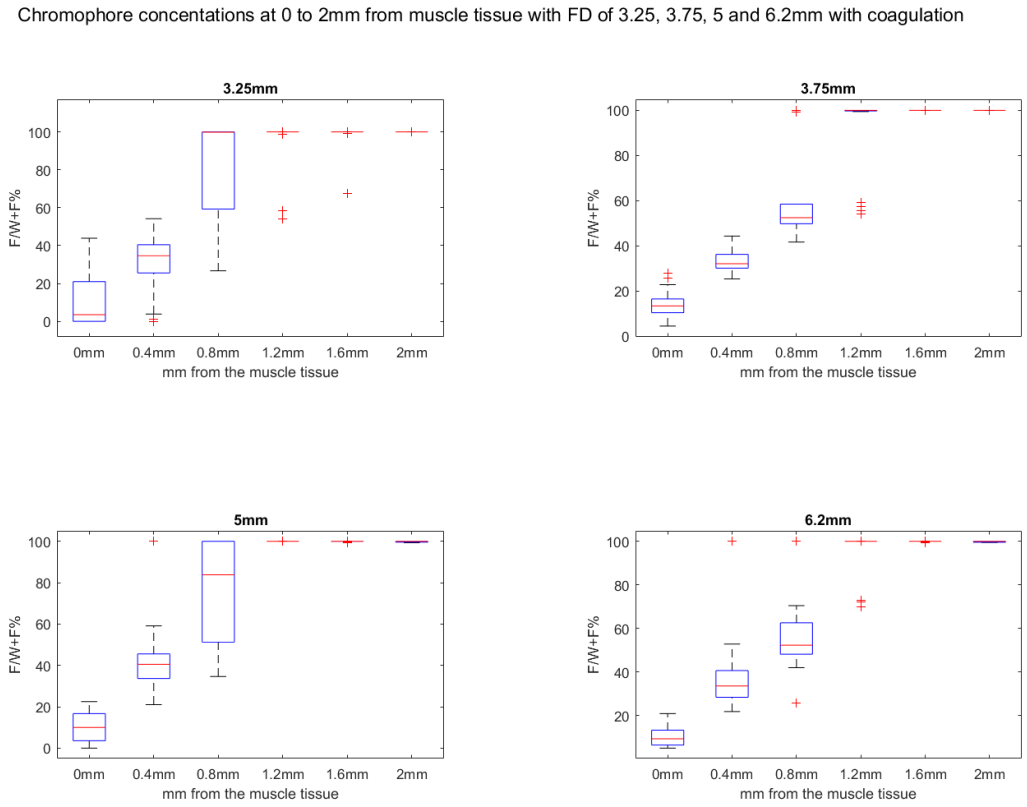

Figure 88: Chromophore concentrations of the fat-water ratio from 0mm (muscle tissue) to 2mm (cut adipose tissue) for various fiber distances (3.25mm, 3.75mm, 5mm and 6.2mm).

Appendix H

Referred to in Paragraph 11.3. All DR spectra obtained while measuring during cutting with and without removing the 'bad' fits. The plot including bad fits shows peaks with a high intensity. Additional, the mean values of all measured spectra during cutting excluded the 'bad' fits in one plot.

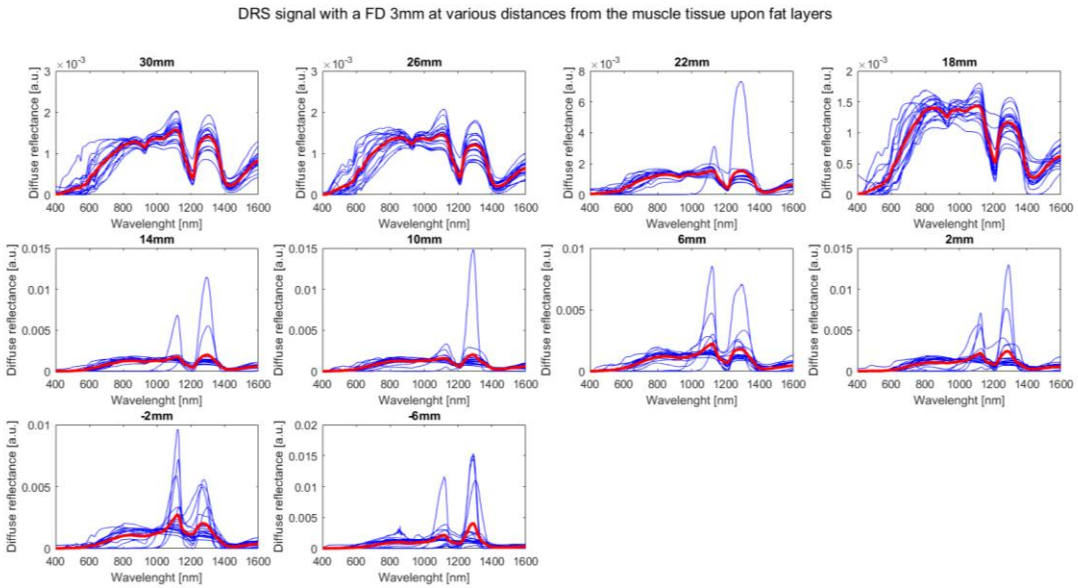

Figure 89: Measured spectra obtained of the transition from adipose (>0mm) to muscle (<0mm) tissue during cutting with an electrosurgical knife. The fit of the spectra is not checked on their correctness (yet). All plots include 20 measurements (blue lines) and the mean of the spectra (red line).

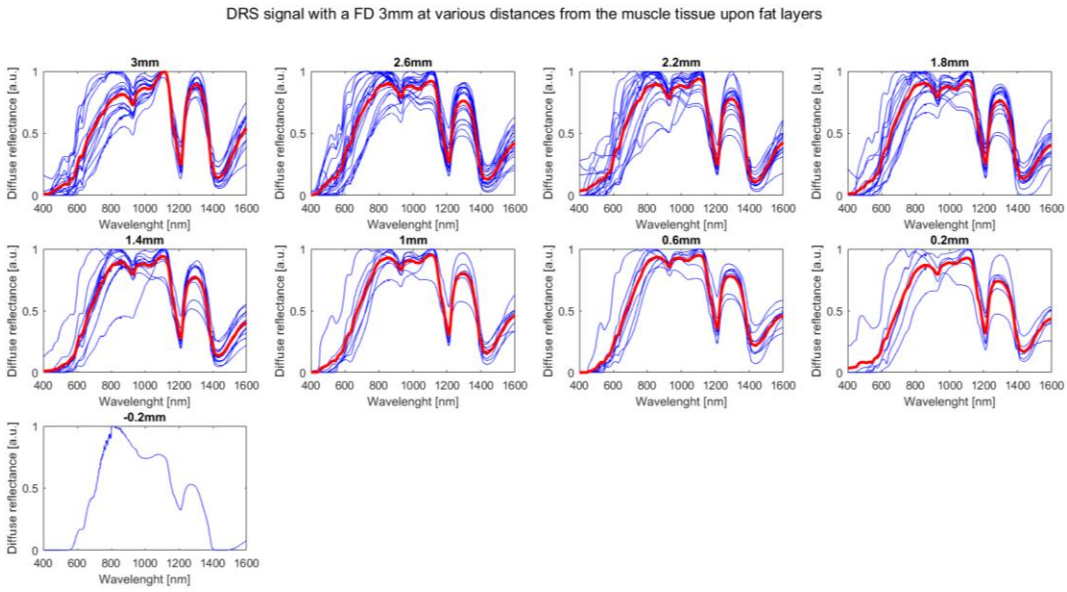

Figure 90: Measured spectra obtained of the transition from adipose (>0mm) to muscle (<0mm) tissue during cutting with an electrosurgical knife. Incorrect fits are deleted. All plots include 20 measurements (blue lines) excluding bad fits and the mean of the spectra (red line).

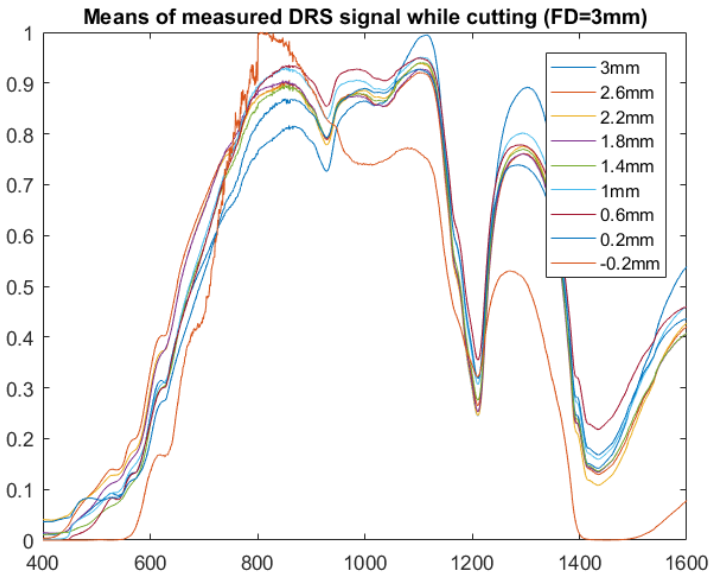

Figure 91: Means of all measured spectra obtained of the transition from adipose (>0mm) to muscle (<0mm) tissue during cutting with an electrosurgical knife excluding the bad fits. The spectrum of (-2mm) is the only spectrum measured in muscle tissue with a good fit.

Appendix I

Referred to in Paragraph 11.4. Examples of 'bad' fits: a low signal, low scattering, a bad fit. A fit is 'bad' if: a low or no signal is present, if the scattering coefficient is lower than the signal, or when the fit does not follow the measured spectrum. In order to compare the spectra, a 'good' fit is added.

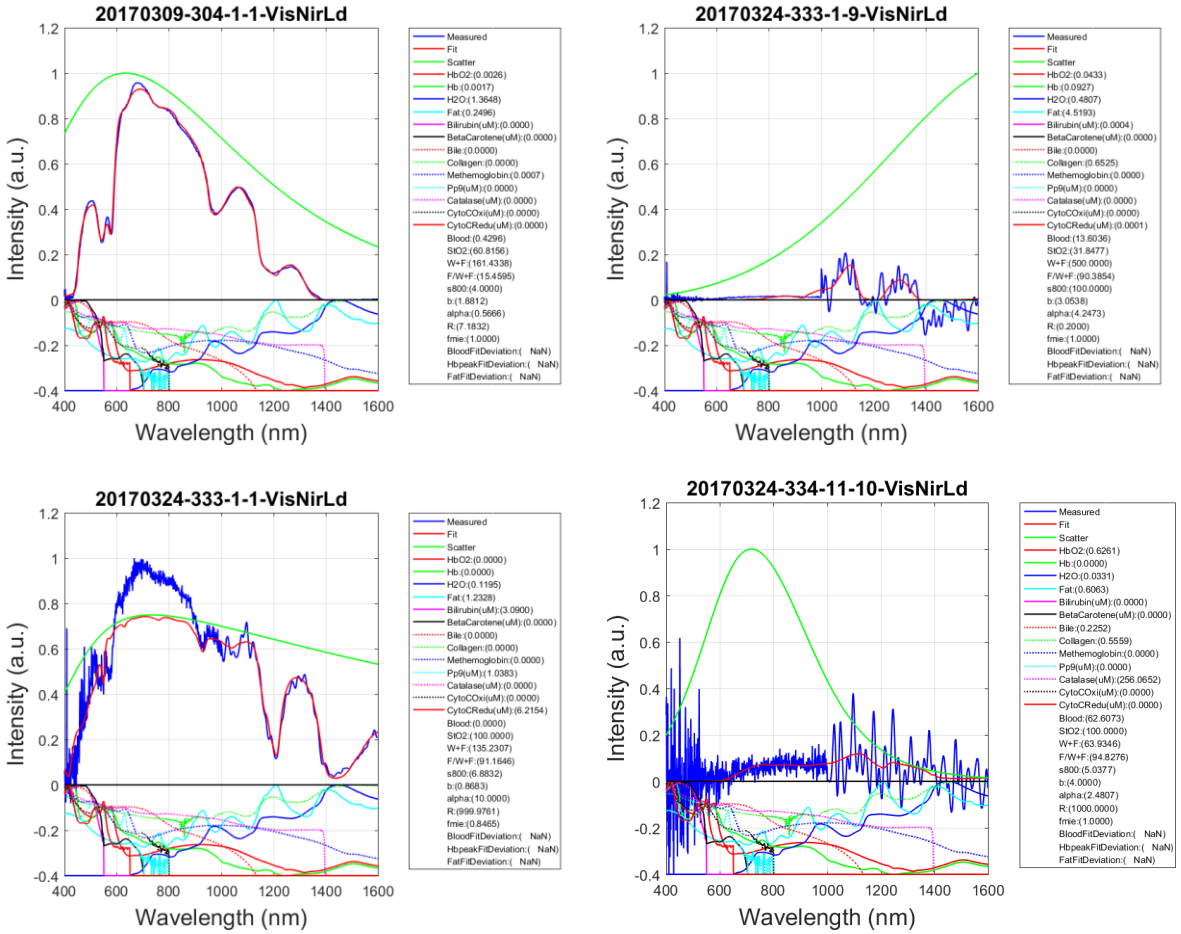

Figure 92: Fits of DR measurements. Top left shows a good fit. Top right shows a low signal. Bottom left shows a scattering coefficient lower than the measured spectra. For the VIS region, this will provide fitted spectrum which does not reflect the measured spectrum. Bottom right shows a wrong fit. The measured spectrum shows large deviations which make the fit in it unusable.

Appendix J

Referred to in Paragraph 11.4. Chromophore concentrations (fat-water ratio, StO_2 and F_{mie}) measured for the transition from muscle to adipose tissue while cutting including the second best and third best fit.

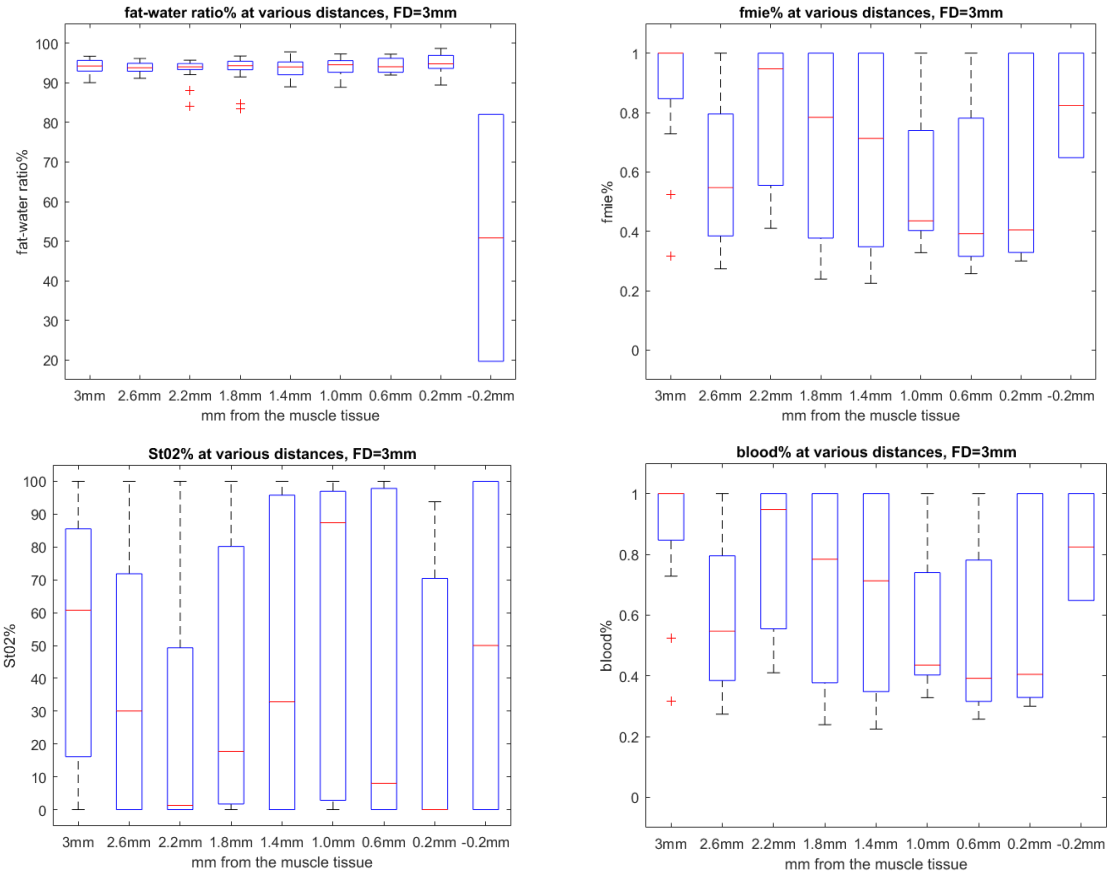

Figure 93: Chromophore concentrations measured for the transition from muscle tissue to adipose tissue. Fat-water ratio (top left), Mie scattering (top right), StO_2 (bottom left) and blood (bottom right) concentration. The second best fit for [-2mm] is included.

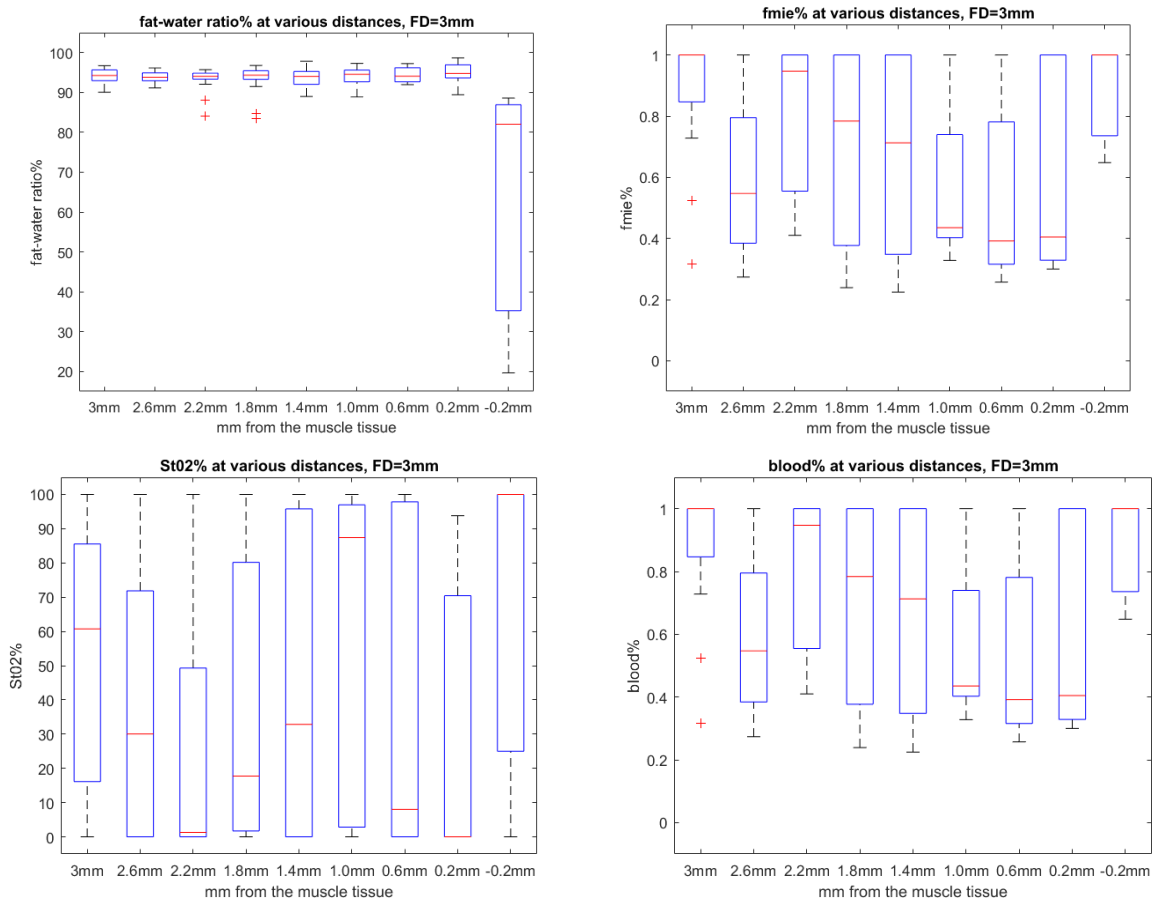

Figure 94: Chromophore concentrations measured for the transition from muscle tissue to adipose tissue. Fat-water ratio (top left), Mie scattering (top right), StO_2 (bottom left) and blood (bottom right) concentration. The second and third best fit for [-2mm] are included.

Appendix K

Referred to in Paragraph 11.4. Chromophore concentrations of StO_2, Mie scattering (F_{mie}) and blood while cutting.

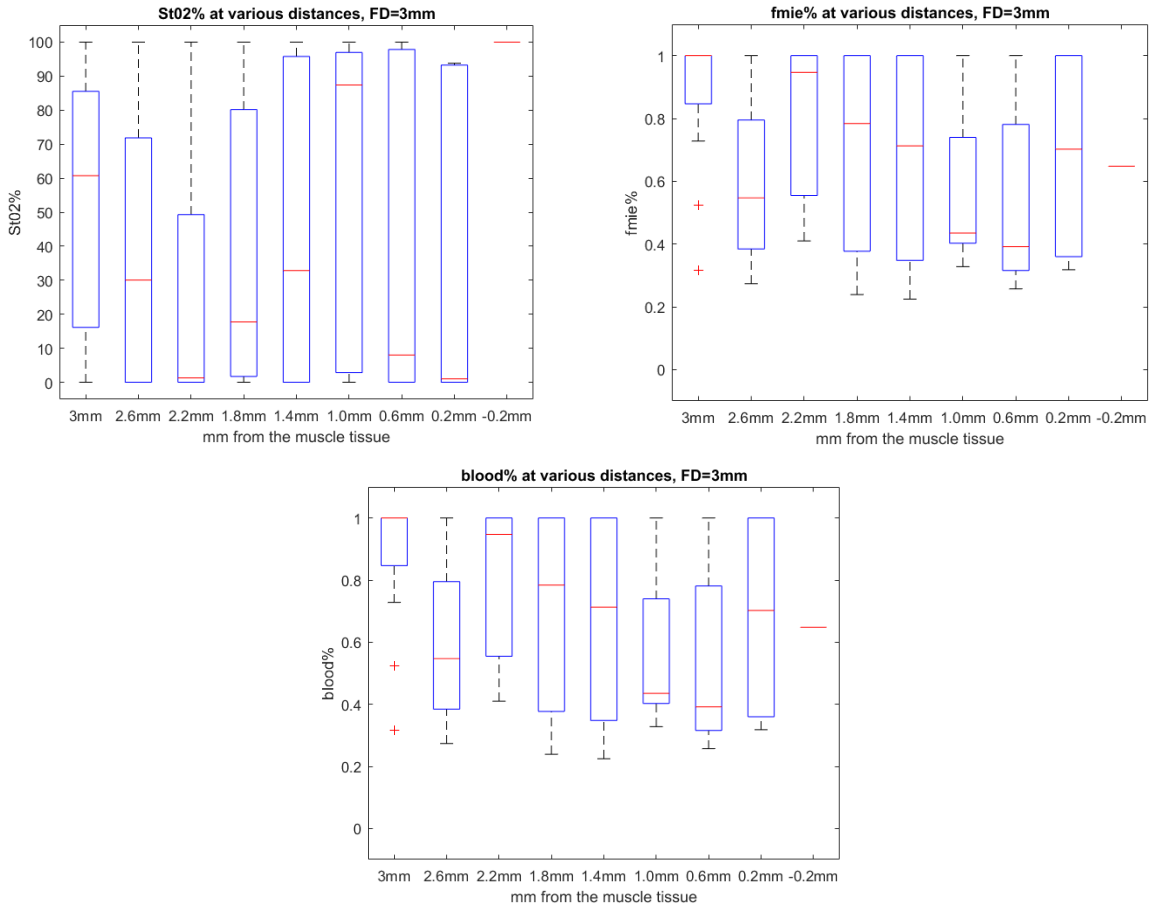

Figure 95: StO2 (top left), Mie scattering (top right) and blood percentage (bottom) of the transition from adipose (>0mm) to muscle tissue (<0mm) during cutting. The FD is 6.2mm and all experimental conditions are performed 30 times.

Appendix L

Referred to in Paragraph 12.1. Values used as inputs for the Monte Carlo model. The absorption and scattering coefficient were retrieved from the DR spectra.

Description tissue	Anisotropy	Refractive Index	Fiber distance
Pork belly	0.9	1.44	3mm
Fat tissue	0.9	1.44	3.25mm
Sowbelly	0.9	1.44	3.25mm
Muscle tissue	0.89	1.46	3mm
Cut pork belly	0.89	1.44	3mm
Cut fat tissue	0.89	1.44	3.25mm
Cut sowbelly	0.89	1.44	3.25mm
Cut muscle tissue	0.9	1.46	3mm

Figure 96: Values used as inputs for the MC model for various tissue types: anisotropy, refractive index and fiber distance.